Developments in reinforced glass beams

TU Delft

Developments in reinforced glass beams

Using post-tensioned GFRP strips, fibreglass fabric and sequential linear analysis

C.W. Hagen

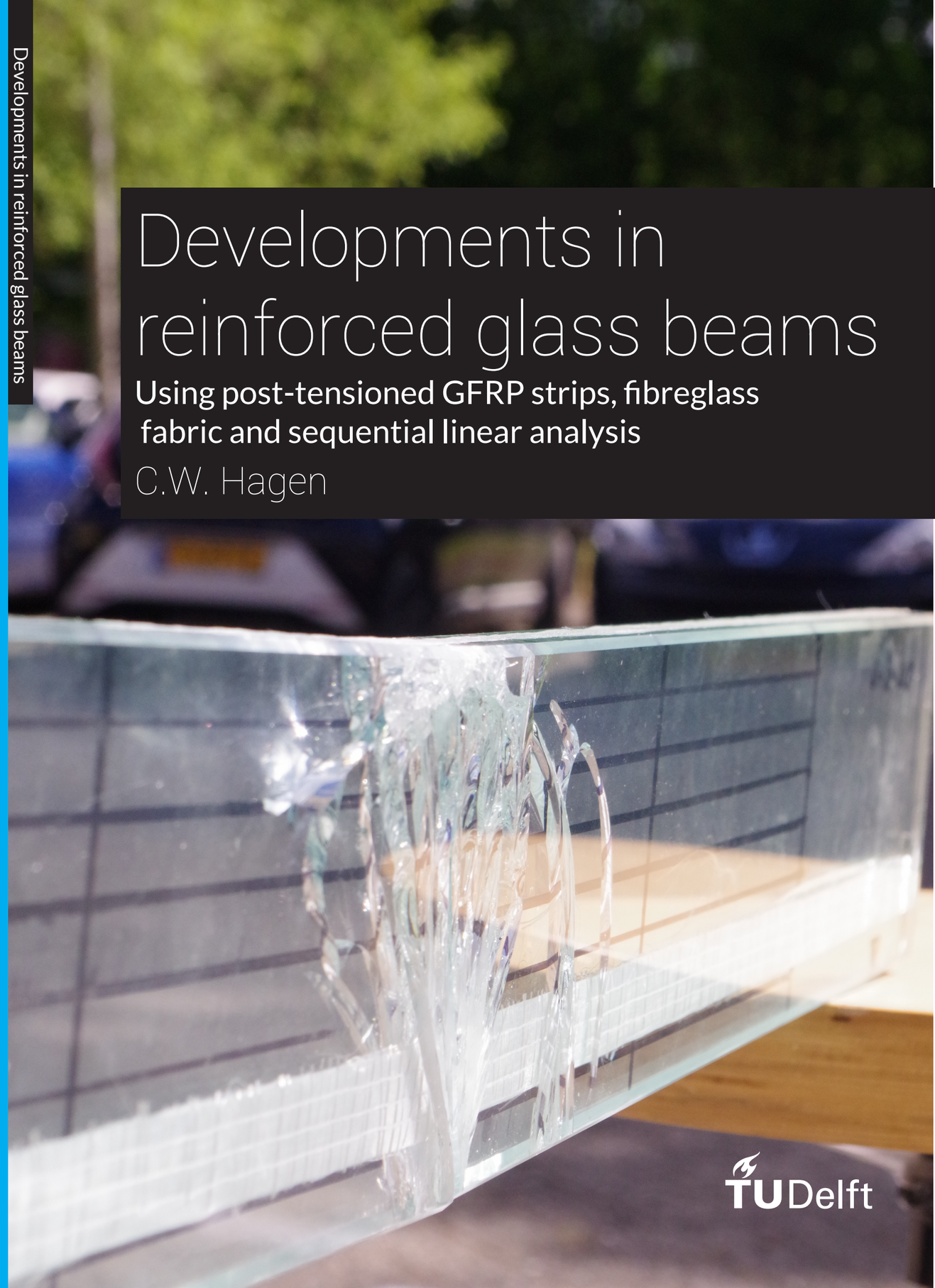

TU Delft

Developments in reinforced glass beams

Using post-tensioned GFRP strips, fibreglass fabric and sequential linear analysis

by

C.W. Hagen

For the degree of Master of Science
on the faculty of Civil Engineering and Geosciences
at the Delft University of Technology.

Date:	September 4, 2017		
Author:	C.W. Hagen		
E-mail:	corne.hagen@outlook.com		
Student number:	4321170		
Thesis committee:	Prof. ir. Rob Nijsse	Chairman	Civil Engineering, Structural Design
	Dr. ir. Christian Louter	Daily supervisor	Architecture, Engineering and Technology
	Dr. ir. Max Hendriks	FEM advisor	Civil Engineering, Structural Mechanics
	Ing. Mark Verbaten	FRP advisor	ABT

TU Delft Delft University of Technology

abt

Preface

This thesis is the final work done in order to obtain the Master of Science degree in Structural Engineering on the faculty of Civil Engineering and Geosciences at the Delft University of Technology. The objective of the thesis is to further develop reinforced glass beams.

After following the course Glass Engineering the behaviour of the material caught my attention. This interest was not only due to the growing application of structural glass, but also regarding the design methods and safety factors which were considered during the course. Thinking about the failure of glass structures the idea came to mind to use tension elements molten within the glass during manufacturing, to act as reinforcement. When talking to the right people it went clear that adhering a tension element was more plausible and that this concept, called reinforced glass, already existed. Hence, the subject of this thesis.

During the course of the thesis, the diversity of applied knowledge really surprised me. Even when the main subject is glass, it feels like only a small part was really about the material behaviour of glass. Besides the diversity of previously learned knowledge, also the range of things I did not know was wide and I have expanded this a lot.

The path of this thesis was not fully predefined and a lot of challenges and decisions in direction were faced. But this makes the process fun to do and satisfying to look back at. Luckily many challenges and uncertainties were not faced alone. I therefore would like to thank my graduation committee, prof. ir. R. Nijsse, dr. ir. P.C. Louter, dr. ir. M.A.N. Hendriks and ing. M. Verbaten for your guidance, expertise and feedback. Also during the execution of the experiments I got some great help and advise, for this I would like to thank, K. Baardolf, dr. ir. F.A. Veer, V. Horbowiec and G. Mulder. In addition to them my gratitude goes to M. Pari and M. Verbrugge for their availability in solving and discussing the SLA issues. Of course I could not have survived this without any daily company and it has been a great pleasure working together with you, A. Koper, C. van Hoogdaalem, M. Mureau, G. van Bolderen, L. Castelein, Q. Li and S. Hengeveld for all the coffee we drank and dealing with the random questions that I asked. Working with you has helped me in my motivation and widen my view on many aspects. My thanks also go to my fellow board members of Pegasus, O. van der Meer, K. Bronsvoort, K. de Nijs and Y. Tjiam, who supported me and I had to miss during the busy days. Last but not least, I would like to thank my family for all the support they gave me during my study time.

Hopefully you will enjoy reading this thesis and if you have any questions regarding the contents or if you desire to obtain some data. Feel free to contact me and I will gladly be of help.

C.W. Hagen
Delft, September 2017

Summary

Glass is gaining popularity as a structural material, this is mainly based on its transparent character. But due to its brittle failure behaviour the safety of these structures is an issue. Several concepts are found to guarantee the safety during the development of its structural application. One of these developments is to reinforce glass with other materials, this concept is known from concrete structures. After fracture of the glass (initial failure), the reinforcement will function as a tension element in order for the beam to maintain its integrity. This creates an additional load transfer mechanism, preventing total collapse of the structural system (ultimate failure) if designed properly.

The objective of this thesis is to further develop reinforced glass beams. In Chapter 1 this is started by defining an abstract concept called the ideal glass beam. This concept is defined as a glass beam which has increased initial failure resistance, ability to maintain its integrity, freedom in manufacturing and all without disturbing the clean transparency of the glass. For the reason of transparency potential all concepts are fibreglass based. Freedom in manufacturing is realised by the use of fibreglass fabric which can be cut as desired and laminated together with the glass panes, just as is done with fully integrated (GFRP) reinforcement. This results in the three reinforcement concepts; post-tensioned fibreglass reinforcement; fibreglass fabric reinforcement; and transparent fibreglass reinforcement. All these three concepts are not yet or only partially developed and thus require research. However only post-tension and fibreglass fabric are chosen to be elaborated in this thesis. The application of transparent fibreglass is briefly discussed in order to assess its plausibility.

Next to these design concepts, some issues exist regarding numerical calculations of glass systems. Most non-linear analysis run into convergence problems. Or computational intensive methods to account for the snap-back constitutive relation. This is due to the relative low fracture energy and high tensile strength with respect to concrete. A new kind of analysing method is in development which uses a series of linear analysis together with a damage model, reducing the material properties at each iteration. This method is called sequential linear analysis (SLA). The stability if this method creates the opportunity to analyse how alterations in design and numerical model influence the performance. These alterations come from differences in modelling approach in previous research, developments in SLA from research in concrete and design possibilities.

The design strategy and philosophy of a reinforced glass beams is different from the current design approach, where additional panes are used to prevent ultimate failure. What these differences are and how a reinforced glass beam should be designed is elaborated in Chapter 3. Here the initial and ultimate failure strength capacities are discussed, how their resistance in affected and how they should be designed in order te create a safe system. In Chapter 4 the origin, feasibility and validation of the concepts are elaborated. In order to validate the concepts and numerical method some validation goals are drafted partially consisting on the former mentioned design philosophy. These goals result in desired data requirements which is subsequently used to described the experiments to acquire this data. Initially only two bending experiments are required, for validation of both post-tension and fibreglass reinforcement. Both are validated using a reference experiment, for post-tension this is a specimen without applied normal force and the fibreglass fabric reinforcement is validated using integrated GFRP strips. In addition to theses experiments tensile data of the different reinforcements is obtained to be used as input during numerical modelling. Also pull-out experiments are done for the fibreglass reinforcements to have a more direct comparing approach and to spread the risk of unsuccessful execution of either experiment.

In Chapter 5 the experiments are designed based on the former mentioned requirements using analytical calculations. This is done to ensure theoretical feasibility of the experiments and to estimate the behaviour. The post-tensioned design consist of GFRP strips adhered on top and bottom after tensioning in order for them to function as reinforcement. No eccentricity is used te prevent crushing of the glass edges as the tensioning is introduced by head sections on either edge. These steel components function as actuators to introduce the normal force on the glass. The fibreglass fabric beams are designed to have equal ultimate failure resistance as the reference specimen.

In the experimental research in Chapter 6 the validation goals are repeated and each experiment is treated. Starting with the tensile experiments, ordinary force displacement experiments are executed on the Fibrolux GFRP strips. These experiments failed at lower values of tensile strength and Youngs' modulus than

expected based on the values given by the manufacturer. This is explained by stress concentrations due to the rectangular geometry and relative low uni-directional (UD) fabric within the composite, according to the manufacturer. The fibreglass composite experiment also failed at a lower resistance than expected. After failure loose fibres are visible implying full saturation is not achieved. Using the theoretical strength of the SentryGlass (SG) it is calculated that approximately 30% of the fibres contributed in the strength resistance. The pull-out experiments are designed as a double pull-out with one lower resistance side which should fail by de-bonding. The difference in resistance can be compared with a reference set which has equal shear resistance to analyse the bonding performance. But due to the same saturation issue as the tensile fibreglass specimen, these fibreglass specimen also failed earlier. Thus making it unable to compare the different reinforcements. The GFRO pull-out specimen did fail properly as is expected from the reference set. Furthermore, the bending experiment using fibreglass fabric reinforcement did perform accordingly. Despite the same internal slipping of the fibreglass, the specimen showed almost sufficient ultimate resistance. After the occurrence of the first crack, the resistance increases again but after some deflection a decrease is observed. This is the consequence of the same internal slip due partial saturation. The final experiment regarding post-tensioning had a fault during the post-tensioning process, resulting in an insufficient post-tension force. The experiments did therefore shown no increase in initial failure. Although the post-tension experiment did not succeed, still a GFRP reinforced beam was experimented and a different failure was observed. This different failure mode occurred due to the low stiffness of the reinforcement resulting in high crack opening and earlier failure of the system.

The numerical analysis is done in Chapter 7. This chapter contains two parts, first the analysis part and secondly the validation part. During the first part a study is done on different parameter and design considerations. This study is based on an experimental data set from former research, this set is also used on a sequential linear analysis (SLA) and non-linear analysis (NLA) validation and is therefore the ideal case to advance the developments. A reference model is made based on starting points from previous research and each aspect is applied on this reference model to analysis the performance differences. This performance differences are analysed based on four aspects: Resistance, deformation, crack density and amount of cracks. After each analysis a conclusion is made using these performance aspects and is graded with respect to the reference case. Two major objectives in this study is to implement the lacking resistance of the SG interlayer and post-tensioning. For the interlayer, the characteristics of SLA are used to construct an equivalent post-cracked resistance using the reduction branches. The post-tension should be implemented as initial stress/strain conditions but as SLA is still in development this is not yet available. A two solutions are found based on the transformation of the material properties. Both result in the increased initial failure, but only one represents the post-cracked behaviour of a post-tension beam in the correct manner. The numerical models of the reference case and post-tension experiments are validated in the second part of this chapter. Initially the fibreglass fabric experiment were planned to be used as validation, but this is not done. Based on the complex behaviour of the reinforcement, numerical analysis of this experiment does not contributed to the objective. The validation of the numerical analysis is done based on the deviation which represents the difference in ultimate resistance with respect to the experiment. For the reference case the deviation in resistance and deflection to the experiments decreased when the findings are applied to the reference model. However the crack pattern is still an issue as T-shaped crack occurred where V-shaped cracks were expected. Also in the validation of the post-tension experiment this V-crack is not present, but due to the absence of SG the cracking pattern is lot more conform the observations in the experiment. This case not only has small deviations in resistance and deflection, but failed in equal manner as the specimen.

All results are summarised and discussed in Chapter 8, from this discussion the conclusions regarding the stated research objectives in the outline are drawn in Chapter 9. In this chapter is concluded that the suitability of GFRP post-tensioning could not be validated due to the fault in the process and the low Young's modulus resulted in higher crack opening and earlier reaching of ultimate failure. The fibreglass fabric did achieve a fair ultimate failure resistance but as they did not have a higher resistance as the initial fracture they did not pass the validation criteria. This was due to insufficient saturation of fibreglass with SG, causing the fibres to slip on one each other, hence not able to reach their full capacity. The analysis of different aspects using SLA resulted in a development in analysing method. Using a grading system the influences on the performance of each aspect are indicated. Creating insight of the influences of different design and modelling considerations. To finalise some recommendations are in place, as this is only the beginning of a broad subject. Obviously, it is recommended to research the third concept as this could not be included in this thesis, to even further develop the ideal reinforced glass beam. But regarding the post-tensioning, more effective systems are recommended as the initial failure increase in the post-tensioned design was quite low,

for example, higher eccentricity and more stable structures. Solutions for higher saturation in the fibreglass fabric to decrease the slip and increase the resistance. Regarding the numerical analysis, implementation of SLA in 3D brick elements and a better more physical correct plasticity model are recommended. Next to these independent subjects reinforced glass in general requires the definition of different failure modes and the prevention of brittle failure modes. Also would it be important to perform force-controlled experiments, possibly in combination with an impact load. Since this is the major reason to apply reinforcements. More recommendations and conclusions are found in Chapter 9.

So in conclusion all the independent subjects converge to the contribution in the developments in reinforced glass beams. The freedom and benefits in application of integrated fabric reinforcement are known and more knowledge is obtained regarding design of reinforced glass structures and influences of (in)correct numerical modelling.

Acronyms

2D	two-directional.
ANG	annealed glass.
CFRP	carbon fibre reinforced polymer.
EP	epoxy.
ESD	element safety diagram.
EVA	ethylene-vinyl acetate.
FE	finite element.
FEA	finite element analysis.
FFR	fibreglass fabric reinforcement.
FRP	fibre reinforced polymer.
FTG	fully tempered glass.
fvf	fibre volume fraction.
GB	acrylate adhesive GB368.
GFRP	glass fibre reinforced polymer.
HSG	heat strengthen glass.
LTM	load transfer mechanism.
NIEM	non-iterative energy based method.
NLA	non-linear analysis.
PT	post-tension.
PU	polyurethane.
PVB	polyvinyl butyral.
R.I.	refractive index.
RG	reinforced glass.
s.d.	standard deviation.
SG	SentryGlass.

SLA	sequential linear analysis.
STS	stainless steel.
UD	uni-directional.

Symbols

ε_e	Elastic fracture strain based on initial Young's modulus.
ε_u	Ultimate strain after snap-back.
$\varepsilon_{u,re}$	Ultimate strain of reinforcement.
ε_u^+	Ultimate strain at the '+' curve curve.
ε_j	Strain at reduction step j.
F_i	Load resistance at glass failure.
$F_{i,p}$	Load resistance at glass failure with post-tension.
F_u	Load resistance at ultimate failure.
M_i	Moment resistance at initial failure.
M_u	Moment resistance at ultimate failure.
$M_{u,mean}$	Mean moment resistance of specimen at ultimate failure.
$F_{u,re}$	Force in reinforcement at ultimate failure.
$F_{u,re,mean}$	Mean force in reinforcement at ultimate failure.
E	Young's modulus.
E_j	Young's modulus at reduction step j.
D	Damage modulus.
f_t	Elastic tensile stress limit.
$f_{t,j+1}^+$	Upper tensile stress limit of saw-tooth at reduction step j.
$f_{t,j+1}^-$	Lower tensile stress limit of saw-tooth at reduction step j.
F_t	Elastic tensile force.
$f_{t,filament}$	Elastic tensile stress limit.
f_u	Ultimate tensile stress limit.
$\varepsilon_{t,y}$	Tensile yield strain.
$f_{t,y}$	Tensile yield stress.
$f_{y,0.2\%}$	0.2% yield stress.
G_f	Fracture energy.
h	Crack bandwidth.
t_{eff}	Effective thickness.
c_{re}	Theoretical cover of reinforcement consisting of edge distance and half the reinforcement height.
z	Distance of internal arm between cumulated reinforcement and compression zone forces.
a_i	Distance between neutral line of total section and part i.
y_{bot}	Distance from neutral line to bottom of glass section.
p	Percentage parameter of f_t; which defines the distance of the upper and lower to the mother curve.
L_1	Distance between support and load introduction point.
EI	Stiffness of the beam.
E_{mean}	Mean Youngs' modulus.
A	Area.
x_u	Height of compression zone at ultimate failure.

Contents

1 Introduction

Glass is in general related to brittle behaviour. One often thinks directly of a window or mirror and a material which should be handled with care. But lately, glass is an upcoming material for structural application due to its unique properties like high compressive strength and transparency. However despite the increase in popularity its application is still limited. In this chapter the current situation of structural glass and the scope of the research project is defined together with the approach and a small part regarding some risk prevention.

1.1. Background

Glass is an upcoming material regarding its application in structures. The high transparency of glass rises the popularity for architects to also design the load bearing structure in this material. But the brittle behaviour of glass brings challenges to its application. Sharp pieces after glass fracture can cause nasty injuries. The idea of using such a risk-full material as a structural material creates sceptical opinions and thus solutions should be found for safe applications.

A few years already this problem is known and in its development some acceptable solutions are found: Over-dimensioning to decrease the likelihood of failure; applying sacrificial layers; laminating panes in combination with stiff interlayer to maintain integrity (glass roof panels); glass composites to increase stiffness and create ductility; reinforce glass to create ductility and preserve transparency; and post-tensioned glass to increase the initial failure moment.

A problem regarding glass design is the ability to calculate these structures due to the brittle behaviour of glass. In most applications finite element (FE) methods are used to easily vary differences in design rather than performing experiments. But due to the brittle behaviour of glass, ordinary NLA do not give satisfying results as convergence is hard to achieve and large deviations are found in the force-displacement curves. A promising numerical analysis method for brittle materials will be used which is called SLA. This analysing method is developed by Rots and Invernizzi [2004] and earlier verifications are done with reinforced glass cases by Louter et al. [2010b], Leung [2010] and Invernizzi et al. [2011]. This method uses series of linear analysis and reduce material properties according to a pre-described damage profile.

1.2. Scope

Reinforced and post-tensioned glass[1] are currently the most promising systems when it comes to design and safety and will therefore be the main subjects of this thesis. The application of reinforcement results in safe failure of the glass beam, but only when the glass is already fractured. Using a compression force by post-tensioning delays this fracture and higher capacity can be applied. Combining these load bearing systems would lead to a structure which benefits both. Causing higher strength resistance in pre and post-

[1] Tensioning the system with another material will be called post-tensioning in this thesis to avoid confusion with internal pre-tensioning (hardening) of glass panes.

cracked stages, the latter will result in an second load transfer mechanism (LTM), thus implying safe failure if a proper design is applied.
In the development of reinforced glass many materials and possibilities are experimented (Martens et al. [2016c]). The use of fibreglass composites in particular is interesting. The benefit of using fibreglass as reinforcement material comes from the developments in transparent GFRP composites (Leung [2010]; Seo et al. [2017]). The transparency should not be spoiled by reinforcement, since glass structures are applied for their transparency. Therefore, transparent reinforcement is very appealing. The potential of fibreglass lies in the small difference in refractive index (R.I.) with SG and the similar properties of the resin which is used in Seo et al. [2017]. An issue in the application of glass fibre reinforced polymer (GFRP) is their availability in dimensions. Structural components are hard to generalise for their all time differing boundaries. The requirements for reinforcement strips differ a lot and thus leading to the challenge to obtain the perfect dimensions of these prefabricated strips. Next to this another issue occurs when full integration of the reinforcement is desired. The use of GFRP strips introduces an additional failure mode as the stresses need to be transferred from the matrix to the glass. This can be prevented by embedding the fibreglass texture directly in the interlayer, making the interlayer both a matrix and adherence. This solution will eliminate this extra failure mode; generates higher potential for transparency as it only contains one material; and higher flexibility in application of reinforcement dimensions. This application is hereafter mentioned as fibreglass fabric reinforcement (FFR), as the fabric is directly used as reinforcement.
Based on the transparency property these subjects are applied using fibreglass, for post-tensioned reinforcement this a new concept as it is only applied using steel. Summarising previous matter, reinforced glass can be developed with the following aspects;

- Increase initial resistance by post-tensioning using GFRP;
- Higher freedom in reinforcement dimensions by combining lamination processes of glass and fibreglass;
- Higher transparency by applying transparent fibreglass reinforcement.

The combination of these aspects is kept in mind as the abstract goal called the ideal beam. This is kept as the main objective in glass development, but can not be analysed as a whole since it is quite abstract and broad to analyse all combined possibilities. From this main objective the three aspects are translated in three subjects which need validation before combination can be done. The three subjects become; post-tensioning with GFRP; fibreglass fabric reinforcement (FFR); transparent fibreglass reinforcement using the interlayer as resin. Unfortunately, not all systems can be validated within the time span of this thesis and therefore only post-tensioning and the fabric reinforcement is treated.
As an understanding of reinforced glass in general is developed, the influences of design choices regarding failure mode and subsequently ultimate failure capacity are currently lacking. Due to the stable solutions of SLA, a study can be performed with respect to physical parameters/design aspects of a reinforced glass (RG) beam. Next to physical differences, some developments are done in modelling by several studies regarding SLA. This study is done to create insight about the influences of design/modelling choices and lead to validation of this developing method.

1.3. Research objective

The previously defined scope is consisting out of three subjects; post-tensioned GFRP reinforcement; fibreglass fabric reinforcement; and developments in SLA. These subjects are part of the whole as their combination results in the former described main objective. The research objective is then described as:

To develop and create a better understanding of the pre- and post-cracked behaviour of reinforced laminated glass, using post-tensioned GFRP reinforcement strips, fibreglass fabric reinforcement and sequential linear finite element analysis.

The following research questions are stated regarding the three main subjects of the main objective. In addition to these research questions some sub-questions are stated as knowledge on these small subjects is also of interest.

- Is GFRP reinforcement a suitable material to use for post-tensioning RG beams?

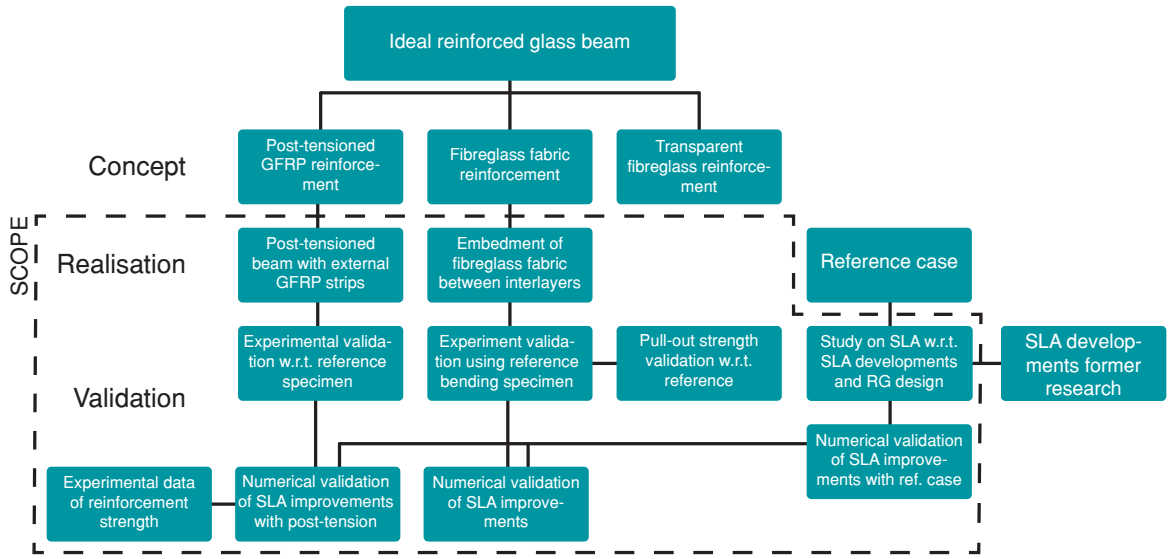

Figure 1.1: Illustration of the scope of this thesis, including the concepts, realisations and their validation

  - How does the relative low Youngs modulus of a GFRP strip perform as reinforcing material?

- What is the post-cracking performance of fibreglass fabric reinforcement with respect to GFRP?
- What are the influences of design considerations and modelling deviations on the (numerical) performance of a RG beam?

  - How can the post-cracked resistance of the SentryGlass be modelled in a 2D numerical analysis?
  - What is the best manner of modelling post-tensioning using SLA?

1.4. Approach

In Figure 1.1 the outline of this thesis is presented. Here is seen that the ideal beam and its three concepts are the starting point of this thesis and the upper goal. First information is acquired from previous research in Chapter 2. All edges of the scope will be looked into and especially the feasibility of transparent GFRP is treated. As RG is a rather new concept as a whole, this also means that a design philosophy should be considerate. Defining how a safe structure should be designed, especially regarding the strength resistance of the second LTM. This definition is done is Chapter 3.
In Chapter 4 the origin, feasibility and validation of the concepts are elaborated. As these concepts are rather abstract they are realised in the designs; post-tensioned beam with external strips and beam with embedded fibreglass fabric as reinforcement. These concepts designs are used for experiments in order to validate the underlying concept. The realisations are based on the design philosophy which will be used to define the validation goals. Then the required data in the form of parameters is determined to fulfil the validation goals, which subsequently form the experiments. To fulfil the design requirements the necessary amounts of reinforcement and post-tension force are calculated in Chapter 5 in a analytical manner. Doing so creates the theoretical feasibility of the validation goals.
Hereafter, the methodology and acquired data from the experiments are presented in Chapter 6. In this chapter also conclusions are made from the observations in behaviour and the concepts are validated according to the stated requirement from Chapter 4. Before the FE method can be validated an analysis is made based on former research. The study in Chapter 7 consists out of developments in SLA over the past years and design considerations. This study will be done to analyse how the modelling of certain elements affects the force-displacement curve and cracking behaviour. In addition to former developments the lack of resistance capacity is considered and an implementation solution for the use of SG will be treated. Finally the found improvements and modelling considerations will be applied on the reference case and the experiments to validate these different cases.

1

1.5. Risks

In the approach is mentioned that the concepts are validated in experimental manner. Experiments have the tendency to create unexpected results, therefore some risks are considered and how this is dealt with. The following risks are only based on prevention of misinterpretation of results and the continuity of the thesis. The risks and their solutions are listed below;

1. Analytical/Numerical prediction, the reinforcement is the major factor in the second LTM. Using the data from the manufacturer could be misleading and lead to inaccurate predictions in the bending resistance of the beam. To create a better prediction of the resistance the actual tensile behaviour of the reinforcements should be know. This is done by performing tensile experiments on the applied reinforcements.

2. Pull-out experiments, the stresses and strains in a bending beam during glass fracture are hard to predict and it is possible to misinterpret the behaviour of the fibreglass fabric reinforcement. The behaviour is simplified to pull-out experiments where the reinforcement to glass bond is tested directly.

3. Reference case, the risk is present that the experiments do not perform as they should. Leading to possible physical behaviours which are challenging to model. For the validation of the SLA improvements, a existing data set is taken as reference case to eliminate modelling defects. This case is the reference case and is applied in the analysis to have the same reference and one changing parameter/principle. After executing the experiments a decision in the numerical chapter is be made if the data set is used for validation.

2

Background

In further continuation of the thesis the background information of different subjects is first gathered to have a broad overview of hybrid glass development, material properties and numerical parameters. Also the transparent potential of fibreglass is discussed. Eventually it is all summarized in a conclusion where is decided to continue on different aspects of design, material and numerical staring points.

2.1. Introduction to glass design

In the outline of this thesis, the reasons of applying glass as a structural material is already covered. To remain within the scope, only hybrid glass is treated in the following sections. The term hybrid glass is used as a collective noun for all sorts of combined glass systems. The goal of combining different materials is to gain as much benefits out of the materials and use them for what they are used best. In glass engineering the main goal of applying this extra material is to remain integrity. Designing glass structures will be further elaborated in Chapter 3, but for now the main theme are the two failure cases, i.e. initial fracture and ultimate fracture. The addition of extra materials create the extra load transfer mechanism, but also additional stiffness, thus increasing initial failure as well. This is dependent on the amount, kind and manner the material is added. Herein, different glass systems can be distinguished in three categories according to Martens et al. [2015], the main characteristics are summarized below;

Glass composites

- Flanges are made from different materials;
- Increased stiffness and thus increased cracking strength;
- Higher ultimate failure due remaining integrity.

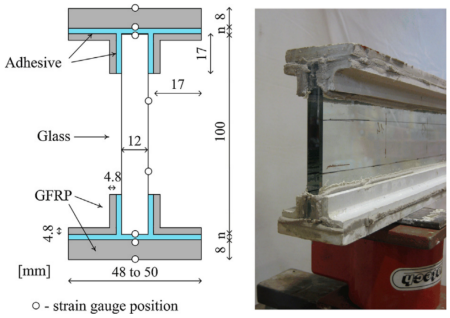

Figure 2.1: Example of a GFRP-glass composite (Valarinho et al. [2013])

2

Post-tensioned

- Increase of initial failure;
- Lateral torsion sensitivity;
- Addition of load introduction mechanism;
- Increased chance of explosive compressive failure.

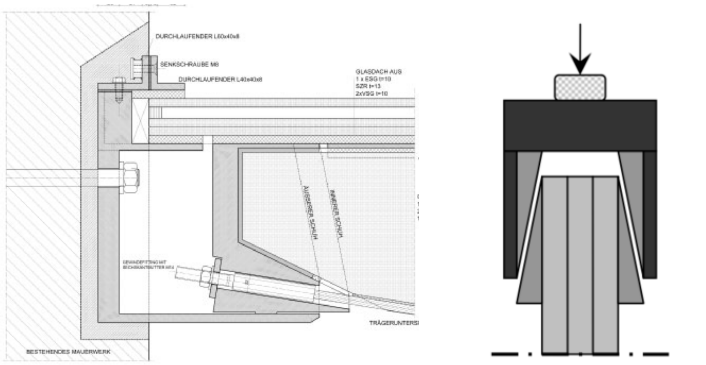

Figure 2.2: Different post-tension load introduction systems by Schober [2004] and Louter et al. [2006]

Reinforced glass

- In -or external reinforcement
- Crack and tensile force distribution function
- Section ratio often lower than 25%
- Reinforcement area based on load resistance after initial failure

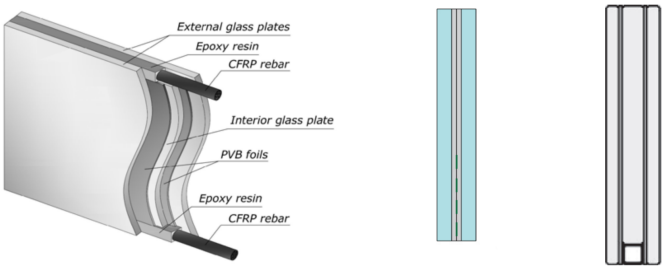

Figure 2.3: Glass section with steel external reinforcement Nielsen and Olesen [2010] and with GFRP internal reinforcement (Leung [2010])

2.2. Previous applications

Some research and applications in projects is already done in the above defined categories. In the subsequent sections the characteristics are discussed for each different application within the category together.

2.2.1. Composite applications

It is rather vague to distinguish composite from reinforced applications since no real boundary is present. The applications differ only in the amount of additional cross-sectional area. Composite action only becomes relevant for initial strength when sufficient stiffness is present. Since this stiffness is mainly dependent on the area, Martens defines this boundary at 25% cross-section ratio. When the cross-sectional ratio is bigger than 25% it is considered a composite and less it is a reinforced application (Martens et al. [2015]). Composite applications are researched in every thinkable application and are all achievable in their own specific way, all of them with their own characteristics, a few examples are summed up below.

Steel

Due to the relative high stiffness and yield strength very efficient to use as increase of initial strength. Also the plastic property of steel results in highly ductile behaviour. Several configurations are executed starting at I-sections by adhering flanges. But also the adherence of smaller steel strips resulting that steel is one composite application which is quite close to the border of reinforcements. Next to ordinary beam sections, experiments are performed using glass-steel composite in a truss application. These different applications are pictured in Figure 2.4

(G)FRP

Experiments with fibre reinforced polymer (FRP) composites are not very popular, mostly GFRP is researched by Valarinho and Correia in both experimental and numerical manner (Correia et al. [2011]; Valarinho et al. [2012a,b, 2013]). Also some experiments are done in laminating with GFRP sheets by Speranzini and Neri [2011]. What they all have in common is the additional LTM and the increased inertia which results an higher initial resistance. Although all applications show a second LTM, the post-cracked behaviour can differ due to variety in stiffness of the different adhesives. Since a lot of experiments are displacement controlled, it suggest that a sufficient secondary LTM is present. This is not always the case, when a low stiffness adhesive is applied it is possible to create a more ductile behaviour in the sense of rotation capacity,

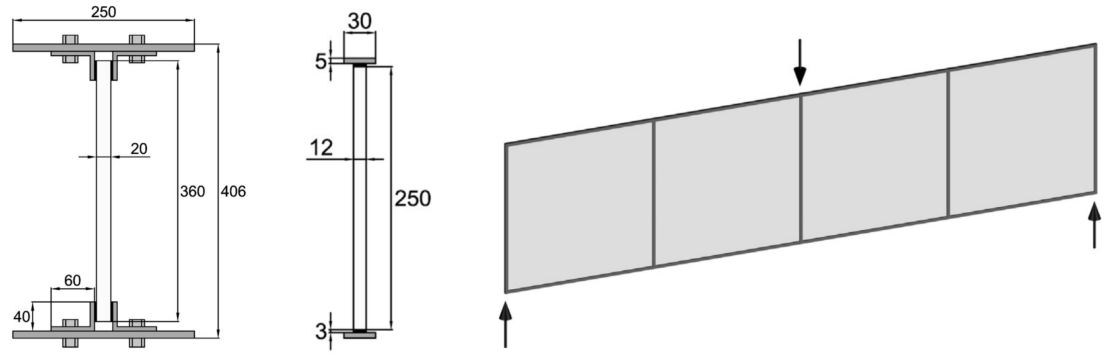

] (a) I-section, Weller-shof [2003

(b) Low section ratio, Abeln et al.

(c) Truss, Englhardt and Bergmeister [2007]

Figure 2.4: Different steel-glass applications

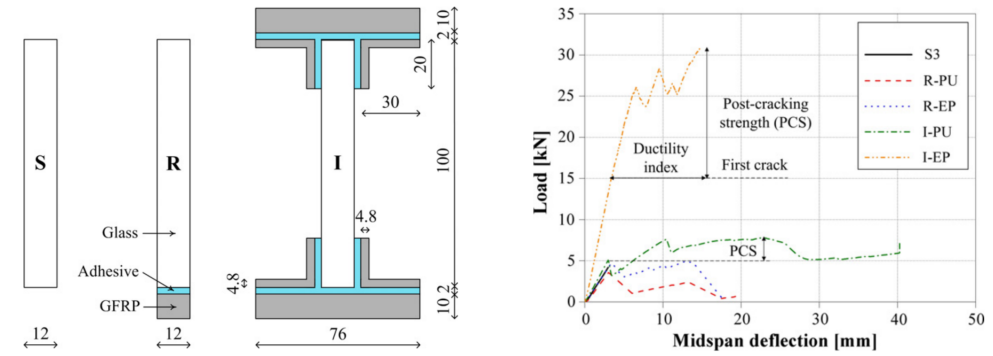

(a) (b)

Figure 2.5: (a) Different sections researched by Correia et al. [2011] using EP and PU adhesives and (b) Force displacement of different configurations

while the resistance capacity is below the initial failure resistance. But if engineered properly, even these application can maintain the minimum resistance ratio. This behaviour is very well seen in the work of Correia et al. [2011] in Figure 2.5, where the epoxy (EP) and polyurethane (PU) adhesives are compared. Here the application of EP result in roughly four times ultimate strength, but also less than half the displacement. It is a matter of definition to assess whether or not both of the applications behave ductile.

2.2.2. Reinforced application

A difference is seen in the reinforced application with respect to composites, here the reinforcing materials have higher characteristic values such as tensile strength and Young's modulus. Therefore less area is needed to create a equally great moment resistance. Again a few applications are discussed.

Steel

The steel reinforcement is an application which is researched most extensively by for example Bos et al. [2004]; Veer et al. [2005] and Snijder [2014]. This is probably due to the convenience of manufacturing and plastic properties of steel. For example a study with respect to configurations is done by Weller et al. [2010], Louter also researched the different glass types with the same configuration in Louter et al. [2012a], the adherence area in Louter [2007] and the temperature and humidity effect in Louter et al. [2010a, 2012b].

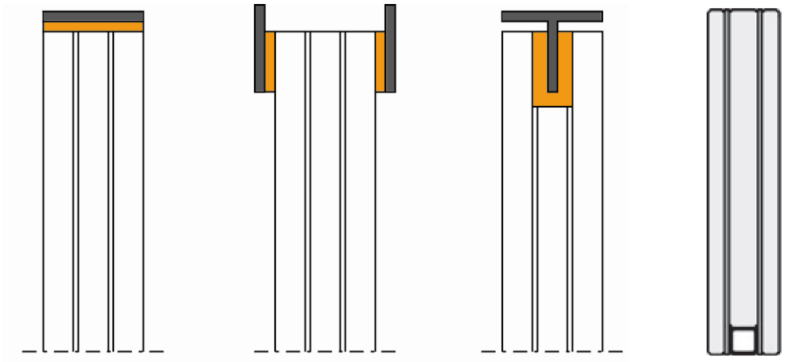

(a) Different configurations, Weller et al. [2010]

(b) Reference cross-section, Louter et al. [2012a]

Figure 2.6: Different steel reinforcement applications

FRP's

Where the FRP's are not very popular in composite application, they are as reinforcement. The work of Palumbo et al. [2005] is considerate one of the first to apply carbon fibre reinforced polymer (CFRP) as reinforcement of a glass beam. After this followed the integration of GFRP rods and strips by Leung [2010]; Louter [2009]; Rademakers [2009]. Also the comparison with CFRP rods is made in the work of Louter [2009], here is clearly visible that CFRP reinforcement creates less displacement. A combinations of steel covered by a polymeric resin is done by Speranzini and Agnetti [2014], yet this did not result in sufficient second LTM due to the lack of steel cross-sectional area and thus lack of tensile strength.

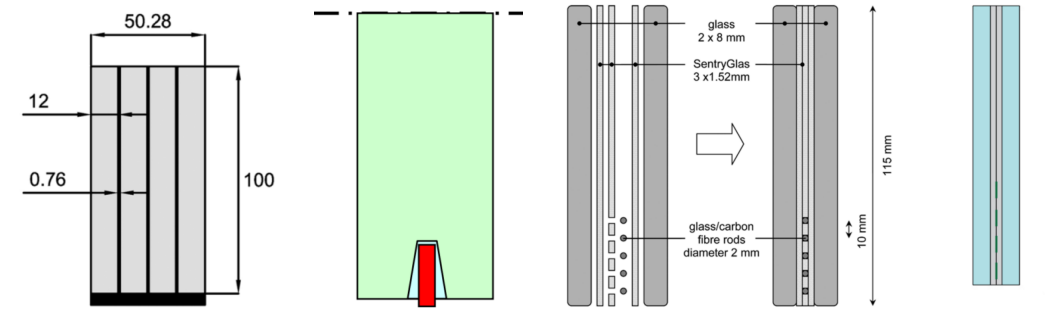

(a) CFRP strip, Palumbo et al. [2005]

(b) Intergrated GFRP, Rademakers [2009]

(c) Integrated rods, Louter [2009]

(d) Integrated strips, Leung [2010]

Figure 2.7: Different FRP reinforcement applications

2.2.3. Post-tensioned

The variety of post-tensioned structures is quite large and some previous application and design considerations are discussed in this section. But first it is necessary to mention some definition which is used in this thesis about tensioned glass structures.

Definition

Let us first focus on the definition of pre/post-tensioned structures. This is worth mentioning since this difference deviates from the definition known from concrete structures. Ordinary pre-stressed structures are commonly structure is either stressed during fabrication or construction. This application is called pre-stressing so it will not be confused with the renovating application of post-tensioning. Here, the already excising structure is given extra resistance capacity during renovation or upgrade after some years. In

glass engineering the difference in pre- and post-tensioning is even more substantial and not specifically mentioned in literature. Therefore the definition used in this thesis is summed up below in order to remain consistent.

Internal pre-stress	Introduction of initial stress applied on the glass' surface of a glass pane[1];
External pre-stress	External application of a normal force in advance of glass lamination;
(External) post-tension	External application of a normal force after lamination of glass panes.

Applications

Pure post-tensioned glass structures are somewhat different than reinforced or composite systems due to the fact that they are not directly adhered to the glass where the other systems are. An example is seen in cross-section displayed in Figure 2.8 (Díaz et al. [2011]) where the tensile elements are only present to introduce a normal force. Due to the normal force the initial failure resistance is increased.

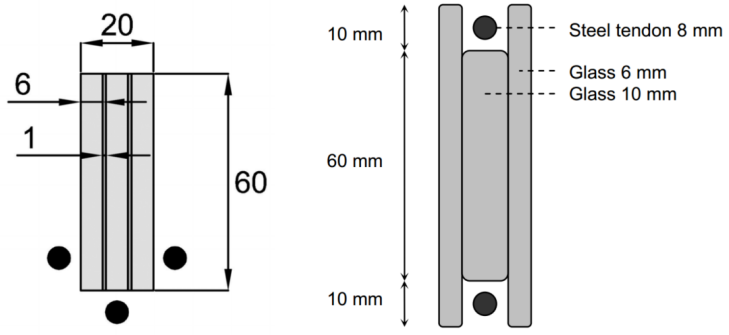

(a) Díaz et al. [2011] (b) Louter and Cupaç [2014]

Figure 2.8: Post-tensile cross-sections where the tendons are not adhered to the glass.

This concept is easily combined with the foregoing reinforcement system resulting in what is done by Louter (Belis [2004]; Bos et al. [2004]) where a curved tendon is tensioned in a hollow section through a glass T-section, displayed in Figure 2.9a and elaborated with post-tensioned stainless steel (STS) and CFRP strips by Louter (Louter and Cupaç [2014]; Louter et al. [2014]) which is seen in Figure 2.9.

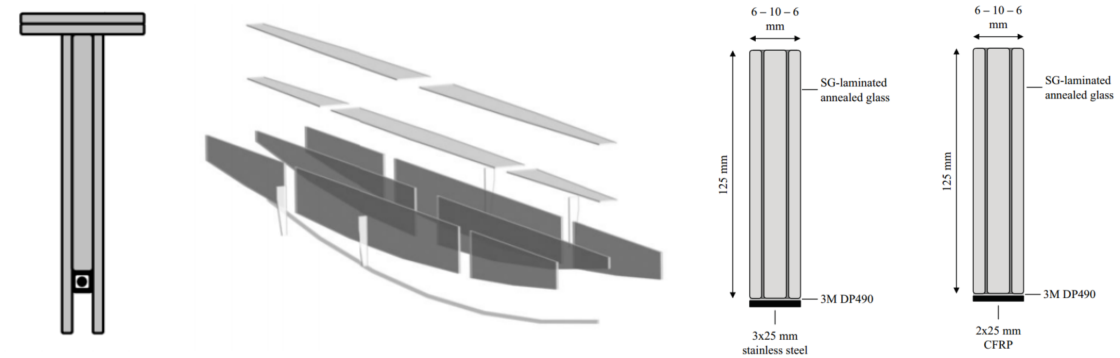

(a) Curved tensioned T-section, Belis [2004]; Bos et al. [2004]

(b) STS strip, Louter and Cupaç [2014]; Louter et al. [2014]

(c) CFRP strip, Louter and Cupaç [2014]

Figure 2.9: Post-tensioned applications in combination with reinforcement.

[1] This is done during manufacturing of glass either by tempering or chemical hardening and is discussed in the subsequent Section 2.3

2

Load introduction

An important aspect of post-tensioning is the load introduction since glass is sensitive for peak stresses. In the work of Louter et al. [2006] some experimentation are done with respect to different load introduction configurations. In Figure 2.10 the four configurations are seen and in Figure 2.11 their respectively force-displacement curve. It is concluded that alignment of transfer area is very important in this application. Method I was able to withstand the highest load, this due to the simplicity which resulted in proper alignment.

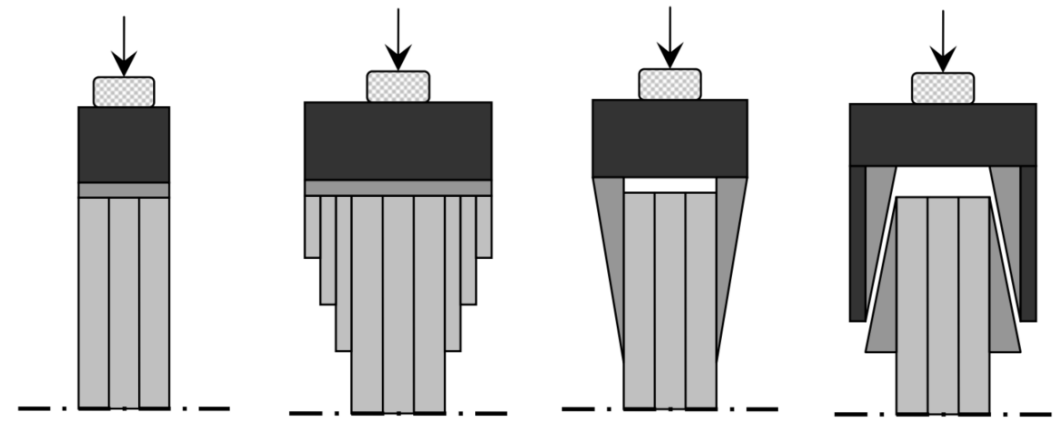

(a) Method I (b) Method II (c) Method III (d) Method IV

Figure 2.10: Four different load introduction configurations from Louter et al. [2006]

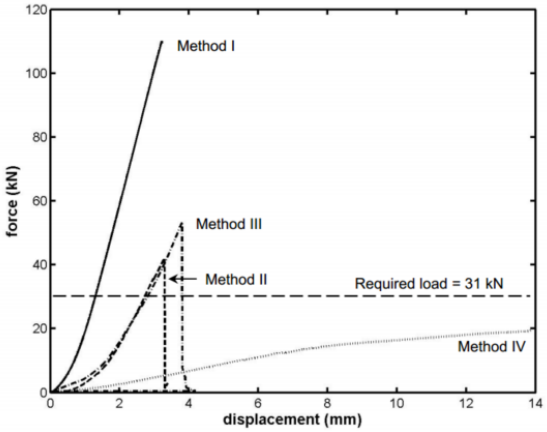

Figure 2.11: Force-displacement curve of different introduction configurations (Louter et al. [2006])

2.3. Glass as a structural material

The most common type of glass is float glass which can be strengthen by temperature or chemical hardening as chemical hardened glass is not applicable for this thesis only the temperature strengthened type will be treated, namely annealed glass (ANG), heat strengthen glass (HSG) and fully tempered glass (FTG). Each having their own distinctive features. To know which glass is suited best for this application all kinds are discussed and argued whether or not they could or should be applied. But first glass itself will be looked at for its chemical composition and structure create a better understanding of its behaviour.

2.3.1. Composition of glass

In general it is known that glass is made by heating sand, this is because sand primary consist out of silicon dioxide or quartz. Which is the main constituent of glass as ii is th main cause of stability and mechanical strength. The ordinary glass panes are silica-lime glasses which contains about 75% silicon dioxide. These

additions are done to decrease the melting point and to create a more complex structure so that in the cooling process the arrangements to form long range crystalline structures is prevented. Glass is therefore categorised as a non-crystalline and often referred to as a super cooled liquid as it is frozen in its glass transition (T_g) state. While glass does display mechanical properties of a solid it is considered a amorphous solid, as the internal structure has both a heigh level of connectivity but low degree of order due to this non-crystalline structure.

2.3.2. Glass types

Based on tensile strength properties, FTG would be the first choice of glass to use ($f_{t,g,k} = 120$ MPa, NEN-EN 2608 [2016]). But for glass engineering this is not directly true since there is more to it than only tensile strength. Due to the temperature hardening is a lot of energy stored in the glass itself, which is all released when one molecular chain is broken, resulting in the characteristic small glass pieces. This is ideal for car industry or façade design where people could get injured. While in design this failure mode is not beneficial due to the fact that designing the small pieces need to be held together. This could be achieved with an interlayer, although only up to a certain amount since the small pieces are not large enough to transfer the inter-laminar forces, causing losses of stiffness and even losing its topology (Figure 2.12,Martens et al. [2015]). Therefore fully tempered glass is not suited for our application, since the goal is for the beam to remain its topology.

The glass type which has almost very opposing properties is ANG, the characteristics of this type are its low tensile strength and large glass pieces after failure. Here, the lower tensile stress ($f_{t,g,m} = 45$ MPa, NEN-EN 2608 [2016]) is not always interesting since the structure should be a lot larger and contain more laminated panes, with respect to fully tempered glass. But its failure pattern is more beneficial due to the large pieces of glass which have sufficient transfer capacity after breakage when laminated. This makes ANG a very good candidate for the application of reinforced glass beams and is therefore seen a lot in research papers for understanding behaviour of certain solutions (Bedon and Louter [2014]; Martens et al. [2016a]; Valarinho et al. [2012b]). But the application of ANG in practice does have a drawback. Namely, glass is known for its property to erode when subjected to water/moisture. The number of flaws will increase over time due this corrosion resulting in lower tensile strength (Perkoff et al. [2001]). Since the beams in practise are subjected to this kind of erosion, maybe small or big, it is not very appealing to apply ANG knowing it chances of failure increase during the lifespan. A solution could be to apply external post-tension, this should theoretical eliminate the eroding process due to the compressive stresses. But only if the tensile zones remain compressed during the lifespan.

The performance of HSG lies in between that of ANG and FTG. this partial tempered glass type has a tensile strength and size of fracture pieces which lies in between that of ANG and FTG glass depending of the amount of internal pre-stress stress in the glass pane. The research of Kreher (Figure 2.12, Kreher [2004]; Louter [2007]) shows the different behaviour of heat strengthened glass in timber-reinforced structures. He differentiates HSG with respect to the internal pre-stress and states that a pane with residual stress below 50 MPa can be considerate to fail in a ductile manner and above 50 MPa will cause brittle failure. The benefit of using HSG is its ideal combination of all types with the right amount of internal pre-stress in present. Since this compressive stress around the edges reduces the corrosion of glass which is the major disadvantage of ANG.

2.3.3. Failure of glass

In general glass is seen as a very brittle material and characterised by its high fragility. Although sheets of glass are thicker thus stronger then a drinking cup it is still relatively easy to break them. In this section some related experiments are mentioned about the differences in failure of (reinforced) glass structures.

When looking at the failure behaviour, a distinguished can be made either due to edge flaws are external events. The edge flaws are micro cracks which occur during the fabrication process. Edges can be either grinded or polished, different finishes are available but will not be elaborated further. This process is done to minimize the larger flaws but can also increase the smaller ones. Further studies to optimise this process are needed in order to diminish the spread in the strength probability functions. External events are not uncommon in practise as is mentioned in Chapter 3. For this section failure by bending is elaborated, since failure by external events in glass in bending is not extensively researched. In Figure 2.13 the cracking patterns of ANG and FTG specimen subjected to bending are shown.

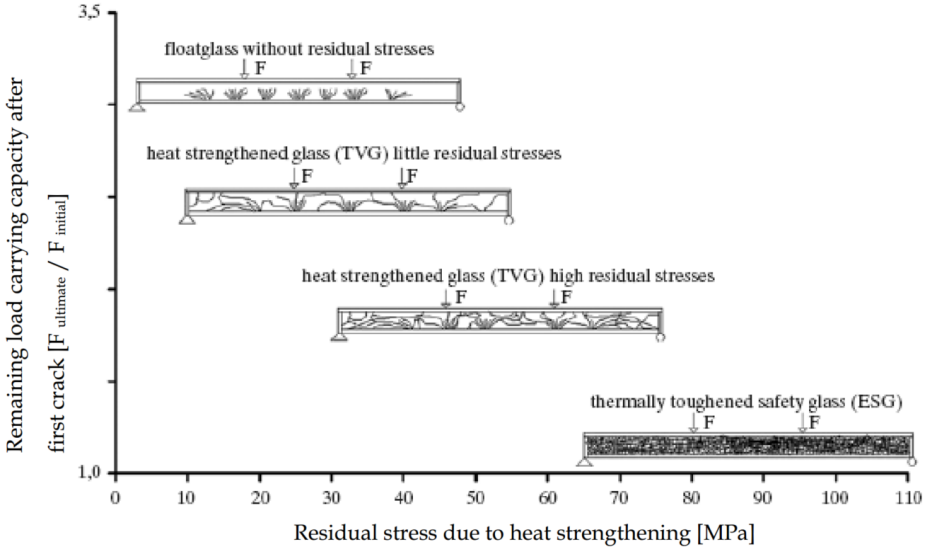

Figure 2.12: Residual load bearing capacity vs. internal pre-stress (from Kreher [2004])

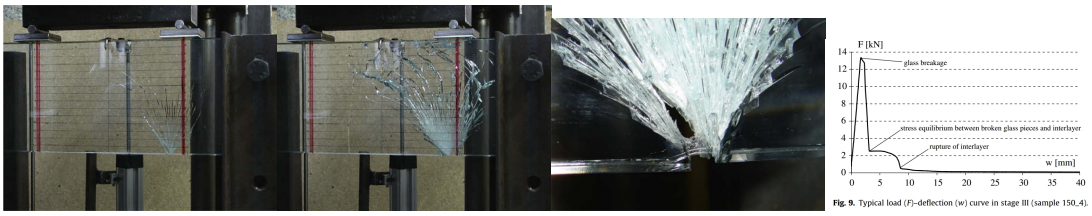

(a) First crack (b) Second crack (c) de-bonding of SG (d) Characteristic force-displacment curve

Figure 2.14: Failure of SG laminated glass beam

Figure 2.13: Cracking patterns of annealed and fully tempered glass pane due to bending, by Veer et al. [2005]

In these pictures the left is the specimen with the lowest strength and the right the one with the highest. This is also visible in the crack pattern, which has a higher crack density since for energy was needed to create them, this is especially visible for the ANG piece. In the work of Belis et al. [2009] the addition of SG interlayer is researched in laminated glass beams. In Figure 2.14 is observed how the first and second cracks are formed and the how the SG interlayer behaves in a glass laminate. It should be notice that the first crack is relative straight and equal in length, further development gives more orientation to the crack.

2.3.4. Failure of reinforced glass

The failure of a reinforced glass beam subjected to in-plane bending can be distinguished in three stages according to the work of Louter [2011] as shown in Figure 2.15 which based on the principle of lying laminated glass from Kott and Vogel [2003]. Although this is true, it implies that glass failure is a single event. While as it is observed the laminate consist out of multiple sheets where one often fails sooner than the other as observed by Belis et al. [2009]; Bos et al. [2004]. Belis explains this occurrence by manufacturing tolerances or load introduction but a local decrease in tensile strength could also be a explanation. Most of the times the remaining structure is unable to carry the load during an experimental test and therefore the

whole section will fail immediately.

Therefore this stage is most of the times so fast that its not even visible as is this stage generalised as one event. For the sake of completeness this should be added to the previously defined failure sequence as it is important when analysing the energy releases, resulting in the following enlisting.

1. Crack in single pane
2. Crack through section
3. Yielding of reinforcement
4. Loss of integrity

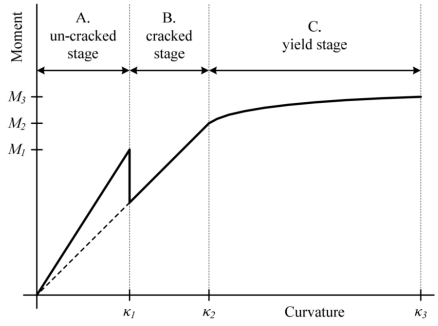

Figure 2.15: 3 stages of reinforced glass failure

For reinforced glass it is interesting to look at these failure patterns and mechanisms as differences are seen relative to the reinforcement material, adherence and used interlayer. Deviations and combinations of the previous mentioned aspect could for different failure modes resulting in different ultimate failure resistances.

Rupture of heat strengthened laminated glass

There is a some risk in the application of polyvinyl butyral (PVB) laminated HSG, Bos [2009] describes a fracture behaviour where the crack initiation and elastic energy release causes a large crack due to the largely stored energy due internal pre-stressing. As the crack pieces are rather large, with respect to FTG, the crack length is shorter resulting in higher crack widths and rupture of the interlayer due to the lack of plasticity. This behaviour is something which obviously is not wanted and therefore further research on this subject in needed. The influence of this phenomenon on RG systems is not know as Bos only looked at laminated glass. However he does mention the possible effect on reinforcement materials which have a low ultimate failure strain. As it is possible to have rupture of the reinforcement when large elastic energy is released, this is an important aspect to keep in mind when designing such a structure.

2.4. Reinforcement materials

From the section regarding previous applications some popular materials come forth as reinforcement, such as GFRP, CFRP and stainless steel (Martens et al. [2016c]). The use of FRP's looks very promising since they are relative strong and therefore can be applied very subtle. Looking further then GFRP or CFRP fibres such as aramid and dyneema are even stronger. The disadvantages of aramid fibres is that they are very sensitive to corrosion and are degraded by UV light and dyneema fibre are hard in application due to their difficulty in creating chemical bounds to a resin.
For this thesis it is chosen to continue with GFRP reinforcement based on previous recommendations from Leung [2010]; Louter [2011]; Rademakers [2009] and with respect to their transparent potential Leung [2010]; Louter [2011]; Seo et al. [2017]. In the subsequent sections both GFRP and stainless steel are highlighted. This is due to the application of stainless steel reinforcement in the reference model.

2.4.1. GF(RP)

Fibreglass is made from extruding thin strands consisting out of a molten mixture based on silica. The strand are either woven in a fabric or stored on coils. In order to make a rigid structure a matrix is applied. In this manner the fibres can work together by redistributing the stresses creating a whole. Different kinds of matrix exist each for specific applications. In this thesis the composites consist of isophthalic polyester and an epoxy resin for the Fibrolux and DPP strips respectively. For the manufacturing different resins also different finishes used an the raw fibreglass texture. As in this thesis the fibreglass is embedded in the SG it is evident to that this should be chosen rightfully for the creation of chemical bounds between the fibreglass and SG. In the patent as guide several silanes are advised to used as primer ar adherence improver between the glass and SG (Niall et al. [2010]). As the fibreglass has an amino-silane finish this should be compatible. When the SG interlayer properties are discussed more about this chemical connection is explained.
The glass fibres and GFRP composites are applied in three different situation throughout this thesis, Fibrolux GFRP strip with a isophthalic polyester resin, GFRP strips with semi-transparent epoxy resin and fibreglass

Table 2.1: Specific properties of fibreglass (composites) used in this thesis

Parameter		Unit	Fibrolux GFRP strips	UD GFRP strips	E-Glass 1200
Yield strength	$f_{t,y}$	MPa	900	2070	2756
Young's Modulus	E	GPa	40	47.58	72.3
Ultimate strain	ε_u	%	2.0	4.3	4.8
Source			Fibrolux	Leung [2010]	AGY [2006]

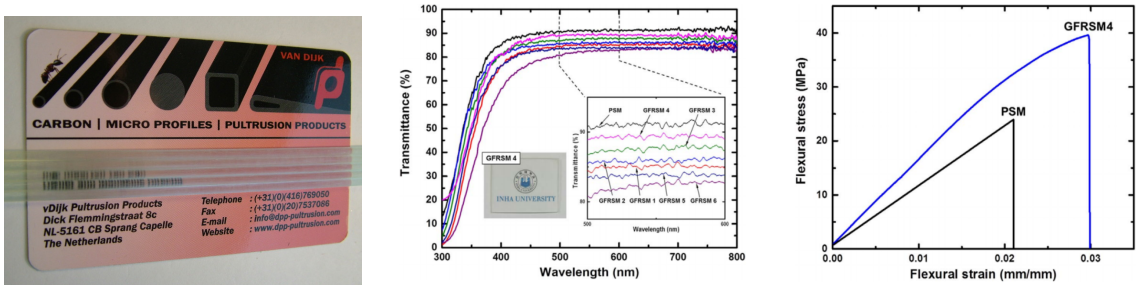

(a) Transparent GFRP strips produced by DPP

(b) Transmittance different matrix combinations

(c) Flexural stress-strain behaviour

Figure 2.16: Different transparent GFRP performances by DPP and Seo et al. [2017]

without pre-fabricated matrix. Their specific properties are listed in Table 2.1 . Fibreglass itself has a relative low Young's mudolus in comparison to steel or CFRP. When the fibres are part of a composite, the effective Young's modulus of the whole is reduced even further. In most cased this means that the Young's modulus of glass. This has an effect of the crack propagation.

Transparency potential

The best reinforcement is the reinforcement no one knows is there, therefore transparent GFRP is a very interesting and feasible concept. A glass fibre composite can be made transparent by using a specific resin. In the thesis of Leung semi-transparent GFRP strips are used, manufactured by DPP. At the moment DPP has achieved an even higher transparent GFRP (Figure 2.16a)
In order to obtain a transparent composite the R.I. (n) of both fibreglass and resin are required to be equal or at least as close as possible. This is seen in the work of Seo et al. [2017] where tunable silazane matrix is developed. The R.I. of this matrix is controlled within the range of 1.51-1.56. and resulted in a GFRP with a transmittance around 80-90% at the range of the visible light spectrum and relative normal physical properties with respect to current interlayer products, as displayed in Figures 2.16b and 2.16c
Looking at the FFR described in the outline of this thesis the goal is to create glass interlayer which can act as a transparent resin if applied in the right circumstances. Looking at SG this has an high potential since it is manufactured as an interlayer. However the R.I. of SG given by the manufacturer is $1{,}5$ which makes no sense due to the fact that significance of this value goes to $10^{-}3$. The department of Mechanical and Aerospace engineering in Missouri S&T also developed a transparent composite. They concluded that clouding could occur when $\Delta n > 0.01$ Menta et al. [2014]. Since the Δn in this case is undefined and probably has a too large difference, transparent GFRP is not achieved. This whole process is partially dependent of the temperature of curing, the amount and type of the glass fibre used and other parameters. This is a specific topic and lies not in the scope of this thesis.

2.4.2. Stainless steel

As is defined in the outline of this thesis, the stainless stain experiment performed by Louter et al. [2012a] will be used as to validate the SLA model. Therefore also these material properties are defined. The stainless steel which is used is cold bended the AISI 304 with the EN number 1.4301. This is an austenitic stainless steel which is characterised by the lower chromium and higher nickel equivalent composition. For its exact composition is referred to the NEN-EN [2017a]. In Table 2.2 the properties of this material are summarized based of Louter [2011]; NEN-EN [2017a,b].

Table 2.2: Material properties of stainless steel

Parameter		Unit	Value
0.2% Yield strength	$f_{y,0.2\%}$	MPa	230
Ultimate strength	f_u	MPa	550
Young's Modulus	E	GPa	200
Elastic strain	ε_e	%	0.115
Ultimate strain	ε_u	%	27.5
Rupture strain	ε_r	%	45

2.5. Laminate

In order to achieve a glass laminate the separate glass panes need to be adhered to each other, popular solutions are PVB, SG and ethylene-vinyl acetate (EVA). In the literature a lot of experiments contain SG as interlayer. For laminating glass the focus will only be on PVB and SG as they are the most common used in previous applications of reinforced glass.

2.5.1. SentryGlas

Sentryglas is becoming quite popular due to its relative high stiffness and strength which is used to maintain the shape of the glass after failure. The thick dimensions (0.9-1.52 with respect to 0.1 of PVB) of SG are used in Leung [2010] to integrate GFRP strips. The same principle will also be used for the FFR and therefore the some chemical properties should be know in order to check the chemical bounding of the two materials. Since it is a patented product very less information is given about the exact chemical composition. The invention is explained in the patent (Niall et al. [2010]) as a ethylene acid copolymer resin including 12 till 30 weight percent of an α,β-unsaturated carboxylic acid, or functional equivalent, having 3 till 8 carbon atoms. The carboxylic groups are partially neutralised with zinc-containing neutralizing agents. This zinc incorporation affects the adhesion, edge seal, de-lamination or visual defects. To improve adhesion optional silane agents/coatings can be used due to the unsaturated carboxyl groups (basic structure illustrated in Figure 2.17a), these groups chemically bound with the hydroxyl groups from coupling agents at elevated temperatures (Shin-Etsu Chemical Ltd. [2015]), e.g. silane coupling agents or coatings. This is particularity interesting in this thesis with respect to the adherence of the fibreglass textures which are available in (amino-)silane coatings. In the work of Louter [2011] it is mentioned that the addition of SG as a reinforcement material, the strength resistant in increased in relation to the same beam with an acrylic interlayer. This effect is explained by the higher strength and stiffness of this interlayer with respect to PVB.

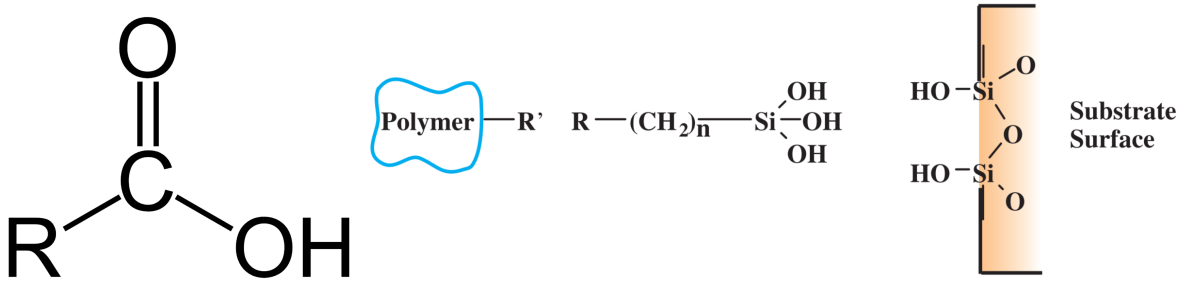

(a) Basic carboxylic structure, reactive groep of SG

(b) Schematic reaction of polymer, silane agent and substrate surface, Shin-Etsu Chemical Ltd. [2015]

Figure 2.17: Schematic of chemical bond of the three components

2.5.2. PVB

Currently PVB is a widely used interlayer in laminated glass structures. It is produced by reacting polyvinyl alcohol with butyraldehyde and is known by many names from different manufacturers, e.g. Saflex, Butacite, Trosifol, WINLITE and others. PVB is a visco-elastic material meaning it behaves differently with different load speeds(Zhang et al. [2015]). The tensile strength and stiffness are quite low and creep sensitive with

Table 2.3: Fracture energy and tensile strength with respect to concrete

Material	G_f^I	f_t	Ratio G_f/f_t
Glass	3.0J/m^2	45MPa	0.06
Concrete	4.15J/m^2	5	0.83
Ratio glass/concrete	0.72	5	

respect to SG (Kuraray [2014b]).

2.6. Numerical calculation

Full scale experiments are interesting to gain insights about the performance and failure modes. But this is very expensive to perform for every project, therefore most structures are not tested in advance, but calculated to determine their load carrying capacity, deflection and other relevant performances to design the right structure. With the eye towards this process it is a necessity for the engineer to be able to calculate the kind structure regarding this research to gain reliable results in this calculation.
Since reinforced glass is a rather new subject, the objective is to simulate the structure's response as accurate as possible using numerical FE calculations. Together with experimental data the numerical model is validated and if this is successful the analysing method can be used without the validation with experiments. To contributed to this process, numerical validation is part of the thesis and therefore previous research in this area is elaborated in this below.

2.6.1. Modelling brittle materials

Differences exist in finite element analysis (FEA) depending on the achievable goal. In the scope of this thesis it is favourable to create a FE model which has a good estimate of both elastic as material non-linear failure moments regarding its load bearing resistance. Since the ultimate failure of the specimen is determined by the post-cracking performance of the material, it is important to have a good understanding of this behaviour, hence the previous material and failure analysis of Sections 2.3 and 2.3.3. Here, is clarified that glass has a brittle failure behaviour and for what it seems almost dynamic crack formation.
Ordinary brittle materials, like concrete, can be calculated with several FE-software by use of a non-linear calculation including a non-linear material module. Some basic material models are brittle and linear softening[2] which are illustrated in Figure 2.19. Since the scope is focussed on tensile failure behaviour as concluded from Section 2.3.3, Mode-I fracture is the most interesting. This fracture mode is one of the three known failure modes which are illustrated in Figure 2.18. The fracture energy is defined as the energy necessary to open a unit area of crack surface and is the integral of the constitutive material curve (Bos [2009]). Since the density of cracks in laminated glass is very high, smeared cracking is used for numerical calculations, meaning that the fracture energy is divided by the crack bandwidth (h), as is illustrated Figure 2.19.
Differences between the brittle and linear elastic material models is the strength after fracture. Where concrete is considerate to have softening after fracture. Glass behaves more brittle, leaving no residual strength after failure, hence no softening is applicable. If the principle of fracture energy is applied in this situation, the integral of stress-strain curve, a snap-back will occur. Meaning, most of the elastic strain energy is released, this is also what Bos has found, only 3.4% of the elastic energy is needed to create a crack and most energy is transformed in kinetic energy (Bos [2009]). To put things in perspective the energy needed to create a crack in relation with the ultimate tensile stress is relative very low with respect to concrete. For example comparing the tensile strength over fracture energy ratio of glass and concrete[3] in Table 2.3. It is clearly seen that the fracture energy with respect to tensile strength is relative low.

2.6.2. Previous research in numerical modelling of reinforced glass

In the published papers some trouble is seen while calculating these structures with the snap-back behaviour of glass, Valarinho et al. [2012b], for instance analyses the influence of fracture energy by taking n times the

[2] More extended modules for post cracking of concrete exist, but since they are not in this scope only the basics are considered here
[3] A typical value for the fracture energy of normal concrete of $4.15J/m^2$ is taken from the validation beam in the work of Invernizzi et al. [2011]

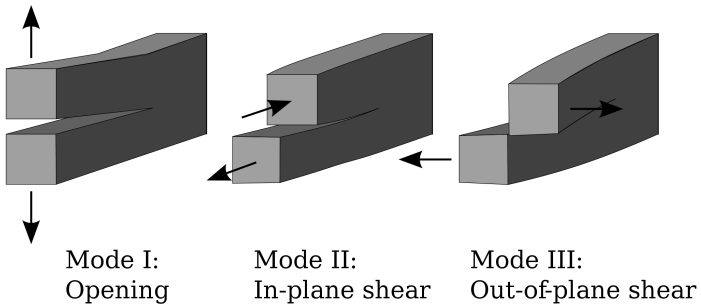

Figure 2.18: Three basic fracture modus

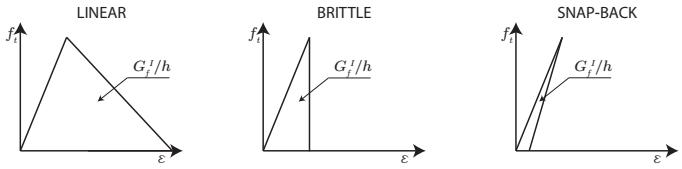

Figure 2.19: Three material models which can be used to interpret brittle behaviour; Linear softening, Brittle and Snap-back

$G_{f,min}$, where $G_{f,min}$ is the minimum fracture energy needed to avoid snap-back. This resulted in a fracture energy of approximate 100 times higher in relation to the values found in literature. This large deviation in the assumption of fracture energy does not seem to interfere with the results since in the conclusion is stated that crack initiation, stiffness degradation, load carrying capacity and crack pattern are predicted with high accuracy. Even though the dependence of crack pattern to experiments, the parameter dependency of crack initiation and load resistance to fracture energy is debatable.

A new kind of analysis is provided by the work of Rots (Graaf et al. [2008]; Rots and Invernizzi [2004]), this is called a sequential linear analysis (SLA) which means that a sequence of linear analyses is performed. At each analysis the critical event is found and damaged according to the predefined damage path. This analysing method is initially meant for concrete but is applied at a reinforced glass beam by Graaf et al. [2008] and later on by Louter et al. [2010b]. Who modelled the UV-curing acrylate adhered beam found in Louter et al. [2008] and was able to create a good estimation and performed a parameters study on this model using SLA. A lot of conclusions were drawn among which, the increase in accuracy by using 10 reduction branches in the reinforcement instead of 5 and about the careful implementation of plasticity. Although the good results were seen in this work, the additional resistance capacity due to the SG interlayer was challenging to be implemented in the 2D analysis.

2.6.3. Mesh dimensions and dependency

Mesh sizes do not differ very much in the papers and are mostly found around 10% of the specimen height. Mostly uniform meshes as in the work of Neto et al. [2015] are found. But with respect to computation time and accuracy in crack patterns this is a subject which needs more attention. For example, the work of Bedon and Louter [2014] stands out herein with a linear scaled mesh density over the height of the beam as pictured in Figure 2.21 using ABAQUS. Due to the small and random mesh and the killing element principle the crack patterns will develop in a more natural way, this should be a goal in further numerical calculations.

For the DIANA SLA modulus a Delaunay mesh algorithm is available. This is used in the work of Leung [2010] in combination with GFRP reinforcement, with the mesh dimensions 12.5, 6.25 and 3.125 for a coarse, fine and very fine mesh. With a constant crack bandwidth varying between 0.001 and 0.01 the obtained crack patterns using a Delaunay triangulation pattern are a lot less straight than seen in a uniform quadrilateral mesh as is seen in Figure 2.22. Although, using the Delaunay algorithm does create large mesh size differences where the cracks are being bend around.

Crack bandwidth in DIANA SLA is determined by the equation $h = \sqrt{A}$. Since smeared cracking is applied the area of the curve is G_f/h the fracture energy multiplied by the crack bandwidth remains equal and thus is mesh independent Rots and Invernizzi [2004].

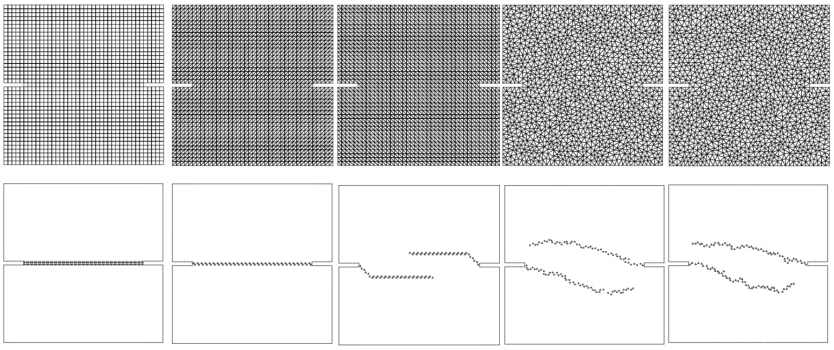

(a) Square mesh (b) Triangular mesh (c) Mirror of b (d) Delaunay triagnulated mesh (e) Mirror of d

Figure 2.20: Nooru-Mohammed test, meshed and corresponding crack patterns, according to DeJong et al. [2009]

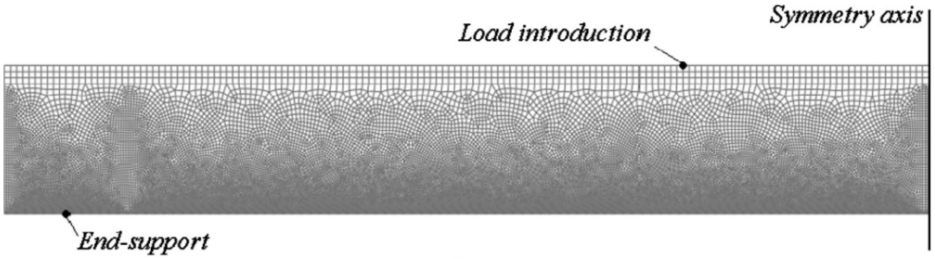

Figure 2.21: Linear scaled mesh density and uniform mesh in compression zone by Bedon and Louter [2014]

In the work of DeJong et al. [2009] the relation between mesh and crack pattern is researched. In Figure 2.20 square, triangular and Delaunay meshes are compared. Here is seen that the influence in pattern is significant and a Delaunay mesh results in the most dynamic crack developing solutions as its directions are the least fixed.

2.6.4. A brief introduction to SLA

As the name states, the analysis method SLA uses a sequence of linear analyses to calculate non-linear effects. This method is developed to model brittle materials, especially concrete and masonry, but this approach can also be used for glass structures. The general concept is to apply a proportional load find the critical element by and reduce it strength by predefined properties. This sequence is summarized up below by Rots et al. [2008]:

- Add the external load as a unit load;
- Perform a linear-elastic analysis;
- Extract the 'critical element' from the analysis. The 'critical element' is the element for which the stress level divided by its current strength is the highest in the whole structure;
- Calculate the ratio between the strength and the stress level in the critical element: this ratio provides the 'global load factor'. The present solution step is obtained be rescaling the 'unit load elastic solution' times the 'global load factor';

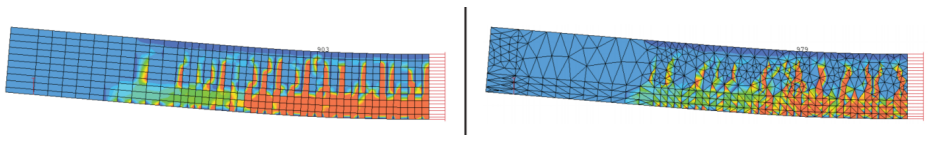

Figure 2.22: Damage indication / crack pattern for uniform quadrilateral and Delaunay triangulation meshes (Leung [2010])

- Increase the damage in the critical element by reducing its stiffness and strength, i.e. Young's modulus E and tensile strength f_t, according to a saw-tooth constitutive law. This corresponds to a local damage 'event';
- Repeat previous steps for the new configuration, i.e. re-run a linear analysis for the structure in which E en f_t of the previous critical elements have been reduced. Trace the next critical saw tooth in some element, repeat this process till the damage has spread into the structure to the desired level.

Current version

Currently the SLA scheme is implemented in DIANA 9.2. In the current version SLA is limited to two dimensional plane stress and interface[4] elements. The integration of truss elements was available in previous versions but is somehow lost in the development and initial conditions can not be applied. Furthermore, the analysis is based on fixed cracking, meaning that the crack direction is set transverse to the maximum principle stress at the initial crack. A large disadvantage of fixed cracking is when the crack direction differs largely from the initial direction, large stresses can occur due to the fixed direction. No large differences in the global crack direction are expected and therefore this should not be a issue.
The initial stiffness matrix used for undamaged integration points is the isotropic relation as seen in equation 2.1. Upon crack initiation the matrix will obtain orthogonal properties due to reduction of stiffness in one direction and is switch to the orthotropic formulation from equation 2.2. Here the n and t are the normal and tangential direction to the crack face respectively, due to symmetry it should hold that $\nu_{nt}E_n = \nu_{tn}E_t$. Where E_n in the reduced Young's modulus according to its definition and ν_{tn} the reduced Poisson ratio according to $\nu_{tn} = \nu_0(E_n/E_0)$. A secondary crack is possible to arise, but only perpendicular to the primary crack since the direction is determined.

$$\begin{Bmatrix} \sigma_{xx} \\ \sigma_{yy} \\ \sigma_{xy} \end{Bmatrix} = \frac{E_0}{1-\nu_0^2} \begin{bmatrix} 1 & \nu & 0 \\ \nu & 1 & 0 \\ 0 & 0 & \frac{1-\nu_0}{2} \end{bmatrix} \begin{Bmatrix} \varepsilon_{xx} \\ \varepsilon_{yy} \\ \gamma_{xy} \end{Bmatrix} \tag{2.1}$$

$$\begin{Bmatrix} \sigma_{nn} \\ \sigma_{tt} \\ \sigma_{nt} \end{Bmatrix} = \begin{bmatrix} \frac{E_n}{1-\nu_{nt}\nu_{tn}} & \frac{\nu_{nt}E_n}{1-\nu_{nt}\nu_{tn}} & 0 \\ \frac{\nu_{tn}E_n}{1-\nu_{nt}\nu_{tn}} & \frac{E_n}{1-\nu_{nt}\nu_{tn}} & 0 \\ 0 & 0 & G_{red} \end{bmatrix} \begin{Bmatrix} \varepsilon_{nn} \\ \varepsilon_{tt} \\ \gamma_{nt} \end{Bmatrix} \tag{2.2}$$

Shear retention

Shear retention always is a parameter which is debated a lot. It defines the amount of shear resistance after failure of the element. For NLA this is mostly defined as seen in equation 2.3 (DeJong et al. [2009]), where β is a constant value. In DIANA this value is default set to $\beta = 0.01$[5]. An alternative is to define the shear behaviour as a function of the normal crack strain, based on the reduced/minimum Young's modulus ($E_{min} = min(E_n, E_t)$), this reduced method is implemented in the current version of SLA (DeJong et al. [2009]; van de Graaf [2009]).

$$\sigma_{nt} = \beta G_0 \gamma_{nt} = \beta \frac{E_0}{2(1+\nu_0)} \gamma_{ns} \tag{2.3}$$

$$G_{red} = \alpha \frac{E_{min}}{2(1+\nu_0 \frac{E_{min}}{E_0})} \tag{2.4}$$

[4] The interface elements are only able to be used in SLA as opening in n-direction and can therefore not be applied to simulate de-bounding in this thesis.

[5] This value is research by a few, among which Louter, he states that this value only has no significant effect on the force-displacement curves, but largely influences the cracking pattern and the default value of $\beta = 0.01$ is in good agreement with experiments (Louter et al. [2010b]).

2.6.5. SLA material models

Some considerations are necessary for the definition of the material models in SLA. The deviations which are applicable for the definition of the material model are discussed below based on findings in previous research.

Fracture energy of glass

Some discussion exists about the mode-I fracture energy which is applicable in the tensile failure behaviour. Different value's for this fracture energy are used in research, e.g. $2.0\mathrm{J/m^2}$ (Martens et al. [2016a]), $8.0\mathrm{J/m^2}$ (Bernard [2013]) and $3.0\mathrm{J}/m^2$ (Bedon and Louter [2014]; Neto et al. [2015]). And in most NLA a brittle cut-off model is used for convergence purposes by avoiding snap-back (Valarinho et al. [2012b]).
Most widely used value for the fracture energy is $0.003\mathrm{N/mm}$ or $3.0\mathrm{J/m2}$ (Bedon and Louter [2014]; Haldimann et al. [2008]; Neto et al. [2015]. In the work of Bedon and Louter [2014] the fracture energy is investigated a little more where also the the values of 8.0 and 5.5 (in between) are used. The value of 8.0 is based on the work of Bernard [2013]; Haldimann et al. [2008], where this value is explained from equation 2.5 found in the fracture mechanics. Here, a practical value for K_I, c is defined for the use of glass fracture energy, namely $0,75\mathrm{MPa}\sqrt{\mathrm{m}}$. Bedon concluded that the alterations did not influence the global resistance of the beams, but did had an impact on the crack pattern. Higher fracture energy resulted in a decrease of cracks, in the numerical calculation chapter this will be verified. Through the extend of this thesis the value $G_f = 3.0\mathrm{J}/m^2$ is applied is not specified otherwise.

$$G_f^I = \frac{K_{I,c}^2}{E} = \frac{0.75^2}{70000} = 8.03 \cdot 10^{-3}\mathrm{N/mm} = 8.0\mathrm{J/m^2} \tag{2.5}$$

As is mentioned above the integral of the stress-strain curve should be equal to the fracture energy over crack bandwidth (G_f/h). This is used to determine the ultimate strain after snap-back (ε_u) based on geometry this yield in equation 2.6 also found in several paper among which Invernizzi et al. [2011].

$$\varepsilon_u = \frac{2G_f}{f_t h} \tag{2.6}$$

Constitutive laws

The quantification of the constitutive law of glass in SLA will not simply follow the mother curve. If the mother curve was simply divided by a few points the area would form the saw-tooth according to Figure 2.23b. This would result in a false interpretation of the fracture energy since the additional area's result in a higher fracture energy than the original curve. Therefore the saw-tooth is adjusted, creating both positive and negative area's in Figure 2.23a. The height of these areas are adjusted with the parameter p which is defined as a percentage of the tensile strength (Invernizzi et al. [2011]; Rots and Invernizzi [2004]; Rots et al. [2007]).
The saw-tooth is assembled according the Invernizzi et al. [2011], two parallel lines are assumed in the vicinity of the mother curve, one upper and one lower representing the '+' and '-' lines. In principle the higher and lower tensile strengths are calculated at each reduction step j, with a drop of $2pf_t$ each. The starting point is elastic failure (f_t and ε_e), from here a drop of pf_t is made to the first tooth ($f_{t,1}^-$) this point creates the first reduced stiffness E_j, starting the iteration process elaborated in equations 2.9 based on the so called softening modulus D and the ε_u^+ according to Invernizzi et al. [2011] shown in equation 2.7. The parameter p which adjusts the upper and lower lines as a ratio of f_t, thus adjust the accuracy of the curve and is directly related to the number of branches.

Defining parameters for the snap-back curve.

$$D = \frac{f_t}{\varepsilon_e - \varepsilon_u} \tag{2.7}$$

$$\varepsilon_u^+ = \varepsilon_u - p(\varepsilon_e - \varepsilon_u) \tag{2.8}$$

Define saw-tooth at reduction step j.

$$E_{j+1} = \frac{f^-_{t,j}}{\varepsilon_j} \tag{2.9a}$$

$$f^+_{t,j+1} = \frac{E_j D\varepsilon^+_u}{D - E_j} \tag{2.9b}$$

$$f^-_{t,j+1} = f^+_{t,j+1} - 2pf_t \tag{2.9c}$$

$$\varepsilon_j = \frac{D\varepsilon^+_u}{D - E} \tag{2.9d}$$

Where:
D = Damage modulus
ε_e = Elastic fracture strain based on initial Young's modulus
ε_j = Strain at reduction step j
ε_u = Ultimate strain after snap-back
ε^+_u = Ultimate strain at the '+' curve curve
p = Percentage parameter of f_t; which defines the distance of the upper and lower to the mother curve
E_j = Young's modulus at reduction step j
f_t = Elastic tensile stress limit
$f^-_{t,j+1}$ = Lower tensile stress limit of saw-tooth at reduction step j
$f^+_{t,j+1}$ = Upper tensile stress limit of saw-tooth at reduction step j

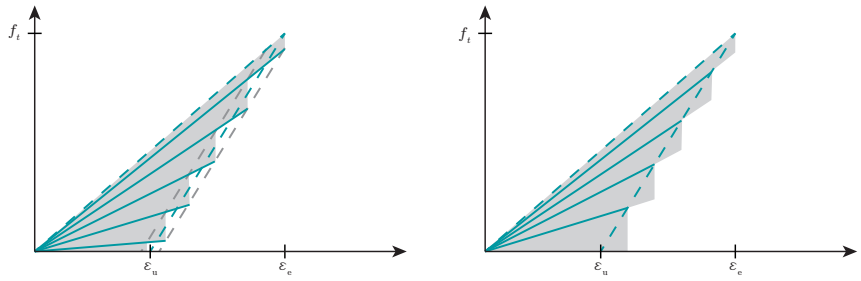

(a) Saw-tooth approach (b) Uniform distribution of mother-curve

Figure 2.23: Reduction curve implementations for snap-back material

Plasticity

The implementation of plastic materials is necessary when looking at materials as steel and SG. Therefore this is brought under attention. It is per definition incorrect to calculate a plastic material with the use of SLA, but otherwise no failure of the reinforcement can be achieved so therefore a reduction method is applied in Louter et al. [2010b] and Invernizzi et al. [2011]. As the analysis method only knows reduction models contain linear elastic materials, plasticity can only be simulated in this manner.
The quantification of this plastic curve has two options, either create a saw-tooth (Invernizzi et al. [2011]; Rots et al. [2008]) or to define a few points of the constitutive relation curve Louter et al. [2010b]. It is debatable which to apply since both approaches are virtually incorrect, aside from the linear implementation of plasticity. The saw-tooth approach has rigid connection between the tensile strength increases and the number of teeth required. Also is the number of teeth bound to the ultimate elongation by this step size. This results in either large tensile strength deviations or a high amount of reduction steps (Figure 2.24a). Looking at the approach from Louter where the curve is followed. This means that the necessary energy until ultimate strain is reduced by the character of this analysis as pictured in Figure 2.24b. Although this deficiency Louter et al. [2010b] was able to get rather satisfying results[6].

[6]It should be noted that the tensile strength in Invernizzi et al. [2011] are based on theoretical values from NEN-EN [2017b] and experimental values from Louter et al. [2010a] in Louter et al. [2010b]

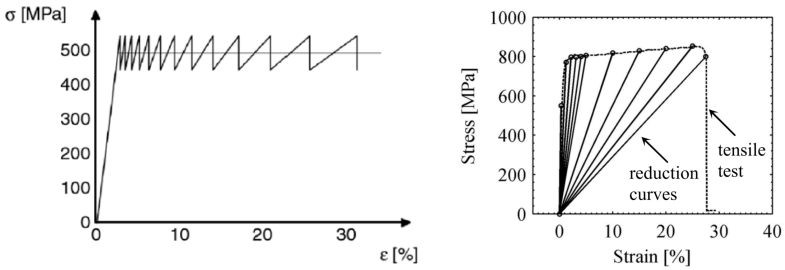

(a) Saw-tooth approach by Invernizzi et al. [2011]

(b) Uniform distribution of mothercurve by Louter et al. [2010b]

Figure 2.24: Reduction curve implementations for snap-back material

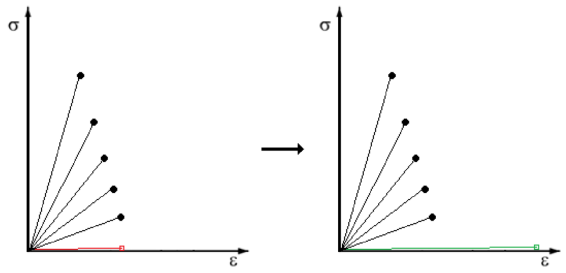

Figure 2.25: Principle of the application of the dummy branch by Kraus [2014]

Number of branches

The amount of branches, highly influences the accuracy of the mother curve approximation. When the number is very low the saw-tooth will automatically be more coarse resulting in large deviations to the mother curve. As the opposite is true for the increase of reduction steps, this consequently increases the necessary iterations, hence longer calculation time. In the work of Louter et al. [2010b] the number of steps is researched, with a difference of 10 and 5, where is concluded that the amount of branches in the steel reinforcement highly influences the force-displacement curve. On the other hand no significant influences are found with respect to the alterations in the glass material model does not highly influences the force-displacement diagram.

Dummy branch

In the work of Kraus [2014] the dummy branch is introduced, this can be compared to the killing element method which is know in ABAQUS. This branch is defined as the last branch of the reduction curve and has virtually no strength. Its function is to strain with negligible resistance in order to create the critical event elsewhere. The additional dummy branch is designed to have a negligible stiffness and strength hence does not have a significant effect of the fracture energy. This principle is pictured by Kraus [2014] in Figure 2.25. In this thesis this behaviour is also referred to as the final branch behaviour.

3

Design philosophy

The underlying goal and initiative for this thesis is to design safe glass structures. So before designs are made, a glance taken at the safety of glass structures in general and the design philosophy. To design safe structures is a rather vague statement at start, when safety has to be described, it is mostly described as the level of risk one is subjected to. Often risk is defined as the product of probability and consequences in a event. While in glass engineering it is assumed that if a possible event exist for the glass to break, it consequently will at some point. Several models are made including one which is now adopted in the Eurocode (NEN-EN 1990 [2016]).

3.1. Difference in glass structures

In order to understand the concept of reinforcing glass beams it is necessary to know where the safety improvement lies and what the differences are in the application of both types of glass structures. In the stated definition of safety a structure with higher chance to failure and low consequences (Structure 1) has an equal safety to one with low chance of failure and higher consequences (Structure 2). Since the product of value of the two is still roughly the same. This is actually the case when looking at glass engineering.

When ordinary glass structures are analysed, a very low probability of failure is present. This design philosophy started in 1990's where extra layers were added to prevent brittle/immediate failure of the structural component (Khorasani [2004]). For example, a beam would have 6 layers, where actually only 3 are needed. Six glass panes are applied due to the existing possibility for the outer layers to get damaged and lose integrity. The other extra one is present to still have enough panes when one glass pane has lower maximum tensile stress, due to accidental/unforeseen flaws. This structure relates to the low-chance, high-consequence example, as the extra panes lower the chance of failure. This is done for the reason to prevent failure as much as possible, because when this beam fails, it will fall down and will have high consequences. On the other hand the concept of hybrid glass structures is proven (Louter [2011]) it ability to maintain integrity in the post-cracked stage, i.e. the beam is able to have sufficient load bearing capacity after cracking has occurred in the glass panes. In Figure 3.2, the experimental data from the work of Louter [2011] is presented[1]. This application provides that the consequences of glass failure are brought back to a minimum due to the additional LTM. This multi LTM is elaborated by Bos [2009] who introduced the element safety diagram (ESD) model. This will be elaborated in Section 3.4.

3.2. Ultimate strength

Now the sense of applying reinforcement is known, a step in the direction of the design in taken. In the thesis of Leung [2010], he strived for a residual load-bearing capacity of 150%. Motivated by load increases due to for example water accumulation. This is not necessary wrong, but the likelihood of the appearance

[1] A four-point bending test is done with l=1500 mm on the cross-sections displayed in Figure 3.1a and 3.1b.

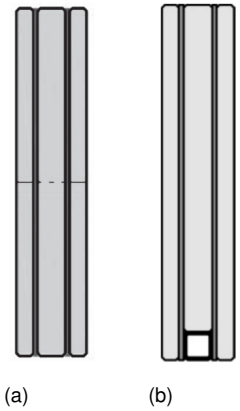

Figure 3.1: Cross-sections of specimen from Louter [2011], (a) with only SG laminate and (b) with SG laminate and stainless steel hollow section

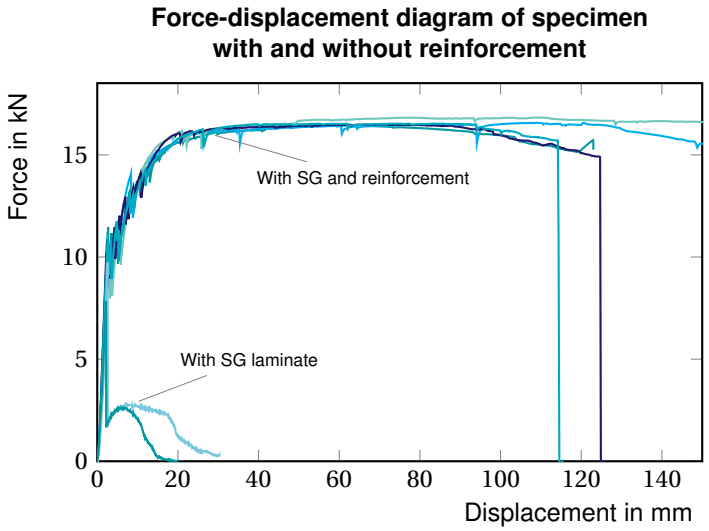

Figure 3.2: Force-displacement diagram of specimen according to glass section 3.1a and 3.1b, without and with reinforcement from Louter [2011]

of an even higher load than the ultimate design load is negligible, since the design load is a load which is defined in the Eurocode as safe[2]. Water-accumulation should thus be accounted for as this is a case which could occur after initial failure.

Let us now take a step back to the origin of reinforced glass, it is a enhancement of the ordinary over dimensioned glass structure. The ordinary glass structures are over-dimensioned because of the assumption that the glass panes will fail. Therefore, glass structure should not be designed with respect to overloading but by physical damage due external action. Hence, the ultimate load should not be compared to initial strength resistance, but in relation to the design load in ultimate limit state. Since this will be the load which could be present when the glass gets damaged. Although the ratio of ultimate and initial strength resistance is not how the ultimate strength should be defined in design, it is an easy way of defining its capacity.

In the previously discussed diagram of Figure 3.2, it is clearly seen that the addition of reinforcement determines the ultimate strength. Adding more reinforcement will only significantly increase the ultimate strength. This would also result in an increase in stiffness, but this is insignificant as is seen in the analytical analysis of Figure 3.3. Here, the initial and ultimate failure strength are calculated according to Appendix Section A.1, based on the dimensions of Louter et al. [2012a]. The reinforcement ratio is the ratio with respect to the full cross-section area, the ratio of the physical experiments is 1.1%.

3.3. Initial strength

Although the reinforcement system is meant to increase the redundancy of glass structures the initial strength is still very important, since this is the first criteria for the beams' dimensions. When more initial strength is needed it is easy to step to HSG or FTG. Since these glass types have internal pre-stress due hardening processes. Here, the question is answered whether this is favourable in reinforced glass design.

FTG is known from its high strength and its failure in very small pieces. This is the logic type one would think of when a glass structure needs to be made, due to the application in roofs or car industry. But when is looked beyond the high failure strength (with a mean of 98.0 MPa Veer et al. [2009]) and to the safety it becomes less convenient to apply. When such a pane fails at one point, all energy is released resulting in small pieces of glass. It is rather difficult to hold of these small pieces together while remaining integrity. Therefore, the reinforcement will be unable to create an internal moment. Therefore fully tempered glass is not suited for this application, since the goal is for the beam to remain its topology.

The glass type which has opposing properties is ANG, the characteristics of this type are its low tensile

[2] In the Eurocode safe is defined as a lower chance of failure of a structural component than a specified chance of failure for a specific reliability class. No further elaboration will be done on this concept, in glass engineering we will assume that if there is a possibility of failure, glass will fail.

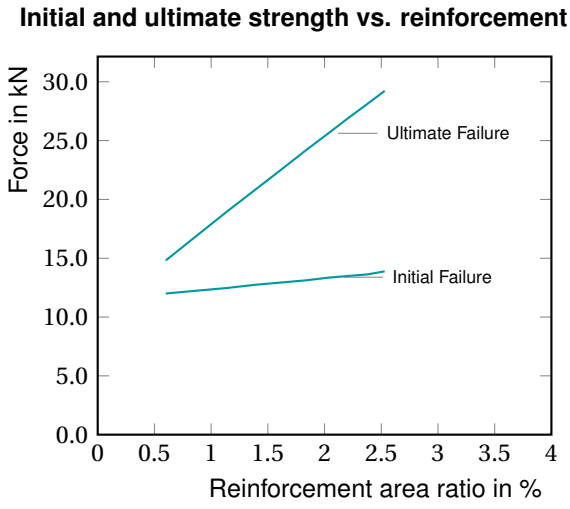

Figure 3.3: Failure forces against increase of thickness of squared hollow section

Figure 3.4: Minimum reinforcement

Figure 3.5: Maximum reinforcement

strength and large glass pieces after failure. Here, the lower tensile stress (mean=27.5 MPa, Veer et al. [2009]) is not always interesting since the structure should be a lot larger and contain more laminated panes, with respect to fully tempered glass. But it does break in large pieces of glass which have sufficient transfer capacity after breakage when laminated. This makes annealed glass a very good candidate for the application of reinforced glass beams and is therefore seen a lot in research papers (Bedon and Louter [2014]; Martens et al. [2016a]; Valarinho et al. [2012b]). It does have a large drawback, since glass is known for its property to erode when subjected to water/moisture (Perkoff et al. [2001]), the number of flaws will increase over time due this corrosion resulting in lower tensile strength. The subjection to this kind of erosion makes the application of annealed glass not very appealing.

The performance of heat strengthened glass lies in between that of ANG and FTG. HSG has a tensile strength and size of fracture pieces which lies in between that of ANG and FTG glass depending of the amount of internal residual stress in the glass pane. The research of Kreher [2004] shows the different behaviour of HSG in glass-timber hybrids. He distinguishes HSG panes based of residual stresses and states that a pane with residual stress below 50 MPa can be considerate to fail in a ductile manner and above 50 MPa will cause brittle failure. The benefit of using HSG would be that it is the ideal combination of all types with the right amount of internal pre-stress. Since this compressive stress around the edges reduces the corrosion of glass which is seen in the ANG.

The above described properties implies that the best applicable glass kind to increase initial strength and prevent glass erosion is to create a small pre-stress in the glass. This can either be done in the described HSG, but also externally by means of post-tension. While eroding experiments on this subject are not yet performed, in theory it works the same as internal pre-stress of glass. However, where the glass tensile stresses are larger than the pre-stress this problem will still occur in both applications.

3.4. Damage model

The relationship between impact and structural damage can be visualised in the ESD, presented by Bos [2009]. Here, the impact refers to the damage sensitivity of the structure and structural damage to the load bearing capacity. An example of this diagram is presented in Figure 3.6a. Here, a triple SG laminated beam is shown. The resistance is seen on the left axis, the damage factor (D_s) on the right and the bottom axis displays the impact. This could be anything, but here is chosen to define this in terms of energy (J), as he does throughout the remainder of the thesis. In the diagram is seen that the design load is $\frac{2}{3}$ of the design capacity and after failure of one pane the resisting strength is still equal to the design load. Using SG as an interlayer results in the small ultimate failure resistance which is seen at the right bottom.

When multiple LTM's are present in a system, more lines can be drawn, yet the highest will always represent

the maximum failure load. In this case two lines are drawn, each representing a LTM, one for the glass panes and one for the SG interlayer. The line with the highest value will be the overall resistance. In Figure 3.6c the same concept is illustrated for a beam with GFRP reinforcement and two SG laminated glass panes. In this case the first damage level is failure of the first pane. The second, failure of the second pane and as third, failure of the GFRP reinforcement.

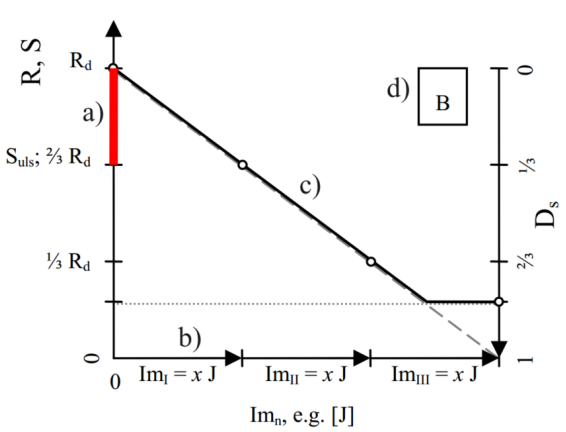

(a) Indicative example of ESD of a triple layer, SG annealed beam, Bos [2009]

(b) Corresponding cross-section

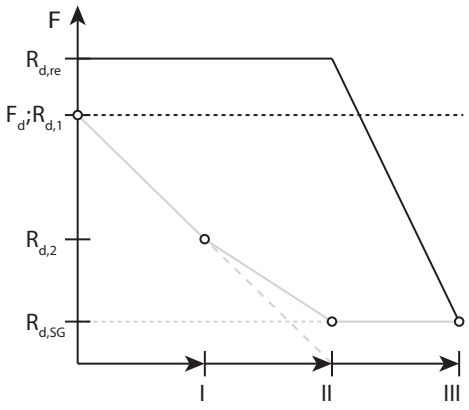

(c) Indicative ESD of double SG laminated glass beam with GFRP reinforcement strip

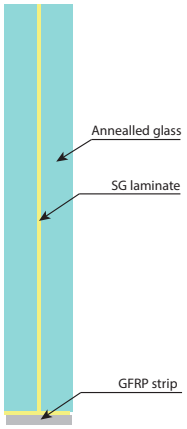

(d) Corresponding cross-section

Figure 3.6: Element safety diagram (ESD) without and with reinforcement

4

Concept

In Chapter 1, two concepts are defined, laminated glass beams with post-tensioned GFRP reinforcement and FFR. In this chapter, both concepts are elaborated with respect to their origin resulting from the expectations in performance of a glass beam in Section 4.1. Subsequently, both concepts are defined together with their purpose and their corresponding validation method.

4.1. Required performance of a glass beam

Regarding previous work discussed in the background of this thesis, the overall goal is mostly to enhance the performance of glass beams. This section summarises what is generally understood by performance. Followed by an overview of currently existing solutions in glass engineering, which have different effect on different properties and requirements. When looking at the performance of a structural element, a distinction can be made in primary and secondary requirements:
Primary requirements:

- Ability to carry design load;
- Limited deflection;
- Specified chance of failure;
- Prevent overall collapse.

Secondary requirements:

- Maintenance;
- Connectivity;
- Aesthetics;
- Construction speed;
- etc.

Now the focus will be at how to improve these requirements, without changing the main material. For increasing the first primary performance of a glass beam, i.e. increasing initial failure, this can be done by either additional stiffness, by means of creating composite glass structures or delay glass tensile failure by post-tensioning (both treated in background Section 2.2.1 and 2.2.3). As for the second and third aspect, which is to create safe failure and maintain integrity of the structural component after fracture[1], is done by any means of connecting the broken glass parts to the unbroken in order to transfer the tensile forces. Therefore only the composite and reinforcement solutions will suffice[2].

[1] Maintaining integrity of the structure is defined as the ability to have sufficient load bearing capacity to carry the design load after cracking of the glass has occurred as defined in the former philosophy chapter 3 (Bos [2009])

[2] This is according to the assumption that the pre-stressed elements are not adhered to the glass beam and is therefore not seen as an reinforcement

Figure 4.1: Flow chart from requirements to data acquisition

4.2. Concepts

Let us now switch to enhancing the performance of glass beams. The main requirement of glass beams next to the primary functions is to be a transparent structure, because this is the reason to apply a glass structure. Therefore a composite glass solution with relative large cross-section ratio of FRP's is considered unfavourable. The combination of reinforcing and post-tensioning a structure will result in the benefits of both.

The study of Leung [2010] shows a glass system where (semi) transparent glass GFRP strips are applied as internal reinforcement due to the possibilities created by the SG lamination procedure. Allowing for a greater transparency in the beams[3]. This can be taken one step further where the interlayer is used as resin for the fibreglass. This creates more dimensional flexibility and the previously stated benefit of transparency potential.

This analysis results in the conclusion that combining the reinforced and post-tensioned structures should theoretically increase both initial and ultimate failure. Incorporating this with fibre glass texture adjusted in a way to be transparent results a highly beneficial glass structure. As is already stated in chapter 1, only the two concepts of post-tensioned and FFR are treated in this thesis. Both of these concepts are elaborated in the subsections below. In the subsequent section the parameters are defined on which these concepts are verified in order to measure their advance.

4.2.1. Post-tensioned beam

The GFRP post-tension reinforced concept is researched separately from integrated reinforcement to keep variation to a minimum. Combining both reinforcement and post-tensioned systems is already performed in the work of Louter and Cupaç [2014] resulting in the expected increases of both initial and ultimate strength. Here, this is done by means of applying a post-tensioned reinforcement strip to the bottom of a glass section (Figure 4.2). This will be the starting point for the application of post-tensioning GFRP reinforcement to the glass section.

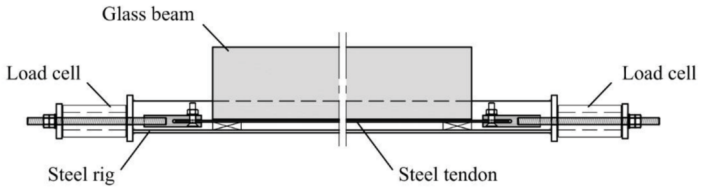

Figure 4.2: Applying method of post-tensioned reinforced steel strip with adherence (Louter and Cupaç [2014])

4.2.2. Flexible reinforcement

In the scope definition in sections 1.3, the FFR concept is briefly discussed. Interest in this concept comes from the benefits summed up below and based on the pull-out observations in the thesis of Leung [2010]. The bond failure mode between interlayer and GFRP strips is eliminated when the fibreglass is directly adhered to the interlayer. The SG interlayer will take over the function of the matrix, creating an even more coherent reinforced glass beam, which improves reliability and strength.

- Higher transparency potential;
- No dimension limitations;
- Less material interfaces[4]

[3] The concept of transparent GFRP is discussed in Section 2.4.1.

[4] The benefit of having less material interfaces is that this diminishes the failure modes.

Naturally, the resin can not be taken away due to its function to transfer the stress to the fibres. Therefore it is necessary to research if this function can be substituted by the SG. As is stated in the SG specification in Section 2.5.1 of the background, a chemical bond is be made between SG's carboxyl groups and the (amino-)silane coupling agent or coating due to the hydroxyl groups. Since the fibre-glass texture has a silane coating this results in a chemical bond and thus is SG a good substitution for the resin.

4.3. Validation

In this section the goals are defined in order to properly validate the concepts. Subsequently the parameters are defined which are needed to acquire the correct data in order to verify the stated goals. These parameters subsequently result in the executed experiments.

4.3.1. Validation of post-tension

The goal of the post-tensioned reinforced glass beam concept is to increase initial failure, while maintaining integrity after failure. These criteria are quantified to at least 15% increase in initial failure capacity (Goal 1). This 15% is based on literature and should be a feasible requirement. Goal 2 applies the design requirement from Chapter 3.

1. 15% increase in initial resistance capacity with respect to initial resistance without pre-tension, $F_{R,P,i} \geq 1.15 F_{R,i}$.
2. At least equal ultimate capacity resistance with respect to design load[5], $F_{R,u,d} \geq F_{E,u,d}$.

The first criterion, increasing initial strength, should be easily achievable is since the definition of post-tensioning is delaying tensile failure using compressive stress on the structure. Therefore automatically increasing initial fracture strength. The latter however is harder to accomplish, since the increase of post-tension force results not only in extra tension reserve in the tensile zone, but also in higher compressive stress in the compression zone. Which consequently leads to higher chances of instability failure modes.

4.3.2. Validation of FFR

The purpose of FFR at first is to create more design freedom and secondly to have equal or higher performance then GFRP strips. The first again is not really quantifiable since just like the post-tensioning, the application of the principle already achieves the goal, one is able to cut the desired size and make a reinforced glass beam therefore has more design freedom. The second part does need validation, this is done by performing four point bending experiments for both fibreglass and the already accepted GFRP strip reinforcement. The specimen are designed to have equal ultimate resistance capacity, therefore the second LTM should have equal or greater capacity, hence Goal 5. As bending experiments could create indecisive results due to the complex behaviour or any unforeseen situations, additional pull-out tests are performed to create equal situations by comparing pull-out strengths (Goal 4). Next to the pull-out, also the bonding itself is assessed during the tensile experiment. This is stated as when the resistance of the reinforcement specimen is greater than the resistance of mere SG should be, bonding between the materials is present. Goal 3 is applicable to this validation. Beside the difference in ultimate capacity the effectiveness of the second LTM is checked for each specimen in Goal 6. The validation criteria then become as follows;

3. Higher tensile resistance than only the SG part of the specimen material, $F_t, FFR > A_{SG} \cdot f_{uSG}$;
4. At least equal pull-out strength with respect to equivalent GFRP reinforcement, $F_{t,FFR} \geq F_{t,GFRP}$;
5. At least equal ultimate bending resistance[6], $F_{R,u,FFR} \geq F_{R,u,GFRP}$;
6. At least equal ultimate capacity resistance with respect to design load[5], $F_{R,u,d} \geq F_{E,u,d}$.

4.3.3. Validation of SLA

In addition to validation regarding the concepts a goal of this thesis is to improve the existing method and to create a better approximation for the numerical analysis. This analysing method thus also need validation, this is done by comparing the force-displacement curves of the numerical simulation to the data of the

[5] In this definition the design load is used since this is what should be used in practise. For this thesis a design capacity is not applicable since a case study is not used. Therefore this value will be replaced by initial fracture capacity, resulting in $F_{R,u} \geq F_{R,i,(P)}$.

[6] The validation is considerate with respect to the ultimate resistance since this is the case where the reinforcement is designed upon.

experiments. The comparison can be quantified by means of the error percentage presented in Equation 4.1. For this method the ultimate failure resistance should suffice. Next to the validation of the improved method, the analysis of the different parameters and design methods should result in more knowledge in the performance of RG structures. In the subsequent section the performance is defined in a few aspects and the independent methods are graded according these aspects.
In the parameter study a reference case is used for adjusting the different parameters. The data from this case is also used to validate the numerical calculation methods giving the analysis method three cases to validate with. Next to the validation, practical values need to be used in the FEA and therefore the reinforcement specimen need to be tested, this will be added as acquirement parameter in the section hereafter. One main development in SLA is the resistance gap due to SG in the post-cracked state. This resistance gap is quite important to be filled and will have its own goal. This all results in the following validation goals.

7. The error at ultimate failure should be smaller using the new SLA method with respect to the starting method (old), $e_{new}(i) < e_{old}(i)$.
8. Grade the influence of each parameter regarding their performance aspects;
9. Increase post-cracked resistance of non-reinforced SG-laminated beam, $F_{R,u} \geq 0$;
10. Increase initial failure resistance in post-tension application, $F_{R,i,p} \geq F_{R,i}$.

$$e = \frac{F_{num} - F_{exp}}{F_{exp}} \times 100\% \tag{4.1}$$

Definition of performance

Previously the performance of the beam is mentioned to be used to quantify the influence of the modelling differences. As this pretty subjective, the performance of the RG beams is defined in four aspects namely;

Resistance capacity The resisting force of the beam after cracking at equal deformation or at ultimate failure;

Deformation The deflection of the beam at ultimate failure;

Crack density The density of the crack, regarding the number of cracked integration point in the vicinity;

Amount of cracks Regarding the amount independent cracks.

In the conclusion of each parameter in Chapter 7 a summary is given about the influence in performance based on the analysis. Hereafter the aspects of performance are tabulated and their difference with respect to the reference is graded with a "-", "0" or "+"", representing lesser, equal or higher results. Using this method, the applied study of the parameter is briefly summarised and distinguished to the reference case. Please note that this grading can not be seen independently from the conclusion as the grade is meaningless when taken out of context.

4.3.4. Definition of validation goals by experiments

Four point bending and pull-out tests are carried out to validate the former state goals. This is achieved by acquiring certain data from the experiments. In the listing below the type of data which is desired is defined. These parameters and the goals from previous section are used to define the experiment in Table 4.1. In addition to data acquisition, each experiment the failure behaviour is observed to analyse the failure mode. Each experiment is elaborated further in the following sections.

- Reinforcement strains;
- Initial failure capacity and displacement;
- Ultimate failure capacity and displacement;
- Pull-out strength and displacement;
- Tensile force and displacement of reinforcements;
- Failure behaviour.

Table 4.1: Performed experiments to achieve goals

Experiment	Goal #	Parameter	Test type	Amount of specimen
Experiment BEN1	1, 2, 5	Reinforcement strains Initial failure Ultimate failure Failure behaviour	Four point bending	2 + 1
Experiment BEN2	4	Initial failure Ultimate failure Failure behaviour	Four point bending	2 x 3
Experiment PULL	3	Pull-out strength	Double pull-out test	2 x 3
Experiment TEN	5	Tensile strength	Tensile test	2 x 3

Experiment BEN1

This experiment will validate the post-tensioned GFRP reinforcement concept. A normal force is initiated in the laminated beam by use of post-tensioned reinforcement at the top and bottom of the beam. The GFRP reinforcement is tensioned to the right amount and adhered to the glass laminate. In this manner the GFRP reinforcement is both tensioned and adhered. The initial and ultimate failure resistances are acquired from the experiment, using the measurements of the reinforcement strains the fracture strength of the glass can be calculated back to analyse its initial fracture increase. The validation is done by using one of the three specimen as a reference without post-tensioning in order to see the differences in failure behaviour and initial resistance. The increase in capacity is compared to the expectation from the linear elastic calculation.

Experiment BEN2

The second bending experiment contains both batches of fibreglass fabric reinforcement (BEN2-FFR), which is done by laminating fibreglass within a SG laminate beam. And is compared with the performance of a reference reinforcement used in the thesis of Leung [2010] (BEN2-REF). The reference set is designed based on the design philosophy and the FFR specimen are designed to have equal ultimate resistance. Both load resisting performances will be analysed to asses the concept.

Experiment PULL

Pull-out tests of both the flexible and reference reinforcement will be executed in order to have a more direct comparison and avoid any unexpected aspects of a bending experiment. These specimen will also be called PULL-FFR and PULL-REF for FFR and reference reinforcement respectively.

Experiment TEN

The verification of the strength of the used materials is done by means tensile experiments. Since the reference reinforcement of experiment BEN2-REF is already tested in the work of Leung [2010] these tests will not be performed. Remaining the the unknown resistance of the FFR called specimen TEN-FFR and the Fibrolux reinforcement used in BEN1, called TEN-FIB.

5

Analytical design

In this chapter the designs which will be used for the experiment are elaborated. Since the experiments should perform accordingly, they are based on the defined design philosophy. Here, the initial and ultimate resistances of the experiments are calculated in a analytical manner. This approach makes the experiments theoretical plausible to achieve their goals. The analytical calculations are based on constitutive relations and force equilibrium.

5.1. Post-tension design - BEN1

First the post-tensioning concept will be designed, preferably the dimensions are equal to previous experiments for example Louter and Leung since they have experimented with the same general concept (Leung [2010]; Louter et al. [2012a]). Their dimensions were 125 x 1500 mm ($h \times l$), unfortunately this was practically not achievable and therefore a beam of similar dimensions is used. The two panes have the dimensions of 10 x 150 1200 mm($t \times h \times l$) and are PVB laminated. This is chosen to prevent the additional strength issue mentioned by in the work of Louter [2011]. The test set-up will have the dimensions ($L_1 - L_2 - L1$) of 375-350-375 mm, as illustrated in Figure 5.1.

Height-to-span ratio

The height-to-span ratio is a good parameter to put the dimensions of the specimen in contrast with previous research. When two 50mm supports are assumed, these dimensions result in a height-to-span ratio of 0.135 mm/mm or 135 mm/m. This is a rather high ratio with respect to previous research of reinforced glass as summarized in Martens et al. [2016c]. Here is mentioned that the mean ratio is 90 (mm/m), with a standard deviation of 19,30. The ratio of this specimen is in relation to these results thus more than one standard deviation, this implies a higher buckling resistance but also higher lateral torsion instability. This fact does not specifically have any consequences for the design since lateral torsional buckling will not be analysed in this thesis, but it is something to keep in mind.

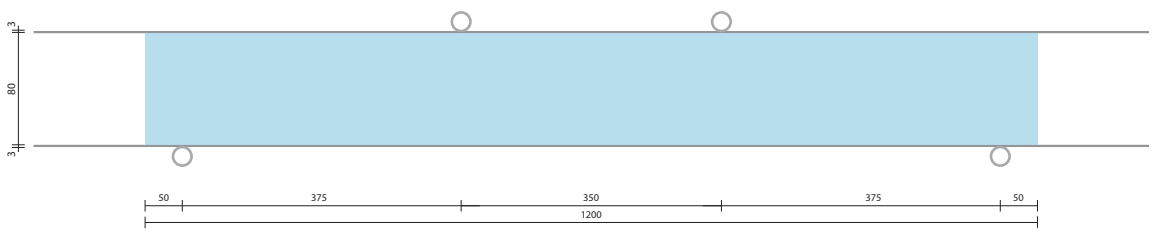

Figure 5.1: Configuration of set-up for experiment BEN1

Table 5.1: Properties of Fibrolux UD GFRP strip

Parameter		**Value**	Unit
Composite dimensions	$h \times t$	20×3	mm^2
Fibre content	-	60	%
Tensile strength	f_t	900	MPa
Young's modulus	E	40000	MPa
Matrix type		Isophthalic Polyester	
Lay-up		1 layer two-directional (2D)	
		UD middle layers	
		1 layer 2D	

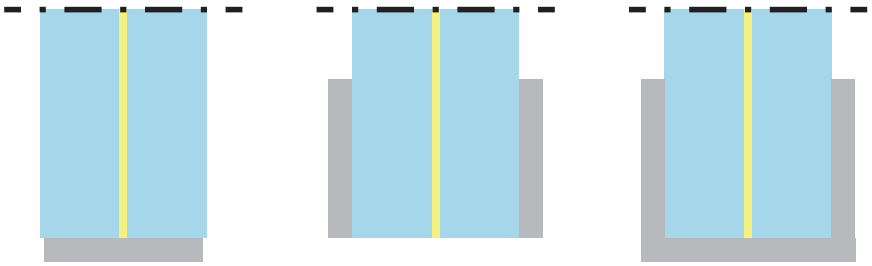

(a) Flat strip (b) Two vertical strips (c) U-section

Figure 5.2: Conceptual possibilities after considered limitations

Reinforcement

For the reinforcement specification there are many of options. As is already stated in Section 4.2.1, external GFRP reinforcement is used in order keep variation to a minimum. Therefore additional influences of SG or complex behaviour from integrated reinforcement are prevented. Concerning the relative heigh tensile strength with respect to steel large sections will not be required. This narrows down the possibilities to the application of strips or U-sections. This leaves the conceptual possibilities to the sections illustrated in 5.2. Regarding the required cross-sectional area, practically available and disturbance of the design, number 1 is chosen to proceed with in this thesis. The chosen strip is specified in the summation in Table 5.1[1];

5.1.1. Pretension concept

Before the design is put together and calculations are made, a glance is taken at the concept of post-tensioning. This with respect to the transition from steel to fibreglass as tensioning material. In the paper of Bos et al. [2004] and Louter et al. [2006] a T-section is used to stiffen the upper flange, resulting in the ability of creating a larger compression zone and decrease the lateral instability of the buckling zone. However, the addition and the type of connection of the flange will in practise always be different, in order to remain to the general idea of post-tensioning glass structures a simple straight cross section is assumed.

As is already stated in the Chapter 4, the starting point of applying the reinforcement is to create tension in the strips using steel bolts. As for the goal of this part of the thesis it is undesired to have adherence defects, which for example lead to slip and consequently decrease in pre-stress force. Therefore it is chosen to introduce the post-tension force by means of steel head-sections, the steel is adhered to the glass in order to flatten tolerances and gently introduce the force and a top and bottom strip is applied to avoid eccentric force and occurrence of local peak stresses. The concept is illustrated in Figure 5.3.

This concept of tensioning the reinforcement is only possible when the GFRP is not adhered to the glass yet otherwise the glass will not be subjected to compressive stresses. Therefore the GFRP strip is strained in advance hereinafter adhered to the glass laminate.

Prospect in development

Although it is not in the scope of this thesis the following is still noteworthy. When the tensioned reinforcement would be embedded in the glass laminate, which is a logical step towards integrated pre-tensioned

[1] The product is chosen in consideration of dimensions, performance, availability and UD fabric.

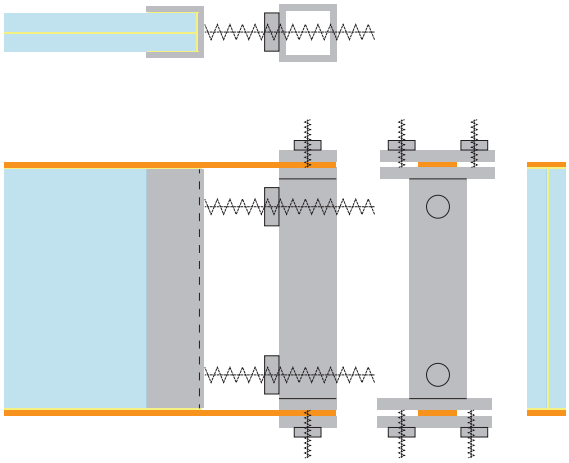

Figure 5.3: Illustration of post-tensioning GFRP reinforcement on a glass beam

reinforced glass design. This has a consequence on two aspects, the pre-tension force should be considered with care due to the non-bounded glass panes and the temperature/shrinkage effect on the GF(RP). When using the buckling calculation method of Blauwendraad (Blaauwendraad [2007]) the lower bound force should be assumed considering this is the force which does not take into account bounding of the panes.

5.1.2. Determination of failure resistances and post-tension force

Initial fracture resistance

To continue the design with post/tensioned reinforcement, it is first looked at the initial failure strength, this is after all the resistance capacity which is increased due tensioning. As already mentioned in the background ANG is used which has a mean tensile strength of $f_t = 45\text{MPa}$[2] (from NEN-EN 2608 [2016]). This results in a initial resistance strength of $M_i = 3.56\text{kNm}$ or $F_i = 19.00\text{kN}$ according to the basic elastic calculation from Appendix A.1.

Post-tension force

In ordinary tensioned structures it is always a challenge to find the optimum configuration and force. Here parameters as drape, angle, friction, creep will all affect the choice of the configuration and applied force. In this case the design is already quite limited due to the simply supported configuration, type of "tendon" and the force introduction with respect to peak stresses. Therefore the post-tensioned force is a normal force and the only remaining parameter to calculate is its magnitude. The post-tensioned force is limited by resistance of the glass section, in this case the most likely failure modes are crushing of the glass at the introduction and buckling of the system. Due to the slenderness of the section, buckling is assumed to be governing and their corresponding stresses are checked to prevent crushing. This done by the analytical calculation found in Blaauwendraad [2007] and can be found in Appendix A.2. The critical load ($F_{p,crit}$) is calculated at 58,19 kN, but due to imperfections this would not be achievable. Based on the second order stress calculation the post-tension force is determined at 20 kN[3], this is in the same order of magnitude with respect to representative post-tensioned structures publish in Louter and Cupaç [2014]. The calculated post-tension force results in the initial failure resistance of $M_{i,p} = 4.09\text{kNm}$ or $F_{i,p} = 21.81\text{kN}$.
Input parameters for this calculation are;

System length	1100 mm
Thickness PVB	0.2 mm
Stiffness PVB	5 MPa (Kuraray [2014b])

[2]This is regarding the design of a specimen, it is favourable to know when the glass fails instead of when it does not fail. Therefore, the mean values are used instead of design values.

[3]Here the design stress value of $f_t, d = 17.0$ MPa is used since this here failure is not desired. A force of 29,8 kN would result in a maximum stress of 16.8 MPa. To be safe 2/3 of this value is taken, hence 20 kN.

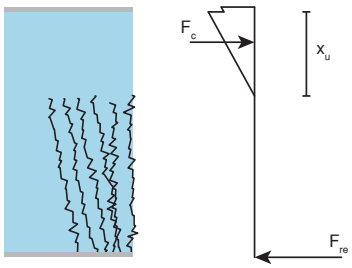

Figure 5.5: Schematic representation of force equilibrium which is used to calculate the ultimate failure resistance

5

The stresses due to deflection of the tensile force are calculated based on a second order calculation, these stresses are displayed in Figure 5.4 . Blauwendraad assumes in his work an imperfection of L/400[4], this leads to a initial horizontal value of 2.75 mm. Given the tolerances in this design with respect to eccentricity of the steel sections this is raised to L/300 this results in 3.67 mm seems a little more plausible.
This tensile force is transformed to strains which are used to measure and control the tensile force in the reinforcement and is elaborated in Appendix Section B.1.1. The required strain for the post-tensile force is $\varepsilon = 1.11 \cdot 10^{-2}$.
For adhering of the reinforcement to the glass and steel the 3M epoxy adhesive DP490 (3M [1996]) is used for heigh shear resistance ($\tau_u = 30\text{MPa}$). The adhesive Araldite 2013 (Huntsman [2013]) is used to adhere the head pieces to the glass since these will only endure compressive force.

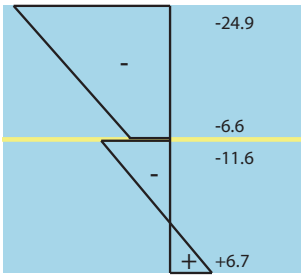

Figure 5.4: Stresses due second order horizontal displacement

Ultimate failure strength

In previous section it is suggested that a strip reinforcement would probably best suitable for this application. Now the initial resistance is known, the reinforcement is calculated according to this requirement stated in Section 3.2 which says that the ultimate resistance should not be less than the initial failure strength. The ultimate failure is based on the force equilibrium calculation which is know from concrete design. Here the cracked cross-section is assumed and an equilibrium of compression zone and reinforcement is present, as illustrated in Figure 5.5. With the properties of the GFRP strip mentioned is former Table 5.1, the ultimate failure resistance is estimate on of $M_u = 6.95\text{kNm}$or $F_u = 37.07\text{kN}$.

5.2. Flexible reinforcement designs - BEN2

The second design will contain either the GFRP strips from the thesis of Leung [2010] or the fibreglass texture. In this manner, the bending resistance can be analysed, therefore the cross-sections and reinforcements' area are both held equal. Both cross-sections are illustrated in Figure 5.6. These specimen are build-up from glass panes with the dimensions 8x80x800 ($t \times h \times l$) and are SG laminated, this is necessary for the integration of reinforcement to be possible. To put the specimen in perspective of previous research, the height-to-span ratio is again mentioned. Since they have a shorter span 25mm after support is sufficient which brings the heigh-to-span ratio to 106 mm/m or 0,106 mm/mm. The experimental set-up is based on the set-up used in Louter et al. [2006], with the dimensions ($L_1 - L_2 - L_1$) of 275-200-275 mm, as illustrated in Figure 5.7.
First the reference design is calculated to design with the right amount of reinforcement strips, since this has the least flexibility. The dimensions of the fibreglass are based on this design and a estimation is made for the ultimate resistance.

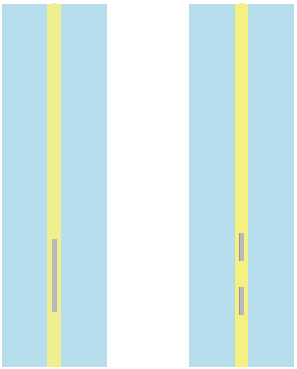

Figure 5.6: Cross-sections containing GFRP strips (a) and fibreglass texture (b)

[4]This assumption is based on the recommendation of Luible 2004

Table 5.2: Summarised SG-fibreglass composite properties

Parameter		**Value**	Unit
Composite dimensions	$h \times t$	$2 \times 8 \times 0.8$	mm^2
Fibre volume fraction	-	60	%
Young's modulus[6]	E	45.4	GPa
Tensile strength	f_t	2070	MPa

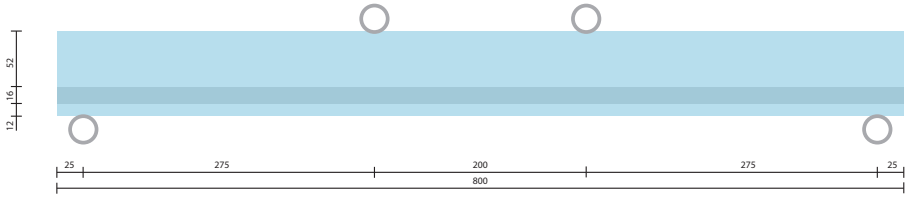

(a) BEN2-FFR configuration

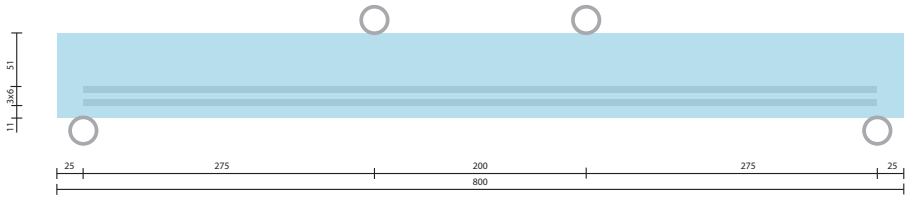

(b) BEN2-REF configuration

Figure 5.7: Experimental configuration of specimen BEN2-FFR and BEN2-REF

5.2.1. Failure resistances and fibreglass design

The initial failure resistance is calculated in the same manner as for design 1 and is found in Appendix A.1 and is estimated at $F_i = 5.61$ and $5.63\mathrm{kN}$ for design BEN2-FFR and BEN2-REF respectively. This small difference lie in the properties of the reinforcements but are not significant. The ultimate failure is calculated with one reinforcement strips using a theoretical cover of $c_{re} = 13\mathrm{mm}$[5], resulting is a ultimate failure resistance of $F_u = 4.826\mathrm{kN}$. This is less than the initial resistance and therefore it is decided to use two strips. With a distance of one strip height (6mm) the fictional cover is designed at 20mm as is seen in the configuration. Based on the analytical calculation this configuration has a ultimate failure resistance of $F_u = 7.71\mathrm{kN}$. With the acquired (experimental) data from Leung [2010], summarised in Table 5.2, the ultimate reinforcement strength is estimated at $F_{u,re} = 2 \cdot 9.74 = 19.48\mathrm{kN}$.

Fibreglass design

Since the fibreglass can be cut as desired, this 20 mm will be the centreline of the fibreglass reinforcement and its height is cut to match the ultimate reinforcement force ($F_{u,re}$). This strength is determined by the type of fibreglass which is used. For this application it is possible to choose two design options, either laminating between the two interfaces of the three sheets or to substitute a small area. In this case a UD $1200\mathrm{g/m}^2$ E-glass fabric is chosen for it uniform direction and high density, thus high strength per unit width. It is thought to be impractical to be use this between the SG sheets, but could also result in higher saturation of the fibreglass.

In order to calculate this force, the strength of the fibres is necessary. This type of fibres have a theoretical filament strength of $f_{t,filament} = 3445\mathrm{MPa}$ from AGY [2006]. Due to surface and moisture defects this strength is normally only 80 % of this stress, therefore a tensile strength of $f_t = 0.8 \cdot 3445 = 2756$ is assumed. Further properties of the used texture are summarised in Table 5.3, because these parameters are quite arbitrary some tensile test should be performed to estimate their exact behaviour.

[5] Theoretical cover is half of the reinforcement height ($3\mathrm{mm}$) and the distance to the edge ($10\mathrm{mm}$). This minimum edge distance is chosen to create sufficient spread in shear in the SG if necessary to eliminate an extra failure mode

Table 5.3: Parameters is used fibres

Parameter		**Value**	Unit
Fibre type	-	E-glass	
Weave type	-	UD	
Orientation	-	$0°/90°$	
Direction ratio	-	95/5	%
Weight of fabric	W	1210	g/m^2
Density of fibres	ρ	$2.55 \cdot 10^6$	g/m^2
Tensile strength	f_t	2756	MPa
Young's Modulus	E	72.3	GPa

Since amount of fibres in the fabric is expressed in density (g/m^2) its effective thickness is estimated by dividing the weight of the fabric over the density ($t_{eff} = W/\rho = 0.475\text{mm}$). Knowing the values of these parameter the height of the reinforcement can be calculated according to equation 5.1, using the 95% of the effective thickness due to the UD properties. The texture will be laminated within the glass panes by SG, this creates the uncertainty of estimating the fibre volume fraction (fvf) of the whole. The total thickness of the SG-fibreglass composite lies between the full interlayer and the thickness of the fibres (thus, between 3.0 and 0.5 mm). Although this in theory does not matter for the overall strength of the reinforcement it does for the elasticity modulus. Therefore a low fvf density of 35% (which is equal to hand laminating) is assumed. This results in a thickness of $t = 100/35 * 0.475 = 1.357\text{mm}$. Which subsequently results in a Young' modulus and tensile strength of $E = 24.2\text{GPa}$ and $f_t = 916$. This is based on the general composite equations elaborated in Appendix A.4. The properties which will be used for the analysis are summarised in Table 5.4. The design having the fibreglass reinforcement is able to resist a force of $F_u = 7.2802\text{kN}$.

$$h_{re} = \frac{F_{u,re}}{f_t t_{eff}} = \frac{19.48}{2756 \cdot 0.95 \cdot 0.475} = 15.6\text{mm} \tag{5.1}$$

Table 5.4: Summarised SG-fibreglass composite properties

Parameter		**Value**	Unit
Composite dimensions	$h \times t$	16×1.357	mm^2
Fibre volume fraction	-	35	%
Young's modulus	E	24.2	GPa
Tensile strength	f_t	916	MPa
	$F_{u,re}$	19.88	kN

5.3. Specimen overview

The expectation of the experiments are seen in Table 5.5 based on the analytical calculations. The calculated deflections are not very interesting as the deflection of initial failure is just linear elastic and influenced by the experimental set-up. And the deflection of the analytical calculation is highly influenced of the failure mode, bounding of reinforcement and elasticity of the reinforcement which does not give a good representation since the analytical calculation is based on rupture of reinforcement, which is based on the relative low elasticity less likely to happen.

Table 5.5: Load resistances at initial and ultimate failure overview of bending specimen

	F_i [N]@[mm]	F_u [N]@[mm]
BEN1	19.0/21.8 @1.96	37 @ 34.96
BEN2-FFR	5.69 @ 1.71	7.66 @ 75.12
BEN2-REF	5.63 @ 1.70	7.78 @ 85.12

6

Experimental research

The experiments are performed according to the described methodology in the following sections. Since the tensile experiments TEN and PULL are used as exploration of the materials and behaviour, the experiments are treated in reversed sequence. Each experiment contains a small analysis/discussion and concluded summary based on the observations and analysis. The last section contains the conclusions regarding the stated goals defined in Section 4.3 and observations.

6.1. Overview of experiments and their goals

The main goal of these experiments is to validate the two concepts, post-tensioned and fibreglass fabric reinforcement. In advance of the experiments an overview is given in Figure 6.1 about the experiments and their relations. In this diagram the two main goals regarding the validation of the concepts are seen at the top and the sub-goals regarding their validation below. These are the sub-goals mentioned from Section 4.3 of the Concept chapter where the validation of the concepts is defined. Besides the experimental validation these test are also done to acquire data to perform and validate the FE analysis.

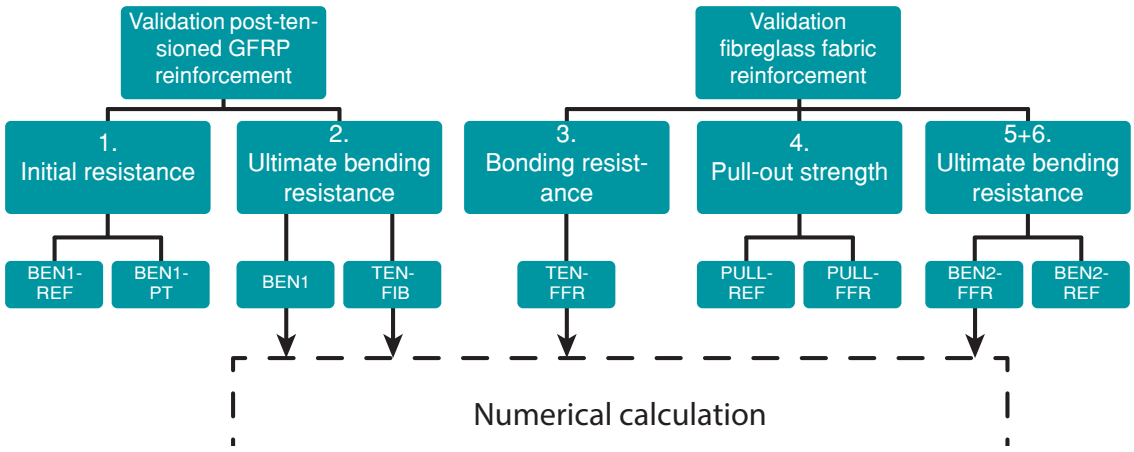

Figure 6.1: Overview of experiments and their relation to validation of the concepts

6.2. Tensile strength experiments TEN-FFR and FIB

Tensile tests are performed to acquire the exact tensile resistance, elasticity modulus and failure behaviour of the used reinforcement. This data is used for validation of BEN1 and 2 in the FE analysis. For these

experiments only the fibre glass texture strips from BEN2-FFR (experiment set TEN-FFR) and Fibrolux GFRP strips used in experiment BEN1 (experiment set TEN-FIB) are tested. Due to the existence of strength properties of the GFRP strips used for BEN2-REF in the thesis of Leung [2010], it is not necessary to exam their performance. In advance of the experiment a small calculation is done for the TEN-FFR, according the the composite calculation in Appendix A.4. The data from this calculation is summarized in Table 6.1. Since the examined materials are not related, they are both treated separately.

Table 6.1: Overview of specimen expectations

Specimen	Tensile strength	Displacement
TEN-FFR, fibreglass-SG, 2.5x16mm	19 kN	9.53 mm
TEN-FIB, GFRP 20x3 Fibrolux	54 kN	5.62 mm

6.2.1. Methodology

The experiments are performed in the Zwick-50 testing system at the faculty of mechanical engineering. Using lever operated clamping and mechanical wedge grips for specimen TEN-FFR and TEN-FIB respectively[1]. Based on practical reasons a length of 250 mm is chosen to be tested, this is longer than the material should need to build into uniform stresses and therefore reduces transverse stresses as much as possible. Including the two times 50 mm needed for the clamping system, this bring the specimen up to 350 mm. In order to gradually build-up stresses, specimen TEN-FFR-1 is performed with a rate of 1 mm/min, as this took longer than expected, the remaining specimen are executed with 5 mm/min as well as the TEN-FIB specimen. Clamping of GFRP is difficult as peak stresses could occur due to the rectangular geometry of both specimen. The SG cover of the TEN-FFR specimen would create a uniform stress distribution so this would not be applicable. For the more rigid TEN-FIB specimen an attempt is done to fit rubber pieces between the clamps, but this resulted in clamping difficulties as the rubber was too elastic. The TEN-FIB specimen are eventually executed without the rubbers.
Initially the fibreglass without any resin were tested, but due to the density of the fibres only the outer fibres were clamped. This created slip between the fibres and the specimen was unable to build-up strength, therefore the SG-fibre composite is made. This would benefit the stress distribution through the specimen and has a better representation of the behaviour in the glass laminate. This composite is made by putting the fibreglass piece between two SG pieces, just as it would be when laminated in the beams, as is illustrated in Figure 6.2. This was then put in the same vacuum bag as the BEN2 specimen, to prevent the breather from adhering to the specimen as well a release film is used, and steel strips for geometry control.

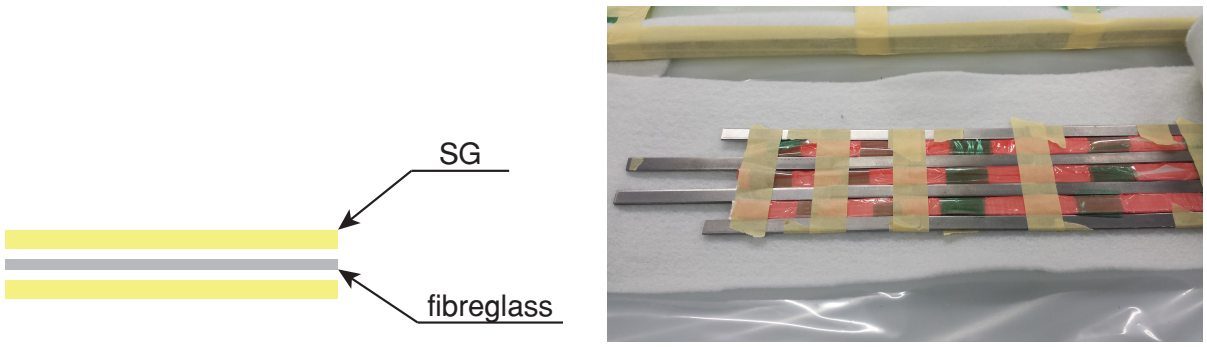

(a) Schematic build-up of TEN-FFR specimen

(b) Specimen during vacuumbag assembly

Figure 6.2: Assembling of SG-fibreglass composite

6.2.2. Results TEN-FFR

In Figure 6.3 the force-displacement curves of experiment TEN-FFR are plotted with the corresponding characteristic values.

[1] The different use of clamps is based on practical considerations and should not influence the results

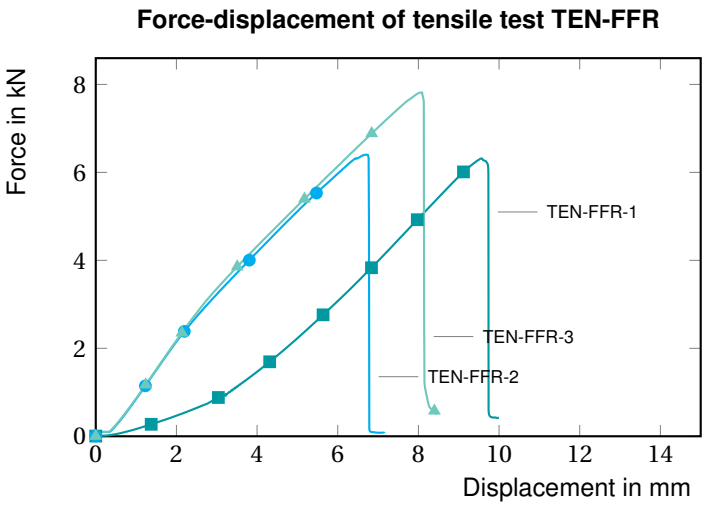

	Tensile failure [N] @ [mm]
TEN-FFR-1	6318 @ 9.73
TEN-FFR-2	6402 @ 6.77
TEN-FFR-3	7816 @ 8.13
Mean	6845 @ 8.21

Figure 6.3: Force-displacement diagram and table of tensile experiment TEN-FFR, in SG embedded fibreglass

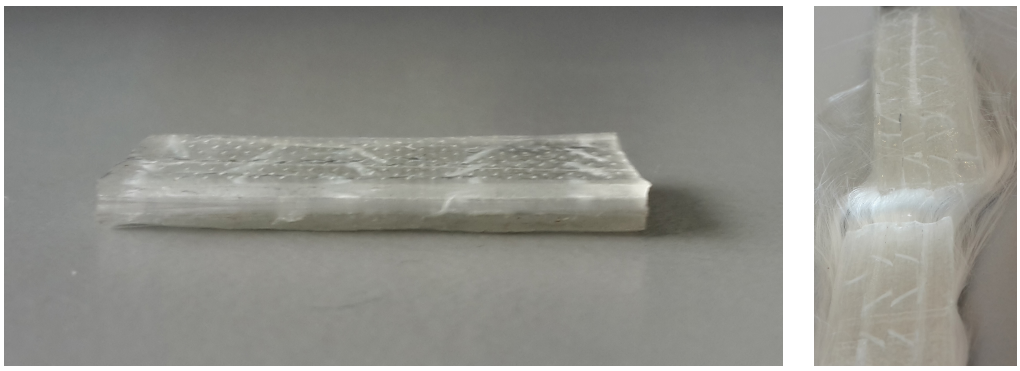

(a) Cross-section of TEN-FFR

(b) Failed specimen TEN-FFR

Figure 6.4: Failure TEN-FFR specimen

6.2.3. Analysis and Discussion TEN-FFR

In the force-displacement diagram two different curves are seen, one with increasing stiffness and two where a slight softening occurs. This curve is related to the first specimen which was tested with a lower speed. It is difficult to say is this is due to the visco-elastic behaviour of the SG or how the clamping works as the other specimen where tightened harder. But the slope and resistance are roughly equal so this would not affect the result significant. Furthermore, all specimen failed between 6-8 kN, which is half of the estimated 15 kN. Also they all failed due to rupture of the SG, which is not expected since the SG has a much lower stiffness and higher ultimate strain. The failure mode can be explained when looking at the failed specimen in Figure 6.4. Here it is visible that the fibreglass in the core of the specimen is not embedded in SG. As a result the composite is not working as a whole as these fibres are not activated in the mechanism, hence reduced properties are observed. Nevertheless, the tensile force is still significantly higher than the value of only SG[2]. This means that although not all fibres where contributing, the principle still holds and approximately 30% of the fibres contributed to the resistance theoretically. This is based on the backwards calculation of the composite resistance according to equation 6.1, where α is defined as the contribution factor. With the assumed effective dimensions of $1.36 \times 16\text{mm}$ from Section 5.2.1 the mean properties of the specimen are

[2]For the SG 2 layers with a thickness of 0.89 mm are used. Assuming the strength of 34.5 MPa as given in the background Section 2.5.1 this results in a force of $F_{t,SG} = 982\text{N}$

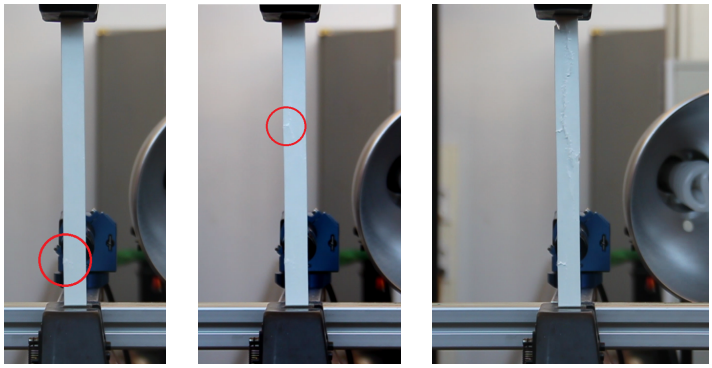

(a) First visible crack in specimen TEN-FIB-3

(b) Second visible crack in specimen TEN-FIB-3

(c) Ultimate failure of TEN-FIB-3

Figure 6.5: Failure of specimen TEN-FFR with visible unsaturated fibres and failure initiation of TEN-FIB

summarised in Table 6.2.

$$F_{t,re,mean} = F_{t,SG} + \alpha F_{t,fibre} \tag{6.1a}$$

$$F_{t,re,mean} = A_{SG} f_{t,SG} + \alpha A_{fibre} f_{t,fibre} \tag{6.1b}$$

$$\alpha = \frac{F_{t,re,mean} - F_{t,SG}}{A_{fibre} f_{t,fibre}} \tag{6.1c}$$

$$\alpha = \frac{6845 - 982}{0.45 \cdot 16 \cdot 2756} = 0.30 \tag{6.1d}$$

Table 6.2: Practical tensile properties of SG-fibre composite experiment

Parameter		Value	Unit
Tensile force	F_t	6.8	kN
Young's modulus	E	7.1	GPa
Tensile strength	f_t	316	MPa
Elastic strain	ε_e	4.4	$\cdot 10^{-2}$

6.2.4. Results TEN-FIB

In Figure 6.6 the test results are visible of specimen TEN-FIB. They all failed in a consistent fashion with a mean load of 34.1 kN and displacement of 10.3 mm.

6.2.5. Analysis and discussion of TEN-FIB

Failure of the specimen occurred consistently at roughly equal load and displacement with the same failure mode. As the failure pattern would suggest the specimen failed due to peak stresses around the clamps edge. Looking at the footage in Figure 6.5, initial failure is introduced at roughly the same position stress concentrations are expected as is visualised in in Figure 6.7. Meaning that when a uniform distribution is present the strips should be able to resist a higher load. But when the detailing of BEN1 is considered, this would result in the same distribution as no counter measures are taken against this principle. From the data the average Young's modulus is calculated via equation 6.2, a displacement range of 2-8 mm is

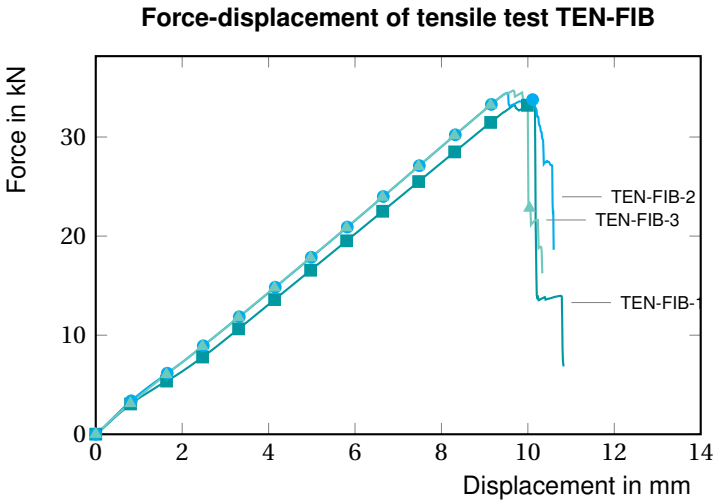

	Tensile failure [N] @ [mm]
TEN-FIB-1	33251 @ 10.00
TEN-FIB-2	34449 @ 10.59
TEN-FIB-3	34674 @ 10.35
Mean	34131 @ 10.32

Figure 6.6: Force-displacement diagram of tensile experiment TEN-FIB, 20x3 GFRP specimen

held on where the stiffness seems linear. This results in the mean Young's modulus of $E_{mean} = 15.33\text{GPa}$, which deviates from the theoretical $E = 40GPa$. This can be explained when looking at the lamination of the specimen. According to the manufacturer the GFRP strips lay-up starts and end with a bi-directional texture and only has a UD texture in the middle of the cross-section. Due to the low thickness (3mm) the two bi-directional textures take up relative heigh area with respect to other UD products where these values are applicable to. The lower tensile strength with a mean of $F_{t,mean} = 34.1\text{kN}$ gives a tensile stress of $f_t = 568\text{MPa}$. In Table 6.3 the properties are summarised.

$$E_{avg} = \frac{1}{N}\sum_i \frac{\Delta F_i \cdot l_{spec}}{\Delta l_i \cdot A_{spec}} \tag{6.2}$$

where:

F_i = Force at data point i

l_{spec} = Length of specimen

Δl = Elongation of specimen at data point i

A_{spec} = Cross-sectional area of specimen

Table 6.3: Practical properties of GFRP strip

Parameter		**Value**	**Unit**
Tensile force	F_t	$34,1$	kN
Young's modulus	E	15.3	GPa
Tensile strength	f_t	568	MPa
Elastic strain	ε_e	3.7	$\cdot 10^{-2}$

6.2.6. Summarised conclusion

For the SG embedded fibreglass it is proven that the chemical bond is present as the resistance is higher than the resistance mere SG. The specimen failed mechanically due to lack of saturation of the SG in the fibreglass. A contribution of approximate 30% is found, based on the tensile strength of the SG and experimental strength.

The experiment of TEN-FIB was executed to gain the true material properties which are needed for the post-tensioning of the glass. A Young's modulus of $E = 15.33\text{GPa}$ is found instead of the 40GPa given by the manufacturer and a lower ultimate strength is observed. The lower Young's modulus is explained by the lay-up composition, were the outer layer are bi-directional woven fabrics. Their performance is lower than

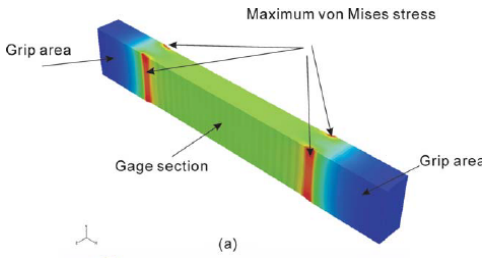

Figure 6.7: Image of stress concentrations due to rectangular geometry

given by the manufacturer as these layers are relatively thick with respect to other (bigger) GFRP products the manufacturer supplies. The lesser tensile strength is explained by the peak stresses introduced by the geometry of the specimen. This is challenging to prevent in the detailing of experiment BEN1 and are therefore accepted. All observations are taken in account in the execution of experiment BEN1.

6.3. Pull-out experiments

To analyse the application of fibreglass fabric as a reinforcing material its bonding behaviour to glass is examined. This is done with respect to the performance of the GFRP strips known from Leung [2010]. A bonding test is performed by means of double pull-out.

6.3.1. Methodology

The glass panes are of the dimension 6x80x145 with the reinforcement configurations of 6mm fibreglass texture and 6x0.8mm GFRP strips. The dimension of the texture is chosen to compare the adherence capacity.

In the work of Leung [2010] it is shown that the minimum transfer length to achieve full bond should be at least larger than 100mm. However, the goal of this experiment is not to find the minimum transfer length or maximum tensile strength of reinforcement, but the differences in the bonding behaviour. Therefore, the transfer length is reduced. The adherence surfaces are held equal so the resisting force can be compared. The length of the glass panes are practically chosen at 145mm and a double pull-out test is performed[3] this implies a maximum of 70mm transfer length with a tolerance of 5 mm in the middle. As is presented in Figure 6.8, the left side has double the adherence surface as the right, which is done to imply failure of the right side.

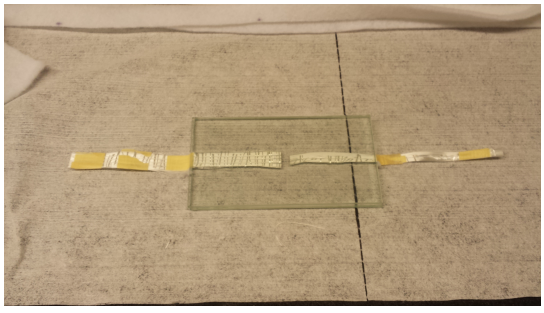

(a) PULL-FFR fibreglass specimen

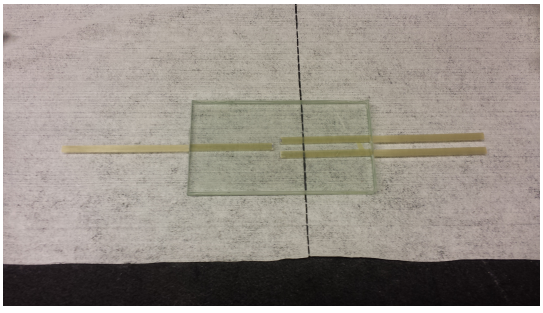

(b) PULL-REF gfrp specimen

Figure 6.8: Finished specimen PULL-FFR and PULL-REF

First the specimens are assembled, this process is not difficult but it does influence the end result and is therefore treated. Its sequence is shown in Figure 6.9, special attention is given to the cleaning, application of primer, not to damage the materials and eliminate air inclusions as much as possible. Cleaning is done with a isopropyl alcohol in order not to damage the materials and the primer is an amino-silane as discussed in Section 2.5.1 and 4.2.2. The specimen are laminated in the oven at 135 °C for at least an hour.

[3] A double pull-out test is chosen to avoid gripping issues of the glass

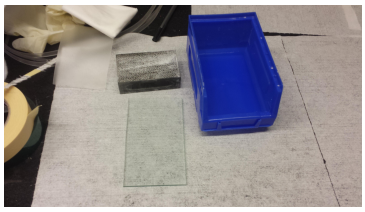
(a) Polish edges


(b) Cut fibreglass texture

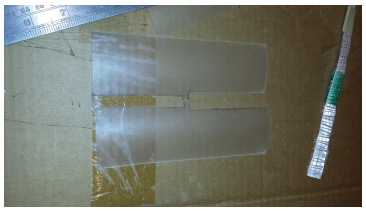
(c) Cut SentryGlas


(d) Clean with alcohol


(e) Treat with silane primer

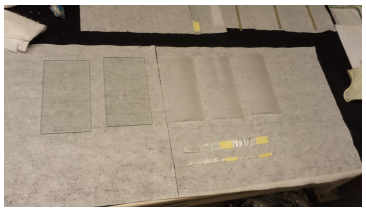
(f) Assemble pieces

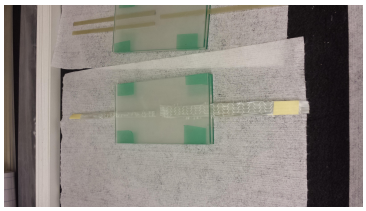
(g) Assembled specimen

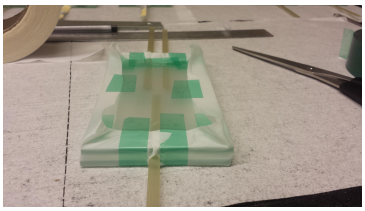
(h) Apply release peel ply

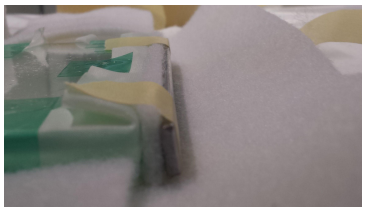
(i) Breather and thickness control

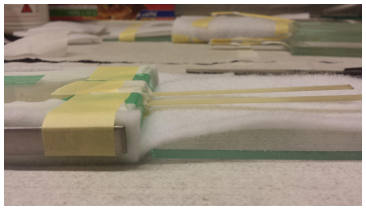
(j) Breather and height control GFRP


(k) Assemble vacuumbag


(l) Put in the oven

Figure 6.9: Assembling sequence of pull-out test specimen PULL-FFR and PULL-REF

Including starting up with 5 $^{\circ}\mathrm{C/min}$ and cooling down with 2.5 $^{\circ}\mathrm{C/min}$. This results in a total oven time of 2.5 hours. This process is based on Hanenberg [2016]; Kuraray [2016] and advised by C. Louter and the SG supplier Kuraray. The hour of constant temperature is necessary for the materials to warm up till the required temperature to create chemical bonding.
An estimation of calculating the shear capacity is done, by this is based on linear elasticity while SG is a plastic material and the specimen are most-likely to have a de-bonding failure mode. The calculated shear resistance is $4167\mathrm{N}$ and calculated according to Appendix Section A.4.1.

6.3.2. Results PULL

The first test batch did not go as expected, due to the slip which occurred between the fibres of the fibreglass fabric it was not possible to create a pull-out. As for the GFRP strips, failure occurred on the outside of the glass laminate. The solutions to solve these problems are listed below. The transfer resistance is reduced and create a transfer length of 30mm instead of the previous 70mm and the fibre glass is also enclosed by SG just as in experiment TEN-FFR. These new specimens are called PULL-X-4/5/6 and are pictured in 6.10.

The force-displacement results of specimen PULL-FFR and PULL-REF are shown in the Figure 6.11 and are summarised in Table 6.5. Their corresponding failure mechanisms are presented Figure 6.12 and 6.13.

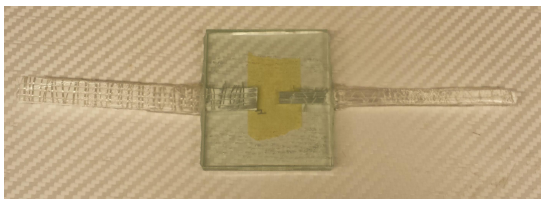

(a) New PULL-FFR specimen

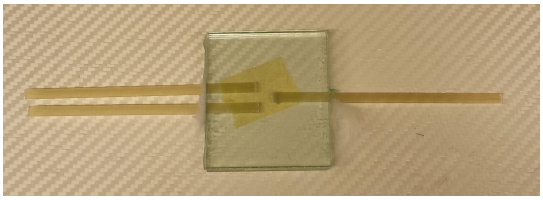

(b) New PULL-REF specimen

Figure 6.10: New specimen PULL-FFR and PULL-REF, with embedded fibreglass and 30mm transfer length

Cause of failure	**Solution**
Slip between fibres	Make SG composite
Failure outside of glass	Lower transfer resistance

6.3.3. Analysis and Discussion

At the first attempt it was concluded that the bonding was too strong and the fibres without resin were slipping in the clamps. Since it was desired to asses the bonding capacity of the material a second attempt resulted in correct failure for PULL-REF, but specimen PULL-FFR failed outside the specimen at a lower force. The same phenomenon as in experiment TEN-FFR is seen, failure in the SG was found while the fibres where still intact and slipping of the core fibres occurred. Specimen PULL-FFR-6 is therefore run a second time to look for any increase in resistance.
Nevertheless, the specimen of PULL-REF did fail and exactly as the were supposed to. The crack patterns are different and specimen PULL-REF-4 seems to be the result of better bonding. But this did not seem to influence the failure force significantly, which is a positive result.

Table 6.5: Summary of PULL experiments and mean values

	F_u [N] @ [mm]		F_u [N] @ [mm]
PULL-FFR-4	1809 @ 4.63	PULL-REF-4	4880 @ 4.02
PULL-FFR-5	1708 @ 4.49	PULL-REF-5	4500 @ 3.34
PULL-FFR-6	1945 @ 4.22	PULL-REF-6	4478 @ 4.73
Mean	1821 @ 4.45	**Mean**	4619 @ 4.03

6.3.4. Summarised conclusion

The goal of this experiment was to compare the bonding behaviour of the different reinforcement materials. The reference specimen had excellent behaviour as it was expected. But since experiment PULL-FFR did not fail as expected no conclusions can be drawn.

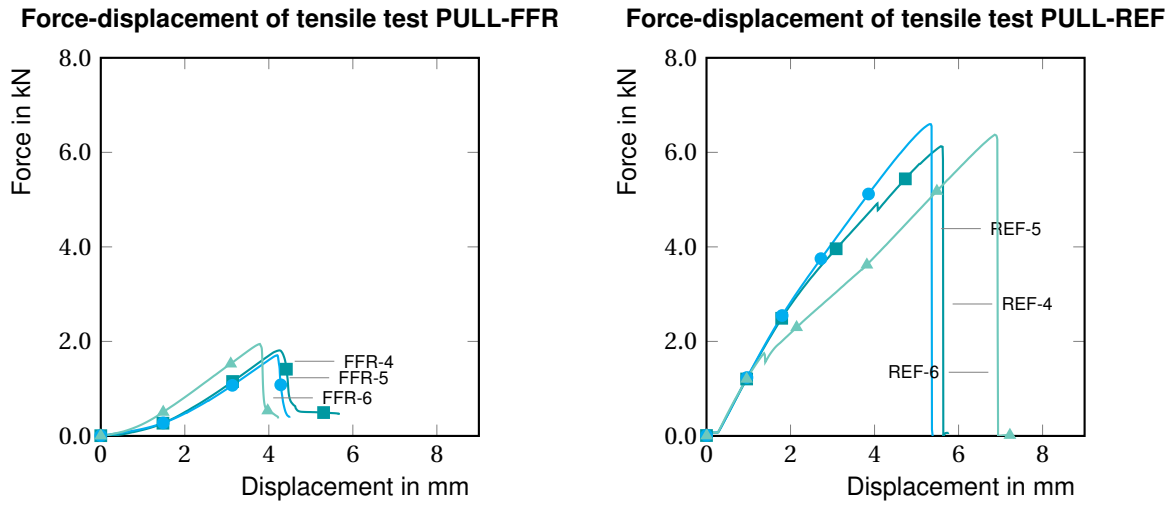

Figure 6.11: Force-displacement diagram of tensile experiment PULL

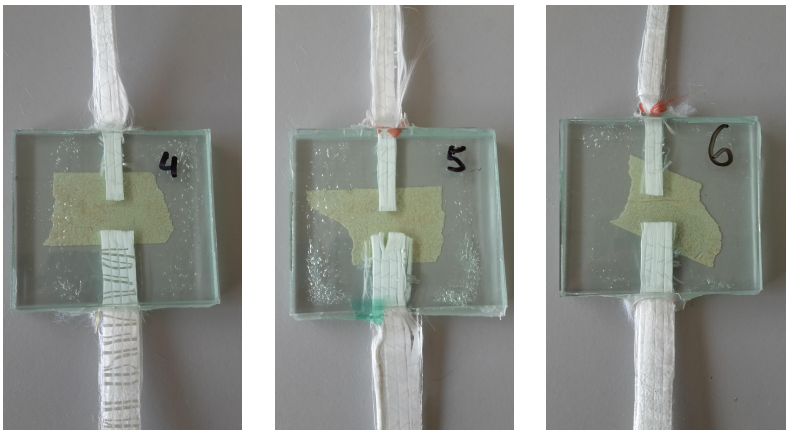

(a) PULL-FFR-4 (b) PULL-FFR-5 (c) PULL-FFR-6

Figure 6.12: Failed specimen PULL-FFR-4/5/6, failure in particular visible in specimen 6 which has been tested twice to look for any resistance increase.

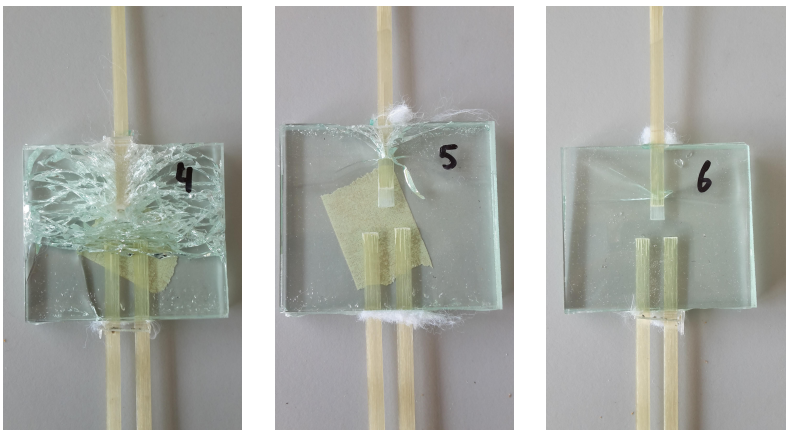

(a) PULL-REF-4 (b) PULL-REF-5 (c) PULL-REF-6

Figure 6.13: Failed specimen PULL-REF-4/5/6, especially at specimen 4 a very good bond is observed.

6.4. Bending experiments with fibreglass fabric reinforcement, BEN2

This bending experiment will incorporate the FFR. Its concept is validated experimentally with respect to the reinforcement type which is proven to have beneficial results (Leung [2010]). The concept will be validated u by the ultimate strength resistance but also failure behaviour is analysed. The expected resistances are found in Table 6.6.

Table 6.6: Analytical values

	F_i [N]@[mm]	F_u [N]@[mm]
BEN2-FFR	5.69 @ 1.71	7.66 @ 75.12
BEN2-REF	5.63 @ 1.70	7.78 @ 85.12

6.4.1. Methodology

Both specimen batches are of the dimensions 80x800mm and build up from 8mm annealed glass panes, laminated with three SG sheets of 0.89mm thick. These three interlayer sheets are practically necessary to laminate the reinforcement inside the glass beam. Specimen BEN2-FFR will have fibreglass fabric with a width of 16 mm as defined in the design Section 5.2.1, specimen BEN2-REF will be the reference containing 2 6x0.8mm GFRP strips, from the research of Leung [2010]. The two sets are subjected to a displacement controlled test with a speed of 5mm/min.

The lamination procedure went the same as for the specimen of experiment PULL and the assembling and finished specimen are shown in Figure 6.14 together with the set-up. The configuration of test rig is 275-200-275 ($L_1-L_2-L_1$) with the extra lengths of 25mm on either side of the support as is mentioned in Section 5.2 of the Design chapter.

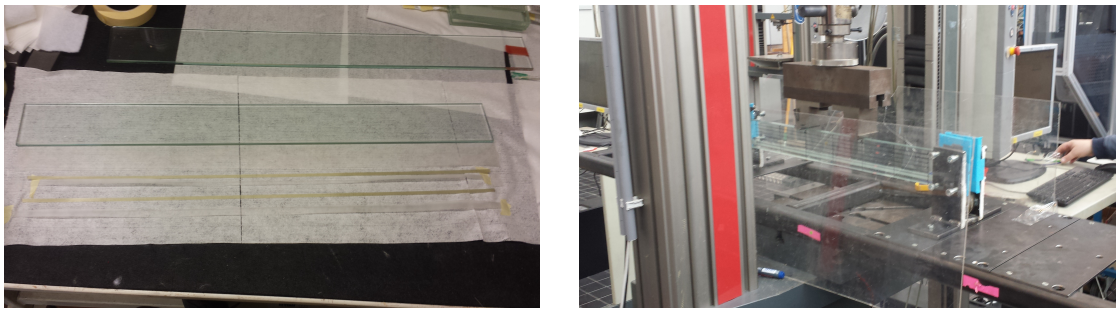

Figure 6.14: Assembling the parts of specimen BEN2-REF and test set-up

6.4.2. Results

In Figure 6.15 the force-displacement curve of the tested specimen are shown and the exact initial and ultimate failure resistances are summarised in Table 6.7.

Table 6.7: Load resistances at initial and ultimate failure summary of experiment BEN2

	F_i [N] @ [mm]	F_u [N] @ [mm]		F_i [N] @ [mm]	F_u [N] @ [mm]
Analytical	5684 @ 1.71	7659 @ 75.12	Analytical	5638@ 1.70	7785 @85.12
BEN2-FFR-1	3762 @ 1.63	3419 @4.91	BEN2-REF-1	5111 @ 2.14	6940 @ 25.83
BEN2-FFR-2	4259 @ 1.78	3864 @ 5.63	BEN2-REF-2	6521 @ 2.77	8045 @ 31.05
BEN2-FFR-3	4974 @ 2.27	3311 @ 5.30	BEN2-REF-3	4528 @ 1.76	6784 @ 12.3
Mean	4331 @ 1.89	3531 @ 5.28	**Mean**	5387 @ 2.23	7256 @ 23.06

6.4.3. Analysis and discussion

The acquired results from experiment BEN2-REF are as expected, building up resistance after initial failure. The BEN2-FFR experiment is very interesting as the resistance is build up but at a certain point gradually

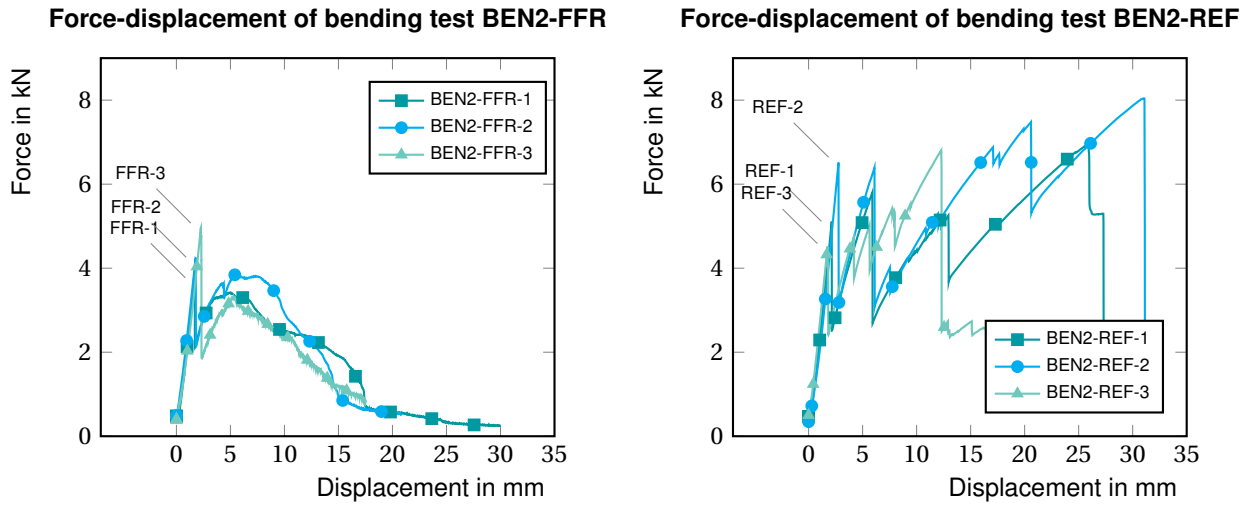

Figure 6.15: Force-displacement diagram of bending experiments BEN2-FFR and 2, fibreglass and GFRP strips

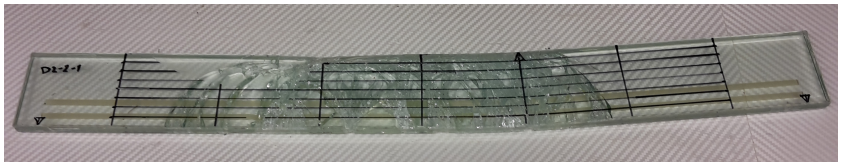

(a) Crack pattern of failed reference specimen

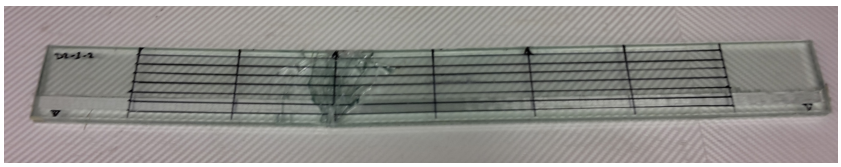

(b) Crack pattern of failed fibreglass specimen

Figure 6.16: Cracks patterns after failure of both specimen

decreases over the deflection. This could be expected looking at the results from experiment TEN-FFR. To analyse the results they are first compared to the analytical values, secondly the differences between experiments are analysed and lastly an estimation of forces in the reinforcement is calculated.

Analytical

When the data is put in proportion to characteristic and expected results, some differences are seen (table 6.7). At first sight the mean values for initial failure are lower for BEN2-FFR and higher for BEN2-REF. A possibility could be that this is mere statistics since only six specimen are tested and all values lie in the same range, except for BEN2-REF-2. This difference could also be explained by the stiffness of the reinforcement. When looking at the stiffnesses of the applied reinforcements[4] an explanation could be that the GFRP reinforcement strips have higher contribution to the initial stiffness in the pre-cracked phase, just as they do in the composite glass systems. But this contribution is almost negligible due to the presence of the SG and the cross-sectional area of the strips[5]. Therefore, it can be assumed that these differences are not dependent on the design and do not influence to results.

[4] Young's modulus for fibreglass texture this is $E = 7100\text{MPa}$ according to tests in Section 6.2.3 as for the GFRP strips this is $E = 45400\text{MPa}$

[5] This contribution of the reinforcement is roughly 0.2 kN, calculated according to the presented analytical calculation in Appendix A.1.

Reinforcement types

As stated above and in Section 6.2.3 about the tensile tests, the measured Young's modulus of the SG-fibreglass composite is significantly lower in relation with the reference GFRP strips. However, after initial failure of the glass, the stiffness (Force/ displacement) of both applications is roughly equal. These differences are quite interesting, an explanation could be the bonding length of the reinforcement. Due to the length of the reinforcement and the occurrence of only sudden local straining, it could act as a fully bond connection, hence having the designed stiffness by full contribution of the fibres. Hereinafter slipping occurs resulting in slowly decreasing stiffness in the fibreglass reinforcement as the un-adhered fibres in the core of BEN2-FFR slipping inside the laminate. Therefore the force is unable to build-up for another crack to occur. This explains the gradual decrease in resistance after the second peak. In BEN2-REF this does not happen and the sequential cracks occur, until brittle failure of either the glass or reinforcement.

Estimation of reinforcement strength

It is interesting to calculate back the force in the reinforcement at the point of failure to see if this is in agreement what was expected, especially for the fibreglass reinforcement. The estimation of the tensile force in reinforcement is calculated according to the following equations.

$$M_{u,mean} = \frac{1}{2} F_u \cdot L_1 \tag{6.3a}$$

$$F_{u,re,mean} = \frac{M_{u,mean}}{z} \tag{6.3b}$$

$$z = 0.9 \cdot (h - c_{re}) \tag{6.3c}$$

Where:
- $M_{u,mean}$ = Mean moment resistance of specimen at ultimate failure
- F_u = Load resistance at ultimate failure
- $F_{u,re,mean}$ = Mean force in reinforcement at ultimate failure
- c_{re} = Theoretical cover of reinforcement consisting of edge distance and half the reinforcement height
- z = Distance of internal arm between cumulated reinforcement and compression zone forces
- h = Height of beam

	$M_{u,mean}$ [Nmm]	$F_{u,re,mean}$ [N]
BEN2-FFR	$485.6 \cdot 10^3$	8992
BEN2-REF	$997.7 \cdot 10^3$	9238

The reinforcement force for specimens BEN2-FFR (fibreglass) is a little higher than the acquired data from experiment TEN-FFR. The limited number and assumption of z could result in a small theoretical deviation. But apart from that the fibres are fully enclosed by the SG resulting in a uniform tensile force distribution instead of forces at the edges but also spread of stress peaks in SG which can occur. Although these plausible deviations, both values are still quite close to each other and therefore it can be said that they act in the same manner. The decrease in comparison to brittle failure can be explained due to the embedding of the glass and SG.

6.4.4. Summarised conclusion

The goal for these experiments is to compare ultimate load bearing resistance and failure behaviour. The load bearing resistance of the FFR is lower than expected due to the slipping which occurred as a consequence of low saturation as is concluded from experiment TEN-FFR. Specimen PULL-FFR has equal failure behaviour as the reference specimen but due to aforementioned phenomenon the load resistance gradually decreases as deflection increases.

6.5. Bending experiments with post-tensioned reinforcement, BEN1

6.5.1. Methodology

This four-point bending experiment is to validate post-tensioned GFRP reinforcement. The steel head pieces are used as actuators to tension the reinforcement up to the designed force and adhered to the PVB laminated glass specimen. As is found that the real Young's modulus of the GFRP strip deviates from the theoretical value, the post-tension strains are calculated according to this achieved value according to the calculation in Appendix B.1.1.

The GFRP strips are attached to steel edge connectors glued and bolted to assure no slip can occur. After curing of this connection the adherence is applied to the GFRP strips on top and bottom of the glass laminate hereinafter the tensioning is applied. The adherence takes 7 days to cure that is the reason for this sequence. In this manner the GFRP strips can be both tensioned and adhered[6]. The tensile stress is monitored by strain gauges on both GFRP strips.

Not only a reduction in Youngs' modulus is found in experiment TEN-FIB, but also a lower tensile strength. In Table 6.8 both values are calculated according to the analytical model. Here is seen that the ultimate resistance is still higher than initial resistance, hence the design is still valid.

Table 6.8: Old and new calculated analytical values

	F_i [kN]	$F_{i,p}$ [kN]	F_u [kN]
According to design	19.0	21.8	37.0
Tested values	18.6	21.3	25.0

Post-tension force

The maximum force in calculated is Section 5.1.2 and transformed in strains according to the calculation in Appendix Section B.1.1. During the tensioning process a fault occurred in the transformation from tension force to the output feedback of the strain gauge measurements. This resulted in a applied post-tension force of 2kN instead of 20kN. An attempt is made to increase the post-tension force by applying additional strain gauges at the vicinity of steel head sections. But since the epoxy was already fully cured this did not have consequences on the normal force in the glass at mid span, since the compressive forces directly flow to the edges. A small FE calculation in Appendix B.1.2 shows the stresses in x-direction for the different cases.

6.5.2. Results

The experimental data is plotted in the force-displacement curve in Figure 6.17 and in Table 6.9 the applied tension strains on the GFRP strips and failure resistance values are presented. In Figure 6.18 the failed specimen BEN1-PT-2 can be seen.

Table 6.9: Post-tension strains and failure resistances

Specimen	$\mu\varepsilon_p$ u.l.	$\sigma_{re,p}$ MPa	$\sigma_{p,gl}$ MPa	$\Delta F_{i,p}$	$F_i / F_{i,p}$ kN	F_u kN
Analytical	11000 / 11000	168 / 168	6.67	2.80	19.0 / 21.8	25.00[7]
BEN1-PT-1	841 / 1086	12.8 / 16.6	0.59	0.24	15.53 / 15.76	11.66
BEN1-PT-2	1009 / 1095	15.4 / 16.7	0.64	0.26	14.17 / 14.43	13.73
BEN1-REF	0 / 0	0 /0	-	0	13.11 / -	12.41
Mean	-	-		0.25	14.27 / 15.09	12.6

6.5.3. Analysis and Discussion

Although the applied post-tension force is insignificant in the specimens, two other interesting aspects are found. In the subsequent sections the expected post-tensioning is put in relation to the glass tensile strength and hereafter the ultimate failure is discussed.

[6] For both glueing applications in shear loading the 3M DP490 epoxy adhesive is used.

[7] Analytical value for ultimate failure is based of the measures stiffness from experiment TEN-FIB, as seen in Table 6.8.

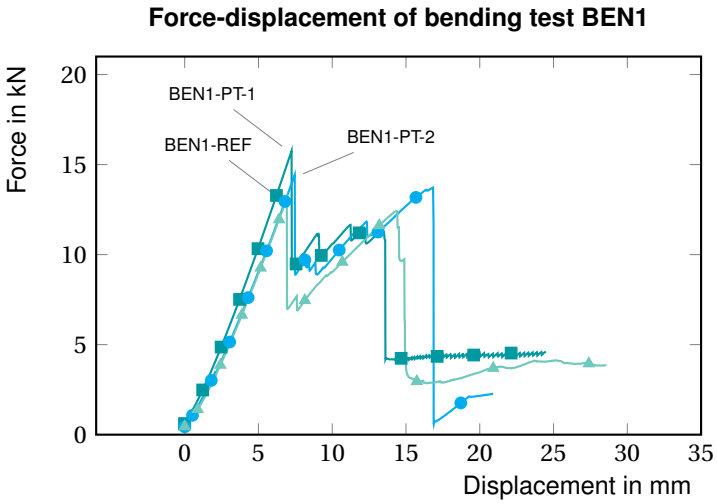

Figure 6.17: Force-displacement diagram of bending experiment BEN1, post-tensioned experiments

Figure 6.18: Crack pattern of failed specimen BEN1-PT-2

Post-tensioning significance

The applied post-tension force in the experiments was too low and a possible increase in initial resistance is insignificant to be observed. Observing the results it does seem that the post-tension (PT) specimen do have increased initial strength due to post-tensioning. But in Table 6.9 is shown that this could not be the case as it could only be increased by 0.25kN. The difference then must come from the spread in tensile strength. When thinking about this concept, the question comes to mind whether the designed post-tension force would be significant enough to be observed. As the estimate is made by analytical calculation a increase of 2.8 kN was expected in the initial failure strength, which is 15% additional resistance on the original value, as designed. Looking at the probabilistic tensile strength properties of glass presented in the research of Veer et al. [2005, 2009] the standard deviations for annealed glass loaded by in-plane bending are 11.8%, 16.1%, 24.3%, 35.3% and 20.1%. To put this in perspective, the standard deviation (s.d.) of glass is about the same order of magnitude as is gained by post-tensioning. So in hindsight, the designed post-tension would have relative low influence on the initial failure. The reasons for this are the safe assumption of the post-tension force ($0.75F_{crit}$), a low critical buckling resistance (F_{crit}) due to the lateral sensitive structure and the normal application of the tension force instead of an extra bending moment. The latter has a high influence. The design would have a better performance when using a more lateral stable design, higher tensioning load and additional eccentricity.

Rotation capacity

Besides the fact insignificance of the post-tension effect, it is observed that neither of the specimens have a resistance higher than initial resistance. This is rather odd since according to the analytical calculation it should have a resistance of at least $F_u = 25.0\text{kN}$. This is not a consequence of the reinforcement strength, as the reinforcement in all specimens are still intact. This raises the question why would the beam not have a higher failure load as it is designed to have? This question is answered when looking at the failed specimen, where cracks are visible in the compressive zone. This is not a compressive zone failure as was observed in Bos et al. [2004] since the present post-tension force was quite low. In this case the cracks are gradually growing towards the compression zone. This is not observed in the case of specimen BEN2-REF and the specimen of Leung [2010] or Louter et al. [2012a]. In these experiments the cracks do not gradually grow, they appear instantly. This is explained by the low stiffness of the reinforcement, relative high strains

are introduced to the glass as the strips are adhered with a high stiffness epoxy. This leads to opening of the cracks and subsequently growing into the compression zone or resulting in bending-shear failure. This failure mode is not often seen in literature and is categorised by the author as a problem regarding the rotation capacity of the beam. This failure mode could be a consequence of the height-to-span ratio and might have a lower effect when SG interlayer was applied.

6.5.4. Summarised conclusion

The objective of 15% increase in initial failure is mentioned as this was an achievable value, but when put in perspective of the failure probabilities of glass it seems insignificant as the design tensile strength is increased to a value which still lies under the mean tensile strength. Attention should be given to the design to increase post-tension effectiveness by applying post-tensioning to more stable system (e.g. box beams,I/T-sections) as is done in Bos et al. [2004].
Sufficient rotation capacity of a beam is required for a glass laminated beam to achieve its full potential. This is limited by the low stiffness of the applied reinforcement, causing earlier ultimate failure. This topic needs further research in order to estimate this bending moment capacity.

6.6. Conclusions

Now all experiments are done and the information is gathered, the validation according to Section 4.3 is carried out. In Table 6.10 the requirements are repeated from the validation-goals. The validation goals are applicable either specific for one case or in general, therefore the specimen name is mentioned or mean values are used. For readability the requirements are transformed to ratio's, to show the magnitude of deviation.

Table 6.10: Overview of experimental validation using the sub-goals from Section 4.3

Requirement	Specimen	Check	Remarks
1. $F_{R,P,i} \geq 1.15 F_{R,i}$	BEN1-PT-1	$15.76/15.53 = 1.015 \ngeq 1.150$	Fault in PT-process
	BEN1-PT-2	$14.43/14.17 = 1.018 \ngeq 1.150$	
2. $F_{R,u} \geq F_{R,i,P}$	BEN1-PT-1	$11.66/15.76 = 0.74 \ngeq 1.00$	Earlier failure due
	BEN1-PT-2	$13.73/14.43 = 0.95 \ngeq 1.00$	low Youngs
	BEN1-REF	$12.41/13.11 = 0.95 \ngeq 1.00$	modulus GFRP
3. $F_{t,FFR} > A_{SG} \cdot f_{u,SG}$	TEN-FFR$_{mean}$	$6845/982 = 6.97 > 1.00$	
4. $F_{t,FFR} \geq F_{t,GFRP}$	PULL-FFR/REF$_{mean}$	$1821/4619 = 0.39 \ngeq 1.00$	No pull-out with FFR specimen
5. $F_{R,u,FFR} \geq F_{R,u,GFRP}$	BEN2-FFR/REF$_{mean}$	$3531/7256 = 0.49 \ngeq 1.00$	
6. $F_{R,u,FFR} \geq F_{R,i,FFR}$	BEN2-FFR-1	$3419/3762 = 0.91 \ngeq 1.00$	
	BEN2-FFR-2	$3864/4259 = 0.91 \ngeq 1.00$	
	BEN2-FFR-3	$3311/4974 = 0.67 \ngeq 1.00$	

From the table above it can be concluded only one of the validation goals is achieved, namely, the tensile experiment which has a higher resistance as only SG. As these are just value, the more specific origin of these results and how this is possible are described in the former analysis and sub-conclusions per experiment. The faults can be summarised as; incorrect specifications from manufacturer, insufficient saturation of fibre-glass and error in post-tensioning process. Although the validation goals are not met, it can be concluded that the concept of FFR is feasible but only needs some enhancement regarding saturation.

7

Finite element analysis

This chapter consist out of two parts, first a numerical study is done using several developments from former research and analyse their applicability on RG beams. Their influence on the performance is analysed using the four performance aspects of Section 4.3.3 and the reference model. This is done by defining the goals, then the numerical and material models and hereafter the study is performed. The second part uses these findings to conclude their influences and are then accumulated in the validation models. Subsequently these are used to validate the models based on the experimental data.

7.1. Problem statement and Goal

As is seen in the background of this thesis in 2.6 some numerical research are already done in several finite element software, where for instance ABAQUS is quite popular. Additional subroutines are used to create a higher stability during the calculation. The counter effect of these solution finding subroutines[1] is the computation time. The SLA method is desirable due to its stability, as this method uses only linear analysing methods. This method is explained in background Section 2.6.4 and it currently under development. The downside of its development is that its functions are still limited. Some promising results are achieved in previous work (Graaf et al. [2008]; Invernizzi et al. [2011]; Louter et al. [2010b]). As the method is still in development, some interesting research is done outside the field of RG, those improvements are worth looking into with the goal to seen for their applicability and influences on RG structures.
As stated in 4.3, the main goal of the numerical analysis in this thesis is to validate the SLA method using newly found solutions for the different reinforced glass structures, to create a reliable estimation of failure moments and behaviour. And in addition to the main goal the post-tensioning and the additional resistance capacity mentioned in 2.6.2 are implemented.

7.2. Approach

In the risk section of Chapter 1 is mentioned that in addition to the experimental data a reliable data set is used to firstly analyse the independent developments in method and parameter application. In the work of Louter et al. [2012a] this case is found, here, the embedded stainless steel hollow section, as pictured in Figure 7.2 is researched in experimental manner. In the work of Bedon and Louter [2014] these specimen are used as reference for a NLA in ABAQUS. The numerical model is based on this work and can also be used to see the difference between NLA an SLA. This model is used to compare the independent parameters/design choices and analyse their influence of the performance. The experimental data sets are used to validate the application to the improved SLA method using the found influences. This approach is visualised in Figure 7.1.
In addition to the parameter analysis based on the reference model, the modelling of post-tensioning is

[1] Subroutines like, arc-length method and double precision are used in the work of Bedon and Louter [2014]

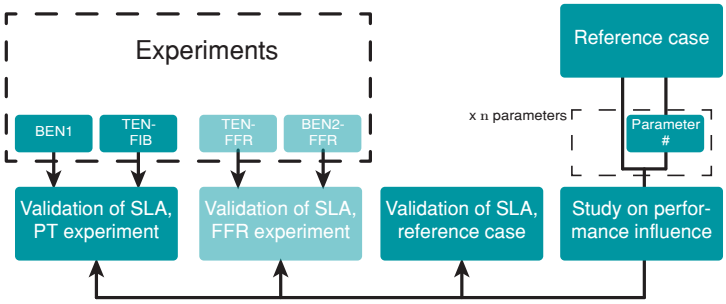

Figure 7.1: Flow chart of numerical research

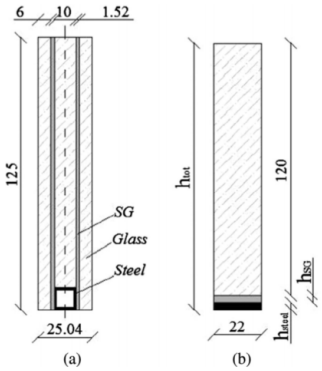

Figure 7.2: Cross-section of reference case specimen (a) and mechanical model (b) from Bedon and Louter [2014]

done based on the BEN1 design. This is done as this experiment is designed for post-tensioning and in this manner the numerical goal of modelling post-tension in SLA can be achieved.
In each independent influence study an analysis and conclusion is made to summarise the performance using the predefined aspects as stated in 4.3.3.

7.2.1. Validation data

In the Chapter 1 is mentioned the risk of uncertain results from the bending experiments which could cause the inability to validate the numerical approach. This was solved using the reference case. Due to the differences in configurations of the experiments, validation of these cases have a beneficial effect and shows the broader application.
From experiment BEN1 it is known that the post-tension was negligible, therefore this experiment can not be used to validate post-tension implementation. On the other hand it still can be used as an ordinary GFRP strips RG structure. Hence, this data set can be used for validation. The experiments BEN2 were executed as they were planned, but the physics of the FFR are rather challenging to model. Together with the lack of truss element implementation (See Section 2.6.4), it is decided not to use this set in the validation procedure and is therefore a lighter colour in the overview scheme of Figure 7.1.

7.3. Numerical model

In this section the numerical models are defined. In total there are two models, Model M-REF, which is used for the parametric study and validation of SLA (Figure 7.4a). And Model M-BEN1 is based on experiment BEN1 which is used for the post-tension implementation and validation (Figure 7.4b). The basic parameters are discussed in Section 2.6 and are the starting conditions for the models. The reference will be used to relate the influences of specific parameters or modelling choices. Since M-REF is based on the model found in the paper of Bedon and Louter [2014], the following starting parameters used in order the recreate an equal model. Besides these parameters, the constant shear retention is replaced by the shear retention based on damage as is explained in background Section 2.6.4. The reference model consist of;

- Single symmetric model;

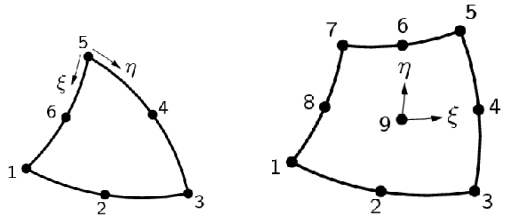

(a) Triangular CT12M element

(b) Quadrilateral CQ16M element

Figure 7.3: Chosen elements which are used in the numerical calculations

- 2D plane stress elements;
- Snap-back glass model ($G_f = 3.0\mathrm{J/m^2}$) ;
- Linear elastic adherence layer, stiffness based on Louter and Nielsen [2013];
- Ultimate strain of snap-back curve / cracked length of element, ($u_{ck} = \varepsilon_u \cdot h = \frac{2G_f}{f_t}$)[2];
- Killing element principle[3].

7.3.1. Model dimensions, mesh and elements

The basic models are all 2D single symmetric models with respect to the length of the beam and are displayed in Figure 7.4. Therefore the displacement restrictions in horizontal direction at the centreline are applied and the vertical support is modelled to move freely in horizontal direction to prevent catenary forces. In the Figure is seen that a uniform single diagonal triangular mesh is used for glass and uniform quadrilaterals for reinforcement. Quadrilaterals are used as rupture of the reinforcement will only occur in transverse direction and crack development is not of interest here, as is mentioned in background Section 2.6.3. In the models 2D triangular and quadrilateral quadratic plane-stress elements CT12M and CQ16M are used[4] and pictured in Figure 7.3. Quadratic order is chosen for higher precision regarding crack formation. Even higher precision for the quadrilaterals was possible using nine nodes, but this is not necessary since they are only applied in the reinforcement, where cracking is not as important as in the glass.

7.3.2. Used material parameters

An overview is given of the basic material parameters in Table 7.1. Unless otherwise stated these are the parameters which are used in the calculation. The GFRP reinforcements are physically orthotropic materials due to their manufacturing lay-up. But their orthotropic properties exist in the third dimension so this will not be used in this 2D model and are therefore simplified to isotropic materials, thus only one elasticity modulus is given in the applicable direction.
Some aspects in Table 7.1 should be noted. Most materials are modelled linear elastic and therefore only a Young's modulus (E) and tensile strength (f_t) are given. As the stainless steel and SG have a plastic behaviour they have additional data. The values for stainless steel are based on the experimental data given by Louter et al. [2010a]. The plastic properties of SG are taken from the manufacturer, although these can differ due to their visco-elastic behaviour (Santarsiero et al. [2016]), but this is not considered. Furthermore, a '/' is used to distinguish manufacturer's and experimental data for the GFRP strips. For the use of SG two values are present, SG1 is based on the manufacturer and used for the interlayer implementation, only tensile straining is assumed in normal direction. Where SG2 is used for modelling the linear elastic adherence between the steel reinforcement acting in shear as is researched in the work of Louter and Nielsen [2013], although in the work of Bedon and Louter [2014] is seen that this does not influence the results. A value of $G = 40\mathrm{MPa}$ is converted to Young's modulus using the Poisson ratio, according to the constitutive

[2] Ultimate crack elongation can only be implemented as ultimate strain, the difference in smeared cracking lies in the multiplication with the crack bandwidth (h), as explained in 2.6.1.

[3] The killing element principle is a sub-routine in ABAQUS, while in SLA this principle is covered by the dummy branch in the reduction curve, this mentioned in Section 2.6.5 of the background and its influence is elaborated in Section 7.6.1.

[4] Similar possibilities are; plane-strain elements which are used for cross-sections of infinite long structures; plane-stress elements with the orthotropic thickness, as both possibilities are not applicable these elements are not chosen.

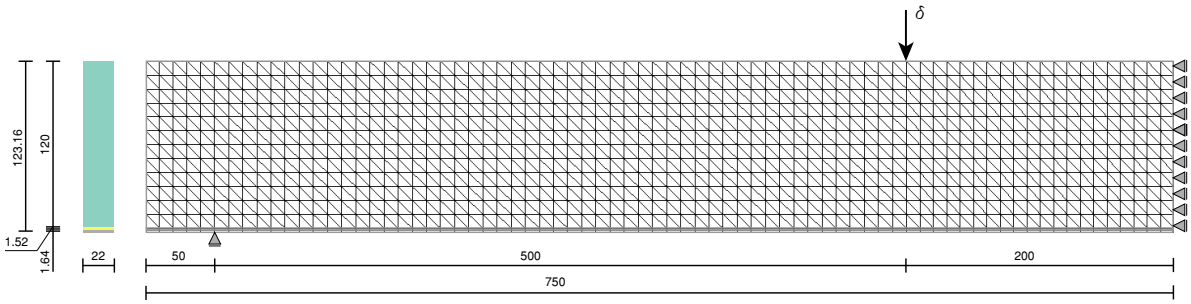

(a) M-REF

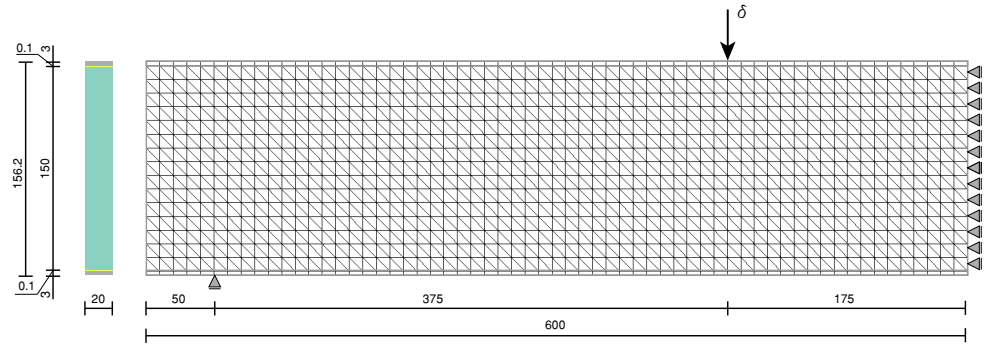

(b) M-BEN1

Figure 7.4: Dimensions of different numerical models which are used.

law $G = \frac{E}{2(1+\nu)}$.

7.4. Material models

In the background Section 2.6.5(figures 2.23 and 2.24) the two possibilities of modelling the material's constitutive relation are mentioned. Either a distribution along the exact mother curve or to create a saw-tooth around it, summarised in Figure 7.5. Both options have their pro's and cons. In the subsequent sections they will be discussed and chosen which is used as starting point for each material.

7.4.1. Glass model

For the glass material model it is easily decided which kind is the best applicable. Due to the importance of the fracture energy the saw-tooth approach is chosen, as is proven by Rots and Invernizzi [2004]. Although small deviations occur in the tensile strength of the reduction curve, the overall fracture energy remains

Table 7.1: Table of the used material parameters for the numerical simulations

Material	E [GPa]	f_t [MPa]	f_u [MPa]	ε_u u.l.	ν u.l.	$h \times b$ mm	Source
Glass - ANG	70	45	-	-	0.23	-	Bedon and Louter [2014]; NEN-EN 2608 [2016]
Steel - EN1.4301	200	220	550	0.275	0.3	1.64×22	Louter et al. [2010a]
GFRP - Fibrolux	40/15.3	900/568	-	-	0.23	3×20	Fibrolux
SG1 - interlayer	0.300	34.5	34.5	4.0	0.49	-	Kuraray [2014a]
SG2 - adherence	0.119	-	-	-	0.49	-	Louter and Nielsen [2013]

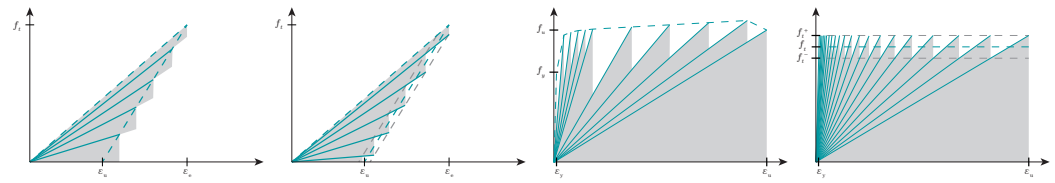

(a) Uniform distribution (b) Saw-tooth approach (c) Divided mother curve model for plastic material (d) Saw-tooth model for plastic material

Figure 7.5: Summary of possible material models for glass and steel

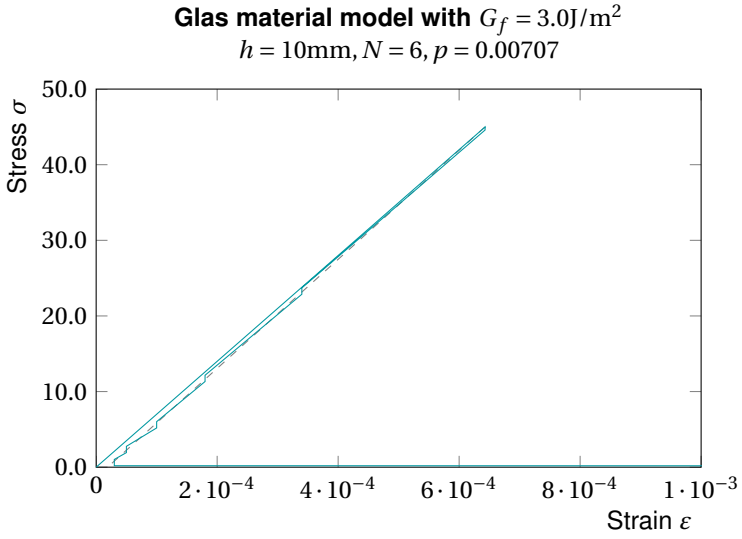

#	f_t [MPa]	ε_e [–]
1	45.0	$6.4 \cdot 10^{-4}$
2	23.7	$3.4 \cdot 10^{-4}$
3	12.1	$1.82 \cdot 10^{-4}$
4	6.0	$9.66 \cdot 10^{-5}$
5	2.76	$5.13 \cdot 10^{-5}$
6	1.02	$2.73 \cdot 10^{-5}$
7	$0.1 \cdot 10^{-6}$	$2.73 \cdot 10^{-2}$ (dummy)

Figure 7.6: General glass constitutive relation used within this thesis

equal and it is off less importance that these $f_{t,i}^{+}$ points are a fraction higher than the snap-back curve. As is already mentioned the fracture energy of $G_f = 3.0\text{J/m}^2$ is used within this thesis and for the reference model a crack bandwidth of $h = 7.07\text{mm}$ is used[5]. These parameters result in the saw-tooth curve of Figure 7.6. The dummy branch from Section 2.6.5 is also visible here.

7.4.2. Reinforcement models

For the brittle reinforcement materials the reduction does not create any issues since the brittle failure model is assumed. The reduction contains no strain alterations and therefore the reduction points lie in a vertical line at ε_e. A uniform distribution of $N = 6$ branches is used. For the steel reinforcement model it is a bit more complicated, as stated in the background, the number of reduction steps is constrained to the height of the teeth. This creates the situation of either heigh number of teeth or large deviations in tensile strength. In this case the tensile strength of the plastic reinforcement determines the post-cracked resistance capacity of the beams. The accuracy of the tensile strength is more important than the energy required till rupture occurs. This does mean that the ultimate strain estimation is not accurate, but this was already not the case due to the sequential linear approach in this analysis. Therefore the material model used by Louter et al. [2010a] is used.

7.5. Reference model

The reference model a extension of Louter et al. [2010b] where it successfully calculated the acrylate adhesive GB368 (GB) glass laminate using SLA, as is seen in Figure 7.7. But as mentioned in the background, it does lacks the implementation of additional SG resistance (Louter [2011]). All information ac-

[5] This is based in the triangular element size of 10 mm, which results in $h = \sqrt{A} = 7.07$ (Section 2.6.3).

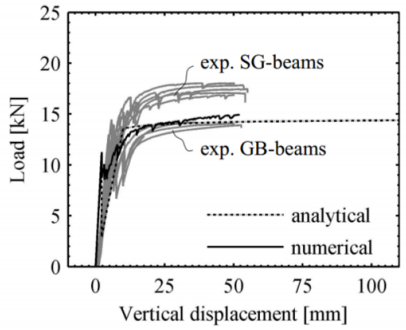

Figure 7.7: Difference between GB and SG adhered specimen from Louter [2011]

quired and calculated previously are used to construct the reference model which is called M-REF[6]. The force-displacement curve of the reference model is displayed in Figure 7.8 here the exact output of the analysis is plotted in thin grey lines. For the sake of clarity of the force-displacement curve a displacement controlled curve is constructed. The simulation is considerate failed after 2342 iterations by rupture of the reinforcement as is seen in its crack sequence in Figure 7.9. Ultimate failure of the model is defined as the occurrence of a drop in resistant force, that is more than half of the resistance before the drop[7]. These principles are maintained throughout the thesis.

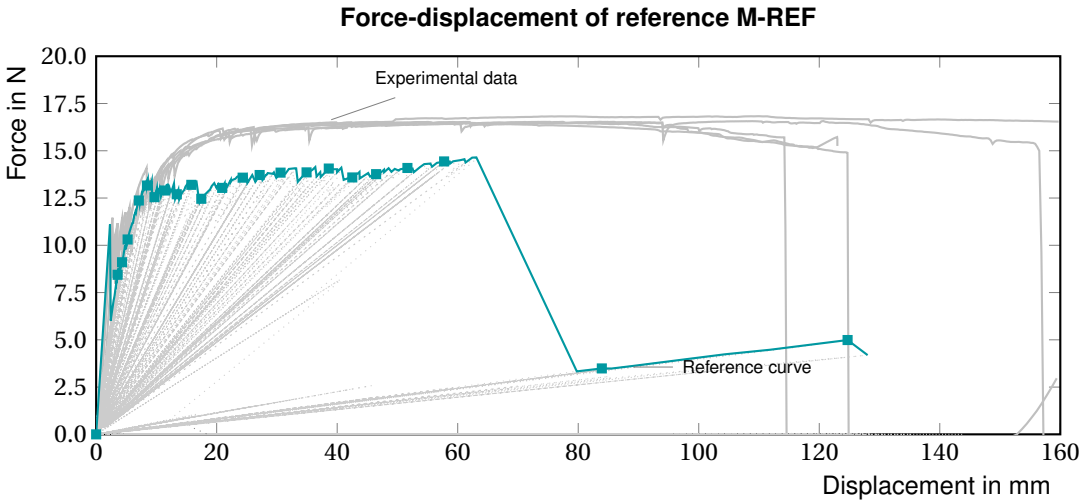

Figure 7.8: Force-displacement curve of reference model

7.6. SLA parameter analysis

Now the reference model is defined, a parametric study is done on the developments of SLA. The influences of some modelling choices are shown and discussed, namely the implementations of;

- the dummy branch;
- SG resistance;
- Adherence layer of reinforcement;
- Material models;

[6] The used material models are based on Section 7.4 where the dummy branches are taken into account. These implementations were not seen in the work of Louter et al. [2010b], it is unsure how is dealt with the residual strength after full damage. More of this effect on the in Section 7.6.1

[7] The quantification of the drop at failure is rather arbitrary as this drop is a consequence of the large straining of the critical element it occurs together with high deflections from which the failure of the system can be concluded.

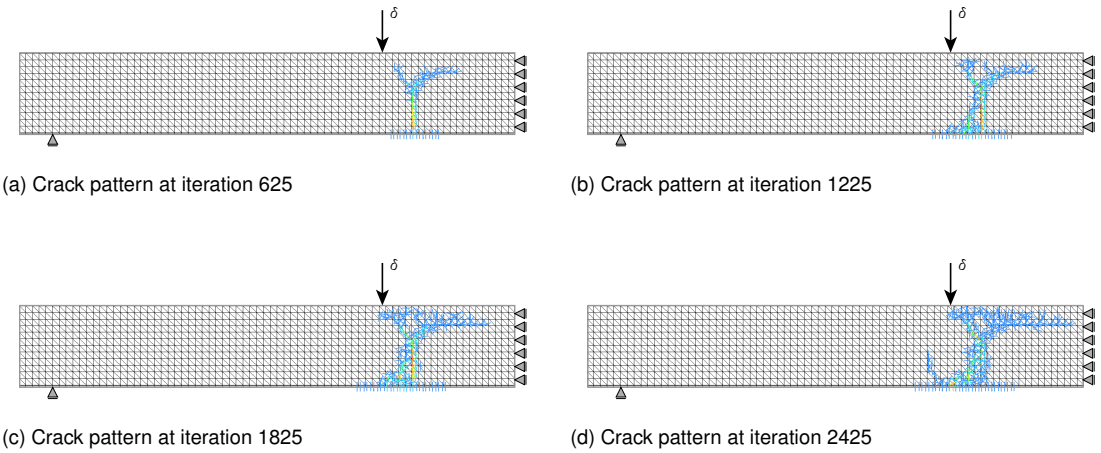

(a) Crack pattern at iteration 625

(b) Crack pattern at iteration 1225

(c) Crack pattern at iteration 1825

(d) Crack pattern at iteration 2425

Figure 7.9: Crack patterns sequence of reference model

- Mesh differences;
- Post-tension.

7.6.1. Influences of dummy branches

As mentioned in the background Section 2.6.5, the dummy branch is the definition of the last branch, which contains high strain limit and low tensile strength. This branch is used to simulate the absence of residual strength after cracking, thus creating the critical even elsewhere. In the work of Kraus [2014] the effect of the dummy branch is already seen for concrete structures. In this section, the force-displacement curve is assessed on model M-REF with dummy branches in both the reinforcement and the glass model and separately. When no dummy branch is applied to last branch (e.g. branch #7 in Figure 7.6 is disabled)[8]. To analyse the affects this has on the crack development, the crack patterns are shown for both cases. Since both crack patterns are equal at the same iteration as M-REF the crack pattern at failure of the model without reinforcement dummy (deflection ≈ 107mm) is taken to analyse how the simulations differ in crack development (Figure 7.11).

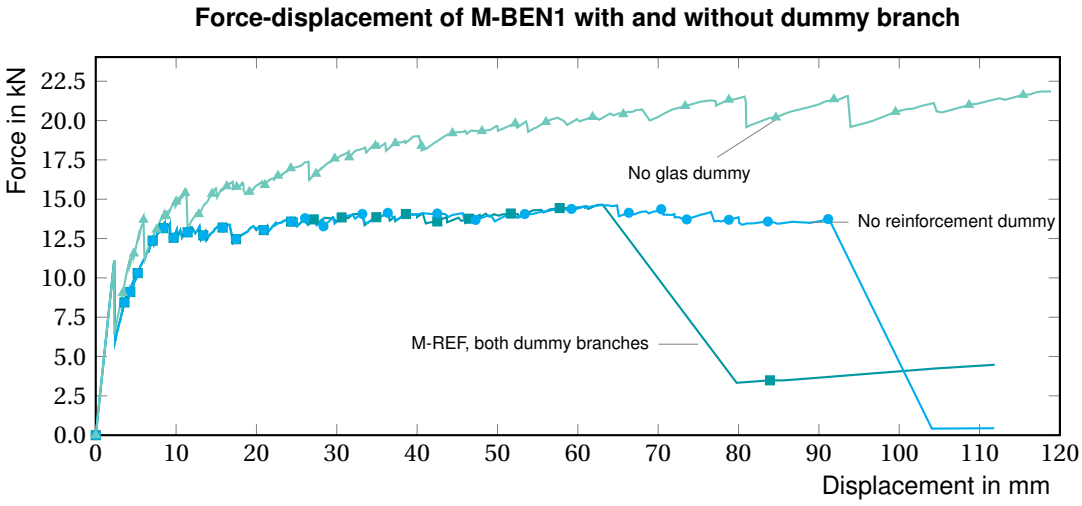

Figure 7.10: Force-displacement diagram of M-REF with and without dummy branches applied in reinforcement and glass models

[8] It should be noted that the magnitude of the dummy branches are not quantified in the work of Kraus [2014]. In this analysis the magnitude is multiplied by 10^3 for the glass case and 2 times in the reinforcement model, which is assumed large enough to observe differences and have negligible influences on the residual strength but its magnitude remains arbitrary.

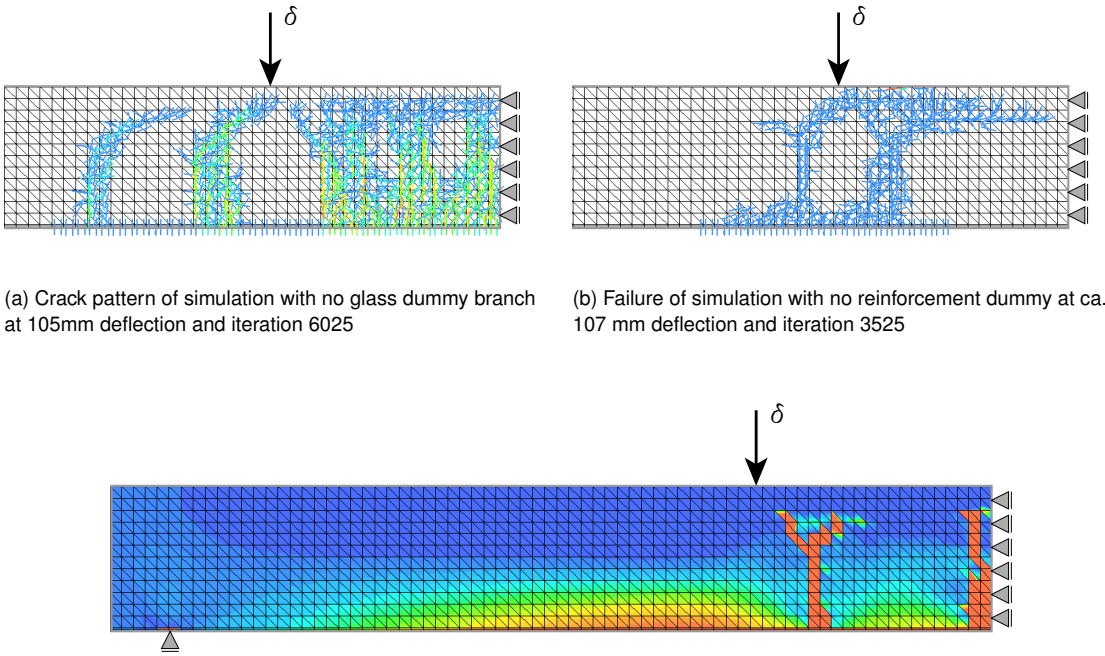

(a) Crack pattern of simulation with no glass dummy branch at 105mm deflection and iteration 6025

(b) Failure of simulation with no reinforcement dummy at ca. 107 mm deflection and iteration 3525

(c) Strain xx in simulation without glass dummy at bringe of crack (iteration 775),

Figure 7.11: Crack patterns development with no dummy branches at equal deflection

Analysis

The absence of dummy branch in the glass model means that glass is left with its residual strength. This leaves the model unable to achieve 'ultimate failure' within the expected range as its strains are limited. Equilibrium is found by creating more cracks at a certain distance from the previous where the force in the reinforcement is lower and thus the stress in the glass is higher, which is seen in the display of strain at an earlier stage (Figure 7.11c). The number of iteration steps and crack density are also higher at the same point of deflection (Figure 7.11a and 7.11b). The is due to the small remaining stresses and strains of the glass with respect to reinforcement stresses and strains, thus more iterations are required to have equal displacement and subsequently more cracks are developed. Looking at the reinforcement model, the absence of the branch leads to a larger deflection of the simulation, since it does not fails by reaching the dummy branch now as it did in the reference model. This create the opportunity for the glass to develop the earlier initiated crack upon reaching their dummy branch, i.e. achieve high straining and failure occurs. It is observed that this case does not increase strength resistance, this is because the ultimate reinforcement strength is already governing for the total resistance and does not add extra resistance when remaining constant.

Conclusion

From the force-displacement curve (Figure 7.10) the influences are clearly visible and their performance with respect to the reference is summarised in Table 7.2. Two cases are analysed, the absence of the dummy branch for the glass and reinforcement model. It is concluded that the absence of the branch with respect to the glass model leaves remaining strength. This is an incorrect increase in the force-displacement curve as this should not happen. Also higher crack density is seen as more iterations are required due to the small remaining strain and stress. As for the second case the absence of the dummy branch in the reinforcement model prevents the reinforcement from rupture. This results in additional deflection as yielding of the steel is spreads. The developed crack pattern is as expected as this is an extension of the reference case. The application of the dummy branch thus create the possibility for rupture of reinforcement and glass crack to open.

Table 7.2: Performance of the application of the dummy branches

Performance aspect	No glass dummy branch	No reinforcement dummy branch
Resistance capacity	+	0
Deformation	+	+
Crack density	+	0
Amount of cracks	+	+

7.6.2. SentryGlass implementation

Based on the definition of the dummy branch explained in the background Section 2.6.5, the dummy branch principle is taken one step further. Where the dummy branch is applied to represent cracked material with no strength left, the SG implementation will be used for defining residual strength after glass failure. Since this is seen in Belis et al. [2009]; Bos [2009]; Louter and Cupaç [2014] some residual strength is left after breakage of the section when a SG interlayer is used, it is concluded that the interlayer does contribute to the load bearing capacity after failure of the glass. In Table 7.3 the properties of SG are shown and it looks quite strong, but this is only a false sight of numbers. Due to the large yield strain and low elasticity modulus the strength at the strain of glass failure is significantly less than the glass. Also, the SG interlayer is relatively thin with respect to the glass. Which all results at a low contribution to the load bearing capacity of the section before initial failure.

Table 7.3: Mechanical properties of SG

Property	unit	value
$f_{t,y}$	MPa	34.5
E_{SG}	MPa	300
$\varepsilon_{t,y}$	%	11.5
$\varepsilon_{t,u}$	%	400

The SG properties are assumed to become active after glass failure, since its strength at ultimate strain of glass is too low to contribute and is therefore neglected[9]. In Figure 7.13a this implementation is shown in the material model of glass, where the specific glass and SG parts are shown in their relation. Due to the difference in thickness, which is roughly 10% in this case, the SG strength properties are reduced. If this is neglected the load resistance would become almost as high as the glass itself which obviously is not the case. This reduction is explained in equation 7.1, where the transformation from glass to SG is represented. By equalising the force in the element with $A \times \sigma$ of both the element and the SG and assuming $A^{(i)}_{elem} \neq A^{(i)}_{int}$, this yields that a adjusted Young's modulus (E^{*}_{int}) is required in order to create equilibrium. Furthermore, this is used to calculate the reduced strength and Young's modulus in equations 7.2 and 7.3 by knowing that the yield strain ($\varepsilon_{t,y}$) the reduced strength is calculated which subsequently is used to calculated the reduced Young's modulus in equation . Here for with the indices i and j for element and iteration respectively[10] is shown in general and its equivalent for the interlayer.

$$F^{(i)}_{elem} = A^{(i)}_{elem} \cdot \varepsilon^{(j)}_{elem} \cdot E^{(i,j)*}_{elem} = A^{(i)}_{int} \cdot \varepsilon^{(j)}_{elem} \cdot E^{(i,j)}_{int} \tag{7.1a}$$

For the adjusted elasticity modulus this yield:

$$E^{(i,j)*}_{elem} \cdot \varepsilon^{(j)}_{elem} = \frac{A^{(i)}_{int}}{A^{(i)}_{elem}} \cdot E^{(i,j)}_{int} \cdot \varepsilon^{(j)}_{elem} = \frac{h \cdot t^{(i)}_{int}}{h \cdot t^{(i)}_{elem}} \cdot E^{(i,j)}_{int} \cdot \varepsilon^{(j)}_{elem} \tag{7.1b}$$

Which is then equal to

$$E^{*(i,j)}_{elem} \cdot \varepsilon^{(j)}_{elem} = \sigma^{(i,j)*}_{elem} = \frac{t^{(i)}_{int}}{t^{(i)}_{elem}} \cdot \sigma^{(i,j)}_{int} \tag{7.1c}$$

[9] It should be noted that the SG strain does not start after failure of the glass but at zero strain just as the other materials (thus $\varepsilon_0 = 0$ and $\varepsilon_0 \neq \varepsilon_{g,u}$)

[10] The elasticity modulus has both indices i and j since it is dependent on the element, i.e. material, and the iteration in consideration of SLA

Thus, by modifying the stress properties of the interlayer to an equivalent stress the interlayer properties remain unchanged.

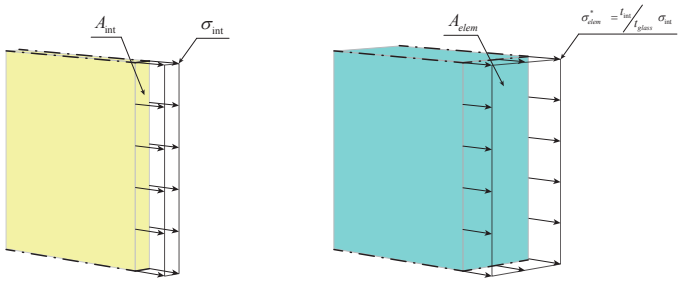

(a) Real stress in interlayer (b) Transformed stress for equal area

Figure 7.12: Illustration of transformation from glass to SG

$$f^*_{t,y} = \frac{t_{int}}{t_{glass}} \cdot f_{t,y,int} = \frac{2 \cdot 1.52}{22} \cdot 34.5 = 4.76\text{MPa} \tag{7.2}$$

$$E^*_{SG} = \frac{f^*_{t,y}}{\varepsilon_{t,y}} = \frac{4.76}{0.115} = 41.4\text{MPa} \tag{7.3}$$

Table 7.4: Reduced mechanical properties of SG

Property	unit	Original value	Reduced value
$f_{t,y}$	MPa	34.5	4.76
E_{SG}	MPa	300	41.4
$\varepsilon_{t,y}$	%	11.5	11.5
$\varepsilon_{t,u}$	%	400	400

The force-displacement curve is plotted in Figure 7.13 where the influence of the SG addition is clearly seen. These results are based on M-REF without reinforcement, as the experimental data is from the reference specimen from Louter and Cupaç [2014] are of equal dimensions as the model reference model. In the force-displacement curve of Figure 7.13 the residual strength due to the SG is seen. The difference in residual capacity is explained by the lack of de-bonding implementation in the model. But for this thesis the SG interlayer is only used as strength increase where rupture of the interlayer not a governing failure mode is, therefore this method can be applied.
In Figure 7.13a the glass reduction curve is plotted with the additional of SG properties. Since the differences in strain are quite large the glass part is flattened against the left axis, but this part is discussed in Section 7.4.1.

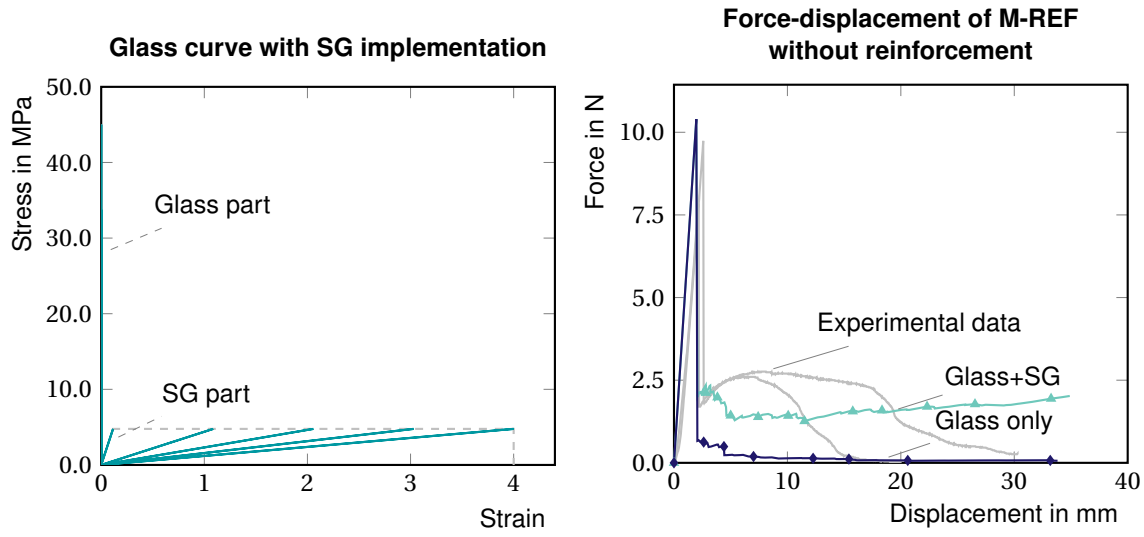

Figure 7.13: Force-displacement diagram with implementation of SG and experimental data from Louter and Cupaç [2014]

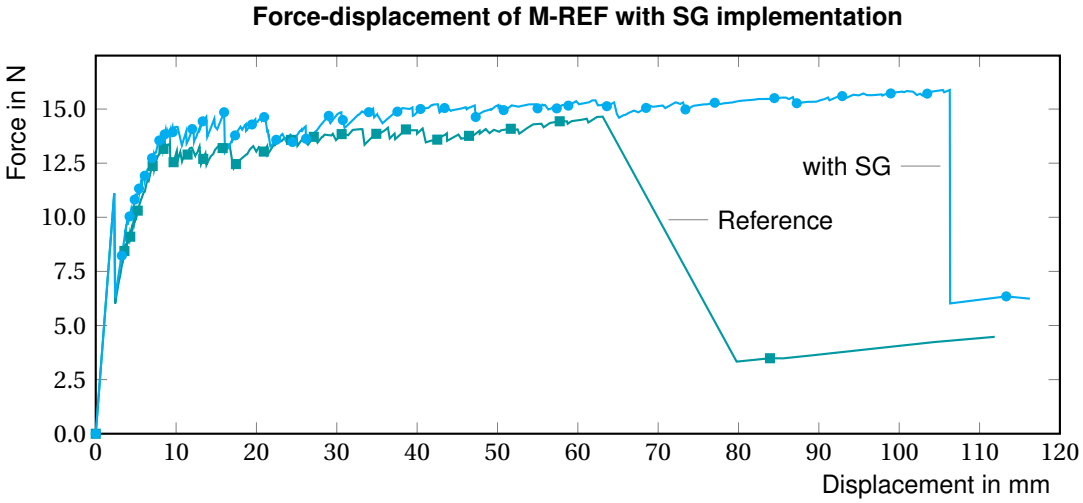

Figure 7.14: Force-displacement diagram with implementation of SG

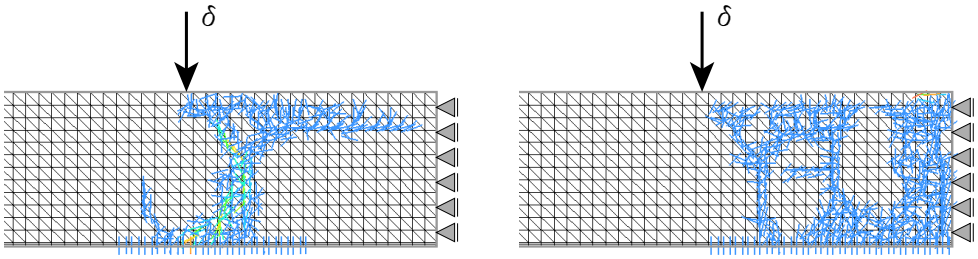

(a) Crack pattern of reference model

(b) Crack pattern of reference model with SG implementation

Figure 7.15: Difference in crack pattern with SG implementation at equal displacement

Analysis

An increase in strength resistance is seen in the force-displacement curve of the SG laminated glass beam without reinforcement in Figure 7.13. Although a post-cracked resistance is found the resistance is only half the strength which is seen in the experiments (Figure7.13). This could be explained in the de-bonding of the SG interlayer to the glass. Also the deflection in the experiments is a lot less than seen in the simulation. This could be the further de-bonding of the interlayer or rupture at lower strains than expected. Both observations requires further research to complete the understanding of the physical performance of the SG. In this case the additional resistance is what was expected although not fully achieved. The deformation difference due to the inability of de-bonding is not a major problem as this is not the governing failure mode for the reference case. In Figure 7.14 the SG branches are added to the reference model causing the predicted increase in resistance capacity. The crack pattern also shows a higher crack density, which is also observed in the absence of a dummy branch in Figure 7.11a. This is the consequence of restrained crack opening as mentioned in the dummy branch Section 7.6.1, this also causes more cracks to develop.

Conclusion

The addition of post-cracked resistance due to the transformed SG properties is proven to have a positive effect on closing the remaining resistance gap. This gap however in not fully covered as the physics of the SG behaviour are not fully known and need further research. This application also results in a more dense crack pattern and a higher deflection as the SG implementation restrains the crack opening. In Table 7.5 the performance is summarised.

Table 7.5: Performance of the application of SG implementation

Performance aspect	SG implementation
Resistance capacity	+
Deformation	+
Crack density	+
Amount of cracks	+

7.6.3. Fracture energy effect

Based on 2.6.5 a small investigation in done for the fracture energy values ($G_f = 3.0, 5.0 \text{and} 8.0$) all in combination with five branches (N=5). This is done to compare the differences in crack pattern to see if the impact of a alteration in fracture energy is significant.

The different glass failure curves are defined by the constitutive laws and the saw-tooth diagram as explained in the background Section 2.6.5. Four curves are observed, with the same fracture energy as in the work of Bedon and Louter [2014]. For the brittle model the failure curve is vertical, resulting in a ultimate strain equal to the elastic failure strain ($\varepsilon_u = \varepsilon_e$). The ultimate strains of the snap-back models are calculated below according to the relations described in the background Section 2.6.5. The triangular element are modelled with a size of 10 mm, as is mentioned in the background Section 2.6.3 the crack bandwidth in this analysis is defined as $h = \sqrt{A}$. For this uniform mesh the crack bandwidth is then maintained to 7.07 mm. Which leads to the following ultimate strains:

Elastic strain $\varepsilon_e = 6.4 \cdot 10^{-4}$;

$G_f = 3.0$ $\varepsilon_u = 1.88 \cdot 10^{-5}$, equal to 2.93% of ε_e;

$G_f = 5.5$ $\varepsilon_u = 3.46 \cdot 10^{-5}$, equal to 5.38% of ε_e;

$G_f = 8.0$ $\varepsilon_u = 5.03 \cdot 10^{-5}$, equal to 7.82% of ε_e;

Brittle $G_f = 144.6 \text{J/m}^2$.

Analysis

These four glass models are plotted in Figure 7.19 and used in a numerical calculation of M-REF resulting in the force-displacement curve of Figure 7.17. In this diagram no significant difference is seen, therefore a closer look it taken at the force-iteration step curve in Figure 7.18. As is mentioned by Bedon, differences in crack patterns are observed which are seen in Figure 7.16, therefore the crack patterns at pre-failure stage are visualised to look for differences[11]. As is seen, these differences are not found, the only difference is

[11] It should be noted that the vertical lines at the bottom indicate the yielding of reinforcement.

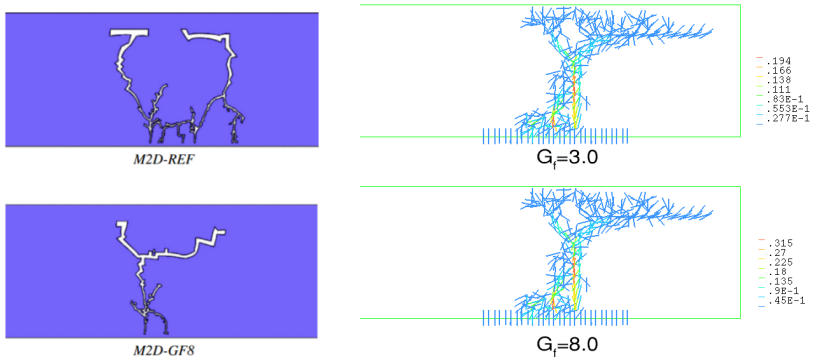

(a) Crack differences from Bedon (b) $G_f = 3.0$ and $G_f = 8.0$

Figure 7.16: Zoomed cracks from different models

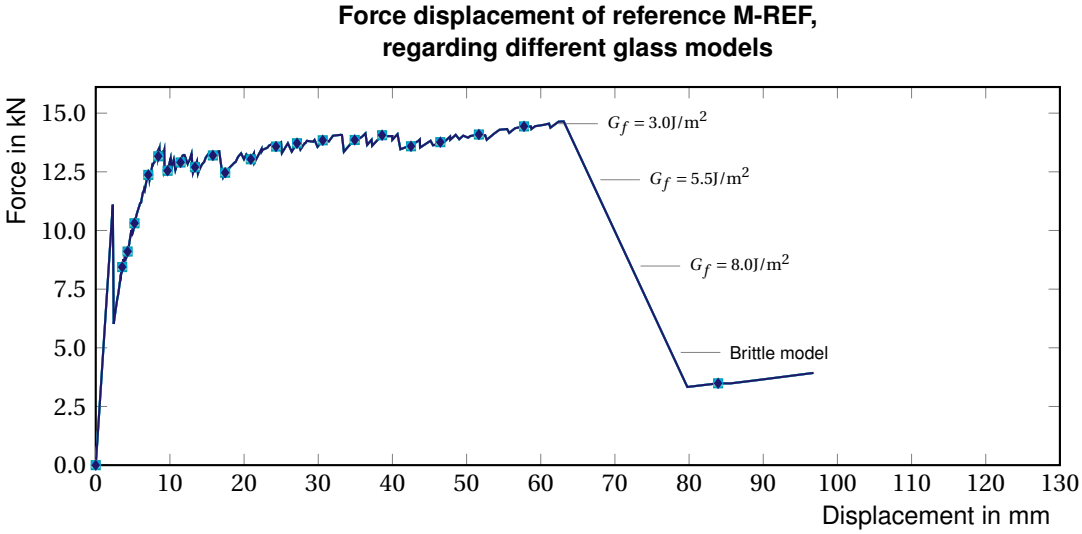

Figure 7.17: Force-displacement diagram from SLA model with different glass models

observed in the force-iteration curve where the brittle model fails at less iterations. A plausible explanation could be that this is caused by the combination linear elastic analysis, fixed cracking and strain difference but this is challenging to prove, as the SLA differs quite a lote from NLA and rotational cracking is not implemented. The shift in iterations in the brittle simulation causes difficulties in finding a sound comparison. For the $G_f = 3.0$ and $G_f = 8.0$ models this can be done as their iterations are synchronised. The crack strains are pictured in Figure 7.16b[12]. Here is seen that the strains are larger for the $G_f = 8.0$ model and thus suggest that the post-cracked strain magnitude is present and the higher strain of the brittle model could therefore cause failure at lower iterations.
Comparing the crack patterns with NLA, the differences seem large at first. But especially for the M2D-GF8 model the same trend is seen, where the crack is growing both horizontally to mid span and directly to the load. The explanation of differences between the ABAQUS models lies beyond te scope of the thesis, as no difference are found in this analysis but they are in the NLA, more research is required to conclude the significant influence of the fracture energy.

Conclusion

Four glass material models are analysed in order to look for the differences in crack patterns as is suggested by Martens et al. [2016b] and Bedon and Louter [2014]. No differences are found in the force-displacement curve as expected. However also no differences are seen in the crack pattern, no solid conclusion can

[12] It should be noted that this is not a governing iteration step as these strains correspond to the 2325 iteration with 13.6 kN at 55mm deflection

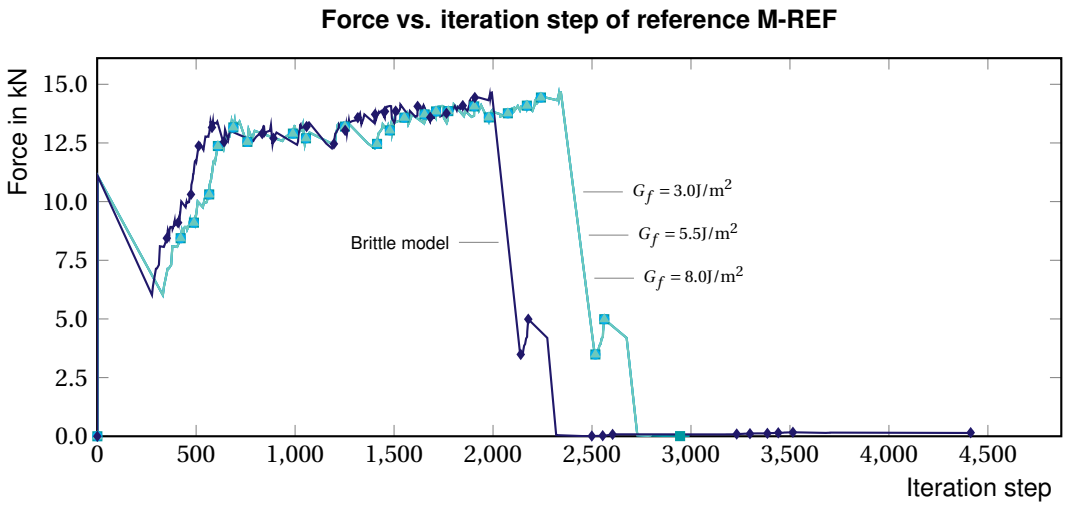

Figure 7.18: Diagram of strength vs. iteration step of different glass material models.

be made why no differences are found and needs further research where the analysing method and the cracking method are the major point of attention. In Table 7.6 the overview is given, but as mentioned before no differences are observed within the performance aspects.

Table 7.6: Performance of the different glass models

Performance aspect	$G_F = 5.5$	$G_F = 8.0$	**Brittle**
Resistance capacity	0	0	0
Deformation	0	0	0
Crack density	0	0	0
Amount of cracks	0	0	0

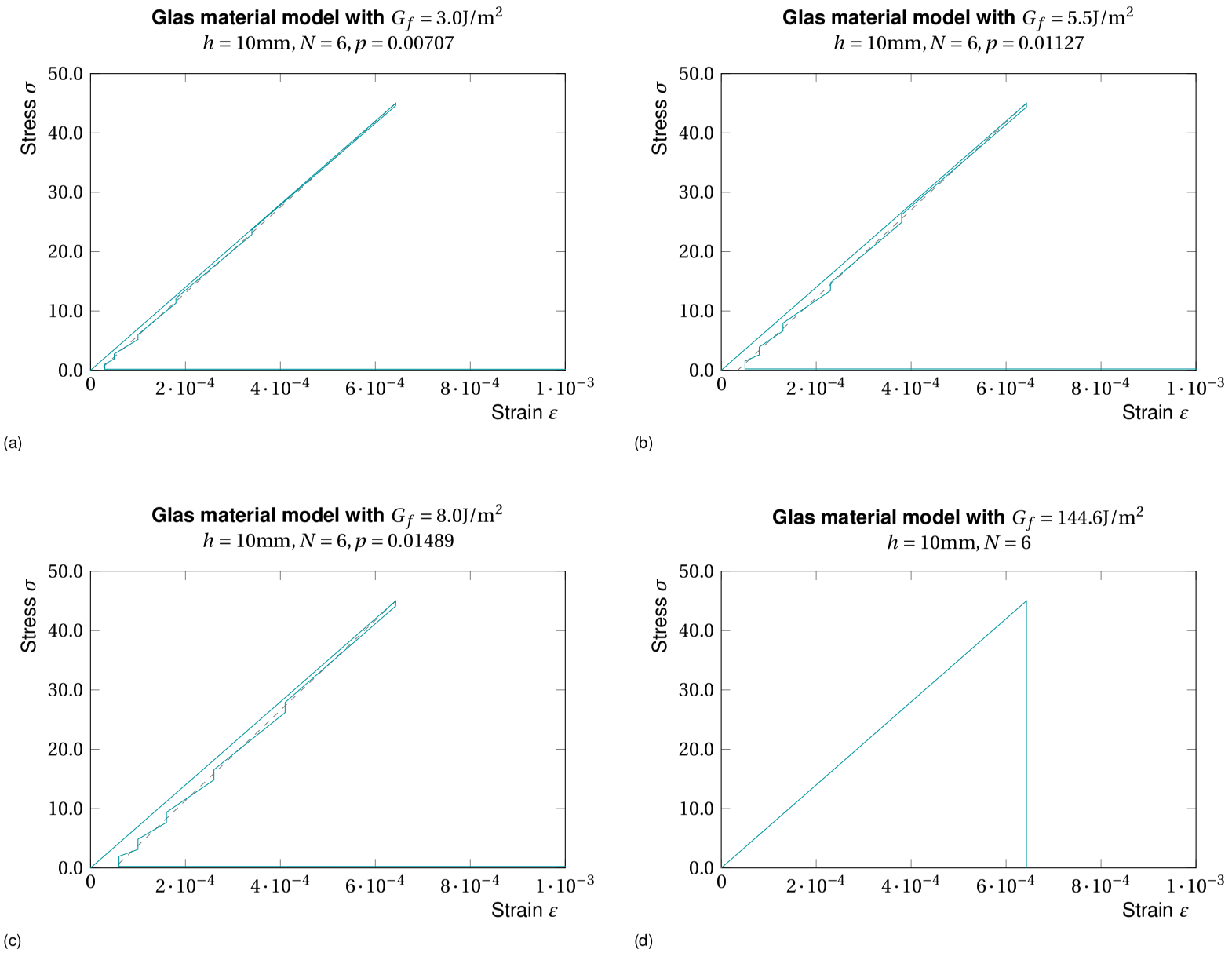

Figure 7.19: Reduction curves for different fracture energy's and brittle cut of relation

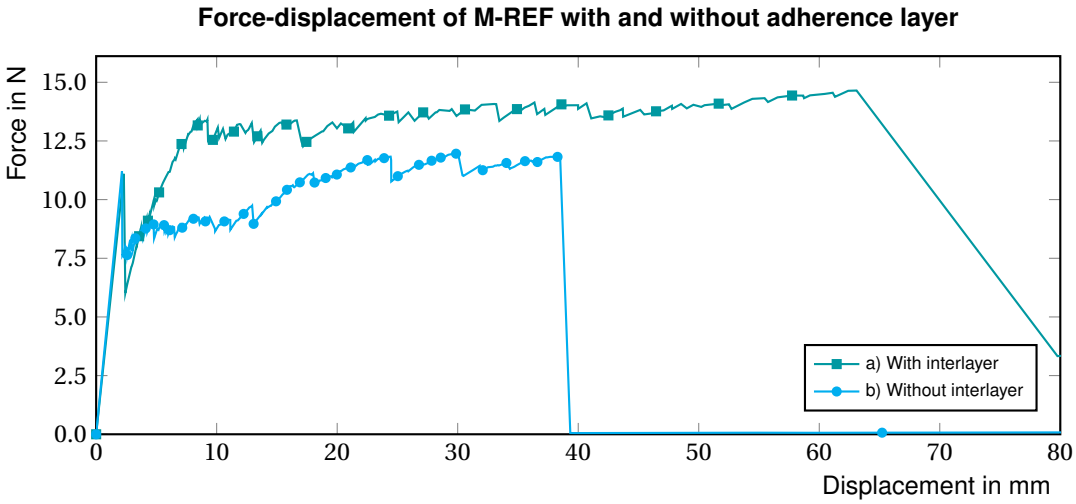

Figure 7.20: Force-displacement diagram of M-REF with and without interlayer between reinforcement and glass

7.6.4. Influences adherence layer between glass and reinforcement

In the paper of Bedon and Louter [2014] an adherence layer is used between the glass laminate and the reinforcement as is seen in Figure 7.2 in Section 7.3. This is also what is done in M-REF, but in the work of Louter et al. [2010b] a truss element is used without interface elements and therefore a full bound between steel and glass is present. Here the effect of modelling this adherence layer is observed by substituting the adherence elements as reinforcement material, creating a rigid connection. While doing this the reinforcement area should be held equal and is adjusted to a thickness of 11.4 mm. Modelling the reinforcement in the rigid manner means that no strain buffer is present between the glass and reinforcement elements. This has an affect on the crack development in the beam and force distribution in the reinforcement and are therefore analysed.

Analysis

In Figure 7.20 the force-displacement is plotted where this difference is visible. Due to the rigid connection the glass is forced to strain together with the glass as is also seen in the crack patterns in Table 7.7. In the force-displacement curve is visible how the limited straining of the reinforcement results in the inability to build up sufficient resistance. At approximate 10mm deformation is seen that the resistance capacity is a lot lower as the glass needs to crack before stresses in the reinforcement can increase. In Table 7.7 the cases with and without adherence layer are presented. Here the stresses are presented at an arbitrary chosen iteration step in the plastic stage of the beam where the first cracks have developed.
A curve is assembled displaying the relative stress in the reinforcement[13] vs. the distance from left edge to midspan. It is seen that the model with adherence layer has a much smoother distribution curve since it has the ability to distribute its stresses. In the model without adherence layer it is seen that the stress increase is present where the glass is cracked and the curve has more discontinuities. Most likely the cause consequence relation here is on the contrary, where the glass is cracked due to straining of the reinforcement in order to create sufficient resistance. The limited strain influences the This behaviour has a influence as is seen in the crack pattern at the chosen moment. This principle is continued until failure. For the model with adherence layer this means extending the growth of this one crack until it grows through the compression zone and for the other model the number of major cracks has increased until reinforcement rupture occurred.

[13] The stresses are taken relative to their maximum since both cases are not a critical case for a reinforcement element nor are they part of the maximum displacement curve.

Table 7.7: Relative stresses in reinforcement and crack patterns of cases with and without adherence layer.

With	Without
Relative tensile stress distribution in beam with respect to the maximum stress of the models	
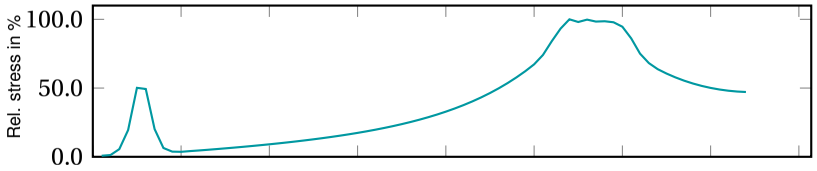	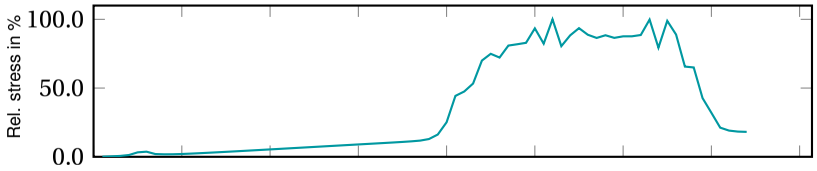
Crack distribution and tensile forces	
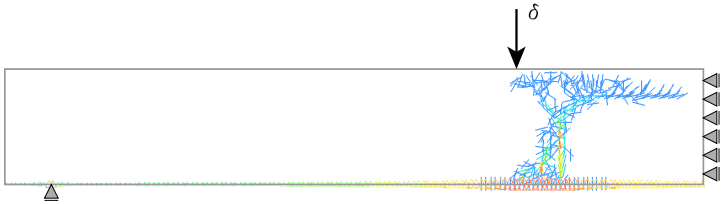	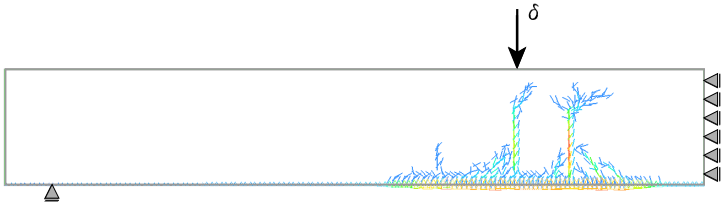
Crack distribution at failure	
	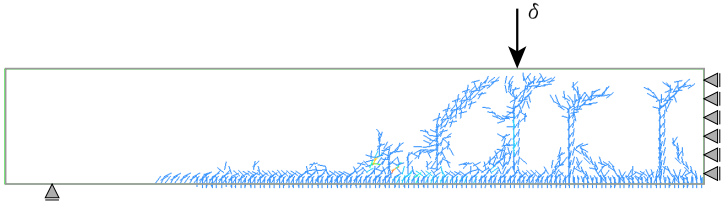

Adherence reduction model

Based on these findings and the effort simulate the adherence layer as best as possible a new concept is brought up. In the reference model, the linear elastic properties of the adherence layer are assumed just as in Bedon and Louter [2014]. But this does not represent the plastic behaviour of the SG material. When it is modelled linear elastic no change is present after reaching the yield point, thus limiting the strain in the reinforcement. To change this, the layer is modelled as a SLA reduction material. Using uniform distributed reduction over the mother curve for now, just as is done with the interlayer implementation. Naturally the original yield strength and Young's modulus are used, the curve is presented in Figure 7.21 and the force-displacement diagram in Figure 7.23 together with the reference model.

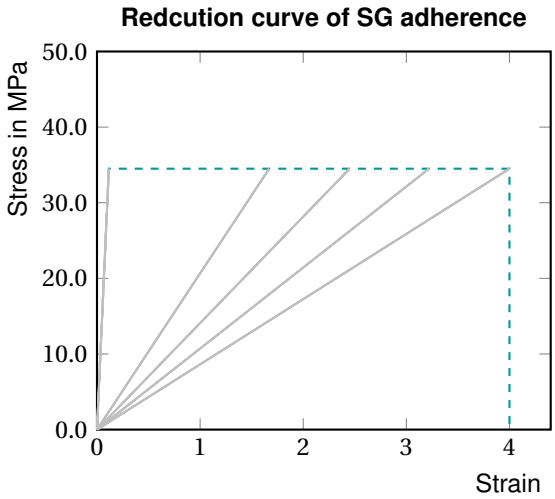

Figure 7.21: SG reduction curve

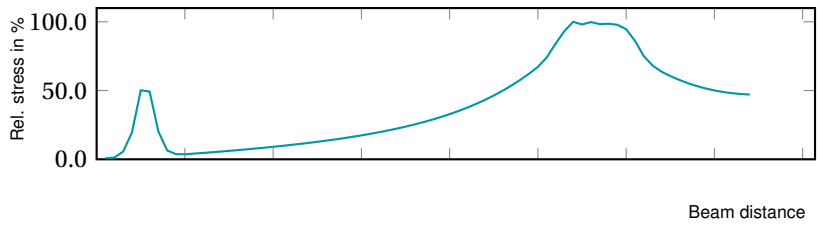

(a) Linear adherence layer

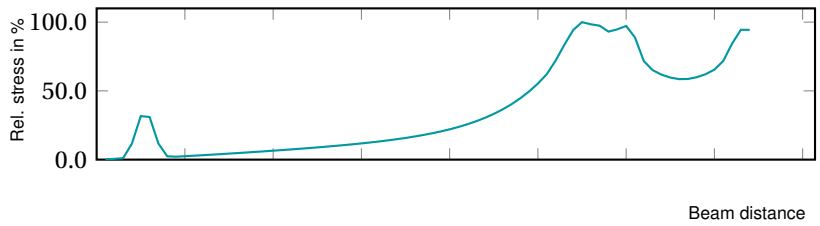

(b) SLA adherence layer

Figure 7.22: Relative stress distribution of linear and SLA model at equal iteration steps

Analysis

The found influence of the presence of an adherence layer is that it is used to spread the tensile forces, when a more stiff connection of the adherence layer is applied, straining of the reinforcement is achieved by cracking of the glass. Using the linear elastic adherence layer, redistribution is possible to a certain extend. The ability to strain plastically results in the more dense crack pattern and higher amount of cracks, just as

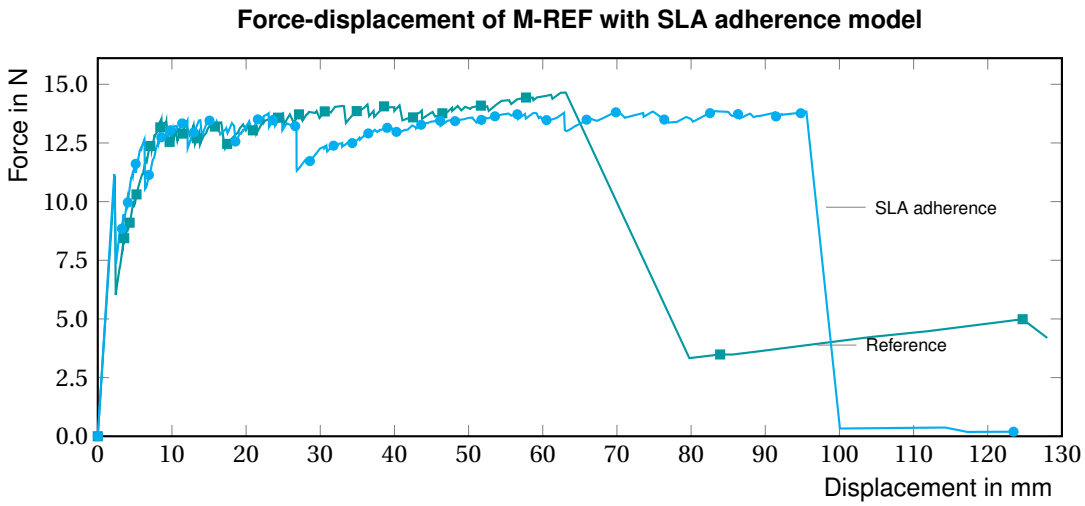

Figure 7.23: M-REF with adherence reduction curve implementation

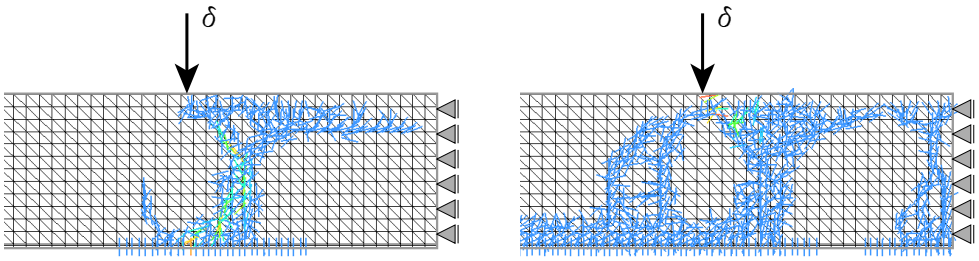

(a) Crack pattern of reference model

(b) Crack pattern of SLA adherence model

Figure 7.24: Crack pattern differences

is seen in the experiments. The physics behind this phenomenon is debatable and requires further research before conclusions can be drawn. In Figure 7.22

Conclusion

It can be concluded that the stiffness of adherence layer has a large influence on the post-cracked behaviour and the build-up of stresses in the reinforcement. When the connection is very rigid the glass must fracture first, resistance can not be build-up by opening of one crack. This is important when force controlled loads are applied as the beams with a stiff adherence layer require a higher displacement to achieve equal force and could fail before achieving this point. This failure mode requires additional research but will be important when it comes to failure definition of RG. This application thus results in more cracks and lower resistance. Beside the difference in stiffness results the use of plasticity in higher amount of crack formation in the glass and redistribution of stresses in the reinforcement. Resulting in higher deformations at approximately equal resistance. This is all summarised in Table 7.8.

Table 7.8: Performance of the difference in adherence layer modelling

Performance aspect	No adherence layer	SLA adherence layer
Resistance capacity	-	0
Deformation	-	+
Crack density	+	+
Amount of cracks	+	+

7.6.5. Saw-tooth in steel reinforcement

The assumed starting material model is equal to the one which is used in Louter et al. [2010b], this model is based on the tensile test as mentioned in background Section 2.6.5. Here the material curve is divided in reduction branches (N) along the mother curve, as is seen in Figure 7.25, in this paper a comparison is made with the same curve divided in 5 branches and it is concluded that the model with $N = 10$ resulted in a better estimation of the force displacement curve. To asses the effect of the different models, a simulation is done with two saw-tooth models, since this is what is used in the work of Invernizzi et al. [2011] and Rots et al. [2008]. A deviation in tensile strength of 5% and 10% is assumed to construct the saw tooth, resulting in a number of reduction branches of 43 and 22. For the ultimate strain the same value is held on as is found in the used experimental data according to Louter et al. [2010a], namely, $\varepsilon_u = 0.275$. This value will be used in the saw-tooth models. The saw-tooth's bi-linear relation[14] is based on a equivalent tensile strength calculated from the strain energy density (Bos et al. [2004]) of the predefined stress strain curve from the research of Louter and is achieved by the integration approach in equation 7.4 and calculated in 7.5, using $\varepsilon_e = f_t/E$ to make this dependent of the Young's modulus instead of the yield strain. This results in the equivalent strength of 819MPa from which a saw-tooth is created, both curves are pictured in Figure 7.26.

$$\chi = \int_{\varepsilon_u} \sigma(\varepsilon) d\varepsilon = \sum_{i}^{N} \frac{f_{i-1} - f_i}{2} \cdot (\varepsilon_i - \varepsilon_{i-1}) \tag{7.4}$$

$$\chi = \frac{1}{2} f_t \varepsilon_e + f_t(\varepsilon_u - \varepsilon_e) \tag{7.5a}$$

$$\chi = f_t \varepsilon_u - \frac{f_t^2}{2E} \tag{7.5b}$$

After analytical manipulation the tensile strength can be described as;

$$f_t = \varepsilon_e E - \sqrt{{\varepsilon_u}^2 E^2 - 2\chi E} \tag{7.5c}$$

When the tensile strength is calculated the saw-tooth is generated according equation ... starting with the first increased tensile strength ($f^+_{t,j+1\,j} = (1+p) f_t$) and corresponding strain ($\varepsilon_j = \frac{f^+_{t,j+1\,j}}{E_j}$). Then the lower tensile strength is calculated which subsequently defines the new Young's modulus which is simplified by Rots et al. [2008], the iterations go on until the ultimate strain is reached.

$$f^-_{t,j+1\,j} = (1-p) f_t \tag{7.6a}$$

$$E_j = E_{j-1} \frac{(1-p)}{1+p} \tag{7.6b}$$

Analysis and discussion

In Figure 7.27 the three curves are used in the simulation of M-REF and a few differences are seen. These differences are mainly steeper slope (beam stiffness) and higher resistance after initial cracking. Also ultimate failure occurred at relative small displacement. These differences are partially expected as the higher tensile strength results in a higher ultimate resistance and as the first branch already has a tensile strength of 900 MPa instead of the previous 550 the stiffness of the beam is higher since the yield occurs at higher stress. Which is more challenging to explain is that ultimate failure occurs at a much lower deflection. And why this even lower when more reduction branches are used. Not only the deflection is lower but also the number of iterations (iteration step 1519 and 895 for Curve P5 and P10 respectively). To explain this the crack patterns are observed in Figure 7.28, here is seen that in both cases the reinforcement has failed and the width of the surrounding yielding reinforcement elements is very small compared to the reference model (Figure 7.9). It seems this is affected by the number of reduction branches, but a clear explanation can not be found.

[14] A bi-linear relation is used, just as in Invernizzi et al. [2011]; Rots et al. [2008], a better approach is to build the saw-tooth around the mother curve. Although this is quite challenging since its most simple form would still have has three linear sections instead of one, this is not done since it is not in the scope of this thesis.

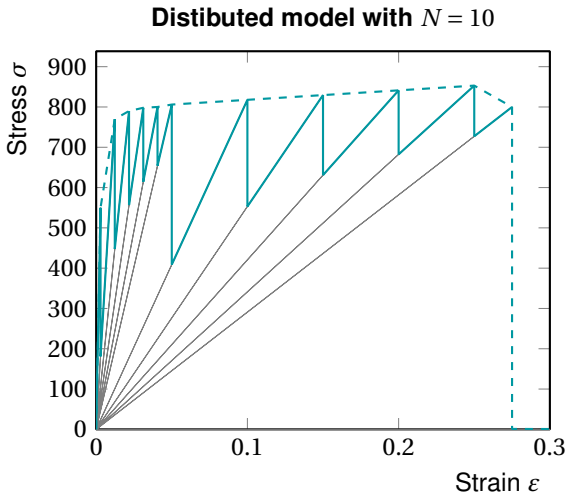

i	f_i	ε_i
1	550	2.80E-3
2	770	1.23E-2
3	790	2.10E-2
4	798	3.10E-2
5	800	4.05E-2
6	806	5.00E-2
7	818	0.100
8	829	0.150
9	841	0.200
10	853	0.250
11	800	0.275
12	0.0001	0.400

Figure 7.25: Curve REF: Reduction curve used by Louter et al. [2010b]

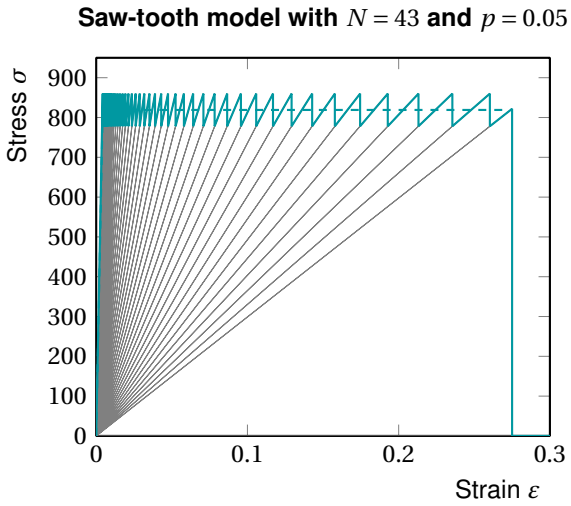

(a) Curve P5

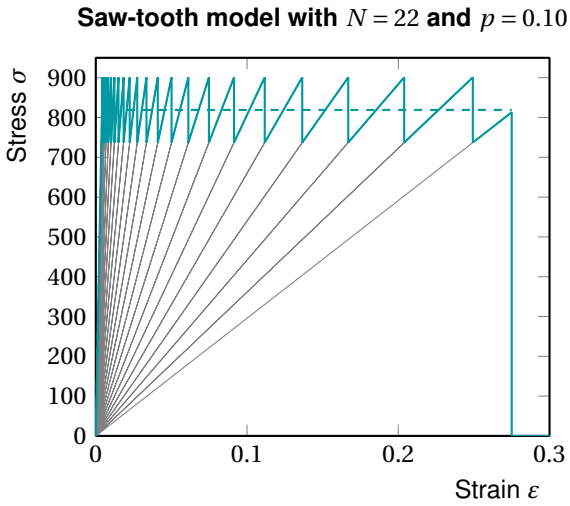

(b) Curve P10

Figure 7.26: Saw-tooth reduction curves based on tensile strength percentage

Conclusion

A large difference is observed in the force displacement diagram and crack pattern as the saw-tooth models fail earlier then when Curve REF is used. Looking at the post-cracked behaviour directly after initial failure the influences are small as is done in Rots et al. [2008]. But in the case of RG structures where the ultimate failure is an important aspect the reference curve is advised. The application of the saw-tooth in the reinforcement model results in a low crack density and an earlier failure. More research is required to clarify this behaviour and to find a proper definition of the use of plastic material.

Table 7.9: Performance analysis of using a saw-tooth for reinforcement

Performance aspect	**Saw-tooth curve**
Resistance capacity	+
Deformation	-
Crack density	-
Amount of cracks	0

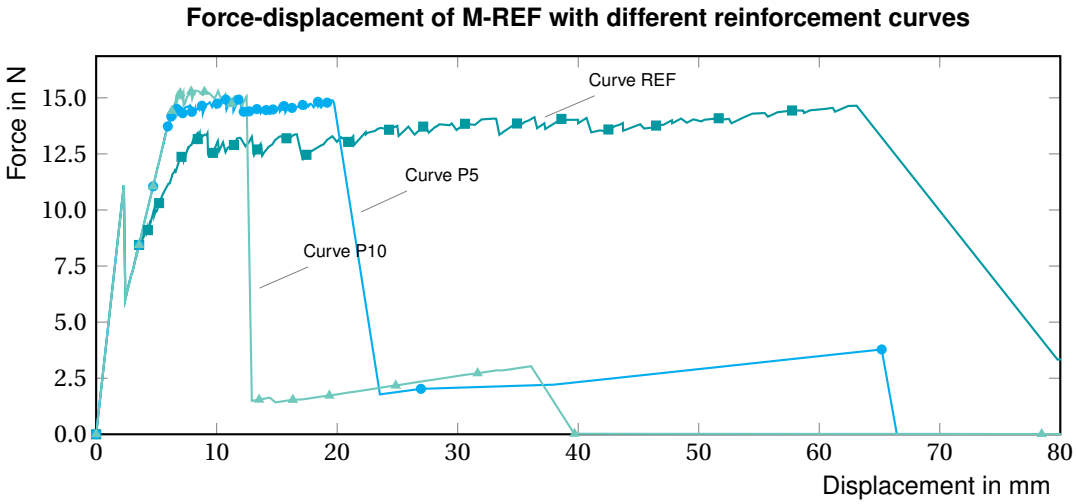

Figure 7.27: Reduction curves for different fracture energy's and brittle cut of relation

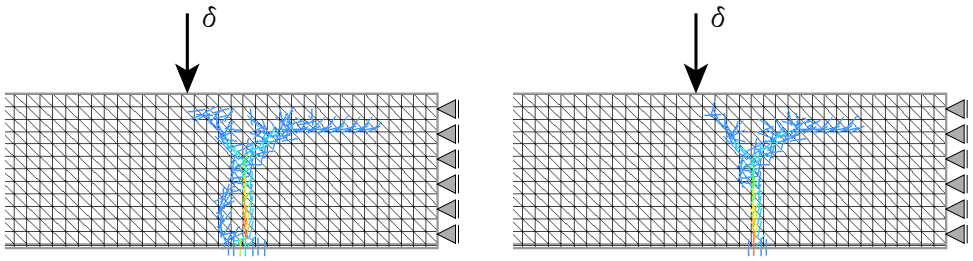

(a) Crack pattern of curve P5 at failure

(b) Crack pattern of curve P10 at failure

Figure 7.28: Crack patterns at failure of simulations using the saw-tooth reduction curves

7.6.6. Influences mesh size on crack distribution

In the background Section 2.6.3 is seen that the crack development can be influenced by the mesh definition. In this numerical analysis the initial model consist of a uniform distributed triangular mesh of 10x10mm. This is done to have a constant G_f/h throughout the model. Although crack patterns from this mesh are not mere horizontal or vertical as was seen in the work of Graaf et al. [2008]; Louter et al. [2010b], the mesh is rather coarse at crack initiation and has a single diagonal with equal direction throughout the mesh. As mentioned by DeJong et al. [2009], a uniform quadrilateral mesh is more likely to have a straight crack development. Thus the vertical planes are minimized by creating the mesh in Figure 7.29. This mesh is still quite uniform but the random Delaunay mesh would result in the same element differences as observed in Leung [2010] which would be unfavourable. As the refinement leads to the development of a crack at the symmetry edge, symmetry can no longer be assumed to have negligible effects and a full beam is modelled. The refinement is done by increasing line divisions, but a slight different mesh is generated in the full beam case. As the maximum line divisions is 99 and the sheet at mid-span is now 2 times wider. While the sheet can be split in half this results in a discontinue mesh therefore this is not desired. These meshes with crack sequence at their pre-fail state are seen in Figure 7.30 and the force displacement diagram of the reference and full beam are plotted in Figure 7.31[15].

[15]Only two simulations are chosen to be plotted as the symmetric beam could be biased due to the crack at mid span and since they are all quite alike, it would be harder to see the differences.

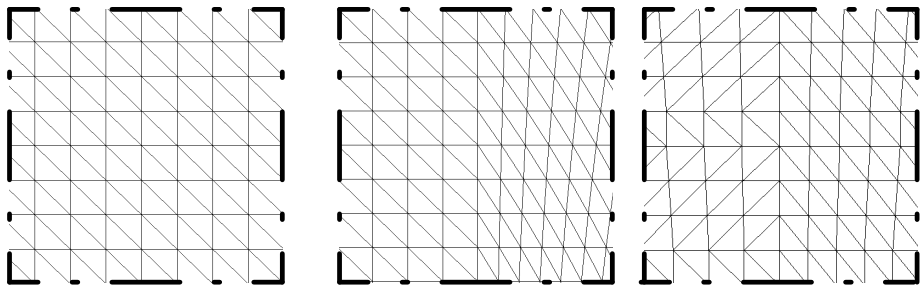

(a) Single diagonal (b) Refined half beam (c) Refined full beam

Figure 7.29: Highlighted different meshes

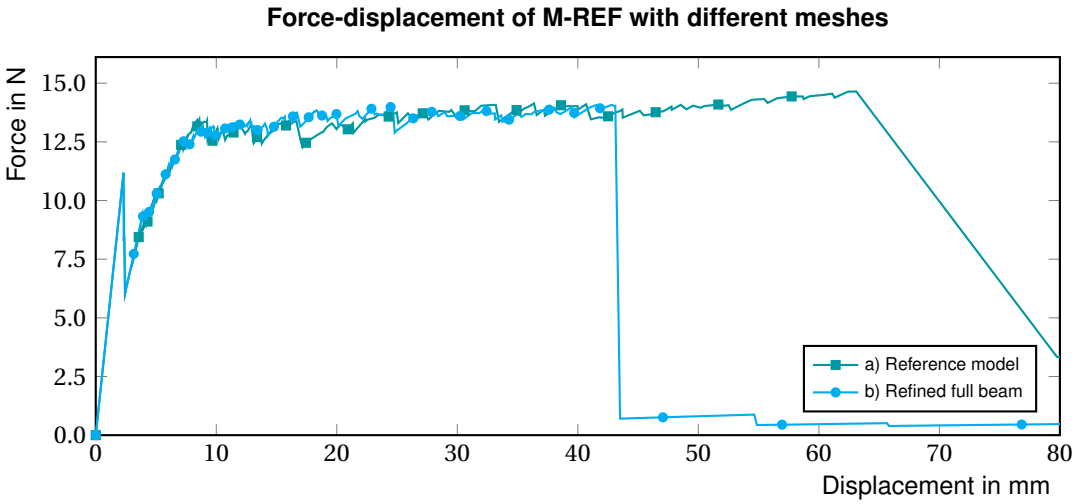

Figure 7.31: Reduction curves for different meshes

Analysis and discussion

The force-displacement diagram is seen that the strength resistance and deflection of ultimate failure do not alter significant with these refinements just as it is expected. Some differences are noticeable though, as the refined mesh results in a smoother curve with less sudden drops. The crack sequence differs from the reference as a crack at mid span develops, why this crack suddenly is present when mesh refinement is applied could have varies reasons in this case it seems that due to the refinement the cracks are at equilibrium and a different critical event is created in the form of a new crack. It is questionable whether this midspan crack occurred due to the refinement or the full beam application. The change in mesh does result in a earlier reach of ultimate failure by failure of the compression zone, it is unclear why the refinement of the mesh results in a different failure mode. This is applicable to not only the full beam but also the refined half beam. Furthermore, the additional crack also has the T-shape crack as is observed by Louter et al. [2010b]. Based on mechanics this sound right due to the absence of shear, but with respect to practice a V-shaped crack should be formed. Unfortunately researching this phenomenon lies out of the scope of this thesis.

Conclusion

The mesh has an influence on the crack development as is seen in the work of DeJong et al. [2009]. Refining the mesh to double direction diagonals and lower dimensions results in a higher crack density, but also lower ultimate failure deformation. This is caused by the occurrence of a different failure mode. In the application of a full beam an additional crack at midspan is observed. The crack formation does still tends to T-shaped cracks were V-shaped cracks are observed in the experiments. The performance is again summarised in Table 7.10, the deformation of the refined half beam is not presented in the graph and therefore filled with "N.A.".

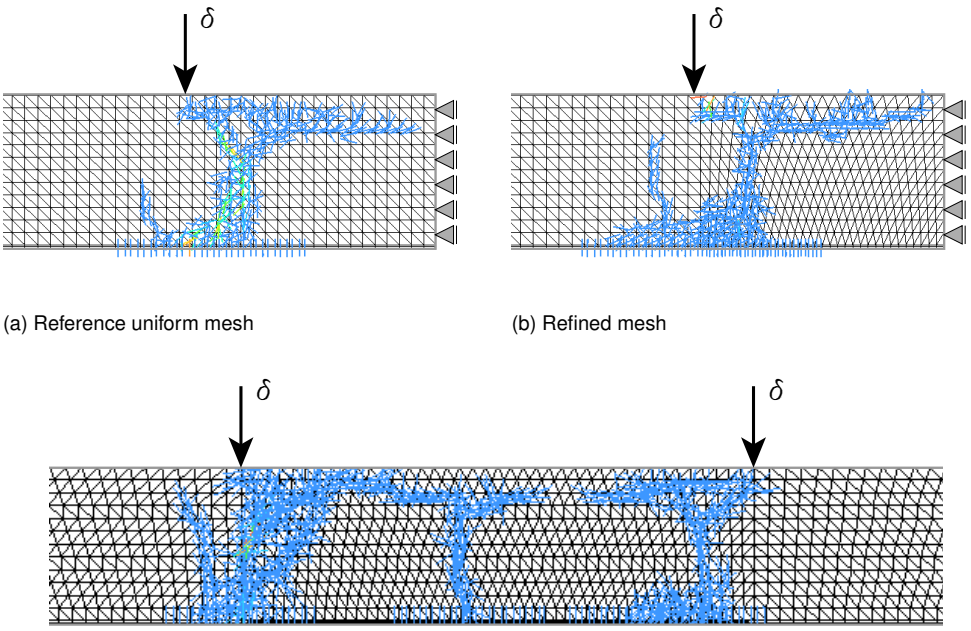

(a) Reference uniform mesh

(b) Refined mesh

(c) Refined mesh full beam

Figure 7.30: Crack strains in reference model

Table 7.10: Performance analysis of using a saw-tooth for reinforcement

Performance aspect	Refined mesh	Refined mesh full beam
Resistance capacity	0	0
Deformation	N.A.	-
Crack density	+	+
Amount of cracks	0	+

7.7. Pre-stress implementation

In Section 2.6.4 already is mentioned that initial conditions are not available yet in this version of SLA. This is unfortunate for its exact representation of the post-tensioned components as it would influence the crack development. Aside from the unfavourable execution of this experiment, the post-tension implementation will be discussed. Design BEN1 will be used as starting point and modelled in Model M-BEN1, two modelling options are treated to create the post-tension implementation using transformations to the material model(s) and non-proportional loading;

Full transfer model Transform initial stress conditions to material model for both reinforcement and glass;

Load model Transform stress conditions only for reinforcement and add non-proportional loading as pre-stress force on glass.

These options are based on adjusting the material models as is seen in Figure 7.32. With this principle the initial conditions are transferred to the material model, so the software does not have to and the material is either increased or reduced in strength. In both cases the $A_i \cdot \sigma_{p,i}$ (where i is the material) stays equal so no energy would disappear. The first method is based on the full transformation of post-tension stress, meaning the post-tension force is taken from the reinforcement and added to the glass model. The second method only half of the transformation is done where the reinforcement model is reduced and added as a non-proportional load on the structure.
When comparing the failure of a continuum element, a slight problem occurs when the first method is applied. In this method the additional strength due to post-tension force is transferred to justification of the

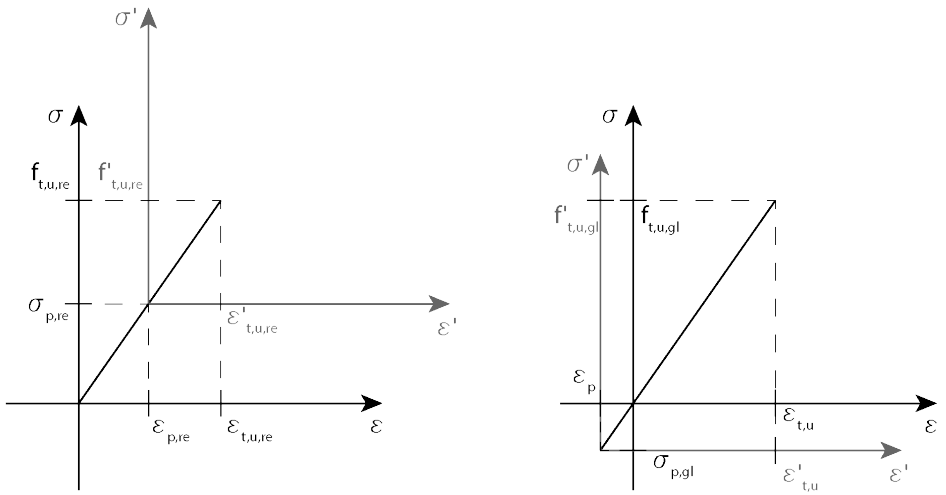

(a) Reinforcement model (b) Glass model

Figure 7.32: Material curves of reinforcement and glass with implementation of pre-stresses

glass material model, it is theoretically inaccurate for two reasons. First, glass fracture occurs not only in x-direction, as is the case with reinforcement, but it could occur at an angle meaning the applied pre-stress force is reduced. Using this method, the failure strength works in principle direction, while the pre-stress is only present in longitudinal/x-direction. Thus resulting in a false material model as energy would disappear from the system, this principle is shown in Equation 7.7 and Figure 7.33.

$$\sigma_1 = f_{t,u,gl} + \sigma_{p,gl} \neq f_{t,u,gl} + \cos(\alpha)\sigma_{p,gl}, \alpha \in (0°; 180°) \tag{7.7}$$

Secondly, next to this physically false interpretation of the post-tension force, it is also the case that this force disappears upon failure of the glass element. Hence, less to non post-tension force is present at ultimate failure which thus reduces the ultimate failure strength in the model. This is also observed in Figure 7.35.

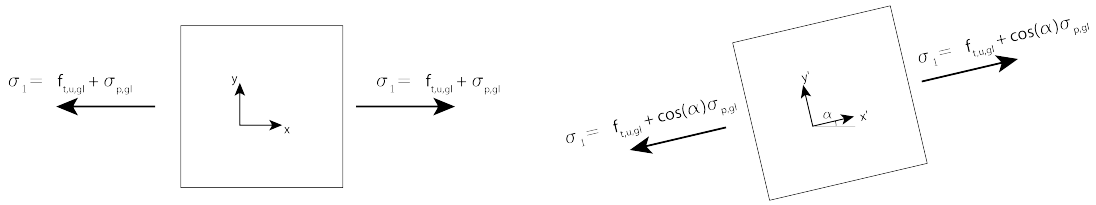

(a) Un-rotated contiuum element (b) Rotated continuum element

Figure 7.33: Continuum element with pre-stress in x-direction to visualise how the additional strength creates a physically false representation

In order to apply the second method, the post-tension force is introduced as a distributed load along the edge of the beam[16]. This physically incorrect since the force is actually introduced by the two bolts, but the distance the glass needs until uniform distribution is approximately 50-85mm[17] which is just past the support. As the cracks in this simulation are not developed at this place, the uniform force distribution can safely be assumed. The force acting on the nodes should be entered as input and is calculated according to equation 7.8. For the outer nodes only half of the force is applied as it is only covered a half length of the edge. For n elements this is fulfilling the equilibrium, $\sum_{i=1}^{n+1} F_{p,node,i} = F_p$.

[16] In SLA this is called a non-proportional loading as the force which introduces bending is scaled to the critical even (proportional) and the post-tension force is kept constant(non-proportional). But this definition does not matter for this case

[17] Based on $45 - 60°$ redistribution capacity over half the c.t.c. distance between the bolts of $\frac{100}{2}$mm.

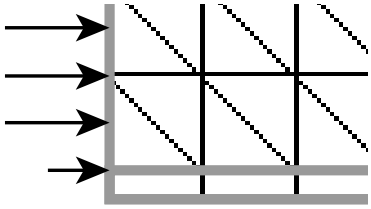

Figure 7.34: Detailed visualisation of force introduction on nodes and edge

$$F_{p,node} = h_{elem} \cdot \sigma_{p,gl}(\frac{t_{glass}}{t_{glass}}) = h_{elem} \cdot \frac{F_p}{h_{glass}} = 5 \cdot \frac{20000}{150} = 666,66\text{N} \tag{7.8}$$

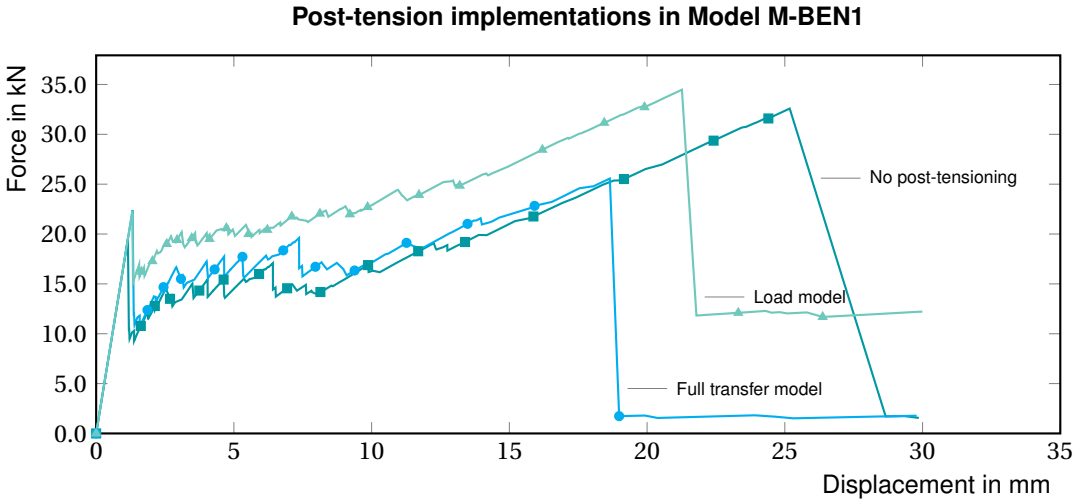

Figure 7.35: Force-displacement diagram with both implementations

Analysis and discussion

In the force-displacement diagram the results of the mentioned differences are seen. As reference the simulation of M-BEN1 without any alterations is shown. For the full transfer model, the initial failure strength is increased which shows that the method works. And it is visible that earlier failure occurs as expected, but also a significant lower ultimate resistance force is visible, this is the consequence of the 'disappearing' force. In the curve of the load method,the same trend is observed as seen in the reference case, but with increased resistance. This is exactly what is expected and it is therefore concluded that this the external force solutions is preferred for this analysis. Unfortunately it is unable to seen the difference using initial conditions as this induces the load directly on the bottom edge due to the adherence. It is recommended to research what this difference result into. In the following Table 7.11 the performance aspects are summarised. Although differences in the crack pattern are observed, they are not presented here as this implementation is mainly about the force-displacement diagram.

Table 7.11: Performance analysis of using a saw-tooth for reinforcement

Performance aspect	Full transfer model	Load model
Resistance capacity	0	+
Deformation	-	-
Crack density	N.A.	N.A.
Amount of cracks	N.A.	N.A.

Conclusion

Two different workarounds are presented and analysed as the implementation of initial conditions are still in development. The first model is the full transfer model where the tension in the reinforcement is transferred to additional strength in the glass. It is found that this implementation is only true in the pre-cracked stage, since after cracking the force disappears and rotated crack planes would bias the post-tension force. The second model uses non-proportional loading at the introduction points of the beam to represent the post-tension force and uses only the transformation in the reinforcement model. This result in both increase in initial failure resistance and approximately equal ultimate resistance. The addition of initial stresses would contribute a lot more as this creates the ability to model how the stress is transferred through the adherence layer.

7.8. Summary and conclusions

In Table **??** all conclusions of the analysed aspects are summarised to create an overview of the influences certain modelling choices have. These conclusions are then used to model the experiments to verify the numerical simulation.

	Resistance capacity	Deformation	Crack density	Amount of cracks
Final branch / Dummy branch	The addition of the negligible resistance branch results in the possibility for cracks to open and reinforcement to rupture. The absence of this branch in the glass models results in a higher force-displacement curve as the glass model is unable to fail. For the absence of the branch in the (steel) reinforcement, higher deflection is observed due to the inability for the reinforcement to rupture.			
Absence in glass model	+	+	+	+
Absence in reinforcement	0	+	0	+
SentryGlass interlayer	The knowledge of post-cracked behaviour from the use of dummy branches is capitalised in the creation of residual strength of the interlayer. The equivalent SG properties result in a positive effect on closing the resistance gap between GB and SG laminated beams and result in more dense crack patterns.			
	+	+	+	+
Fracture energy	Expected deviations in the crack patterns did not occur, only higher crack strains are observed. More research is required regarding the fracture energy.			
All models	0	0	0	0
Adherence stiffness	The stiffness of the adherence layer has large influences on the stresses in the reinforcement. Lower stiffness creates the ability to spread stresses and rigid adherence results in more cracks as the glass limits straining of the reinforcement.			
Rigid connection	-	-	+	+
SLA adherence	Using plastic SLA material causes the material to deform plastically and higher deflection is observed together with an expanded crack pattern. The physics behind this are debatable and require further research.			
	0	+	0	+
Plasticity	Using a saw-tooth as plasticity model creates too large deviations in tensile strength for a practical number of reduction branches. It is unclear how this saw-tooth results in the low deflections at ultimate failure. Therefore a approximation of the mother-curve is advised, although this still does not represent plasticity due to the linear characteristics. Further research is required on this aspect.			
Saw-tooth model	+	-	-	0
Mesh	Refining mesh orientation and size in the crack initiation zone results in a smoother force-displacement curve and higher density in the crack pattern.			
Refined mesh, full beam	0	-	+	+

7.9. Validation

The final part of this chapter is the validation of the mentioned data sets. In the subsequent sections both M-REF and M-BEN1 are adjusted according to the found performances to simulate the best representation of the experiment and are validated with their experimental data. In this validation the performance with respect to experiments is analysed.

7.9.1. Reference model

The experimental data is shown in the force-displacement diagram of Figure 7.36 together with both the full beam model consisting out the parameters which are listed below. In addition to the experiments and

the SLA, the NLA results from Bedon and Louter [2014] are also presented to put the different analysis in relation.

Glass model Fracture energy of $3.0\mathrm{J/m^2}$ is used;

Reinforcement Application of reinforcement Curve REF, following the experimental curve;

Final branch Final branches of negligible strength and high strain are used for both material models;

Interlayer SG implementation in glass model;

Adherence SLA material model for SG adherence with the reinforcement;

Mesh Full beam refined mesh, using double direction diagonals.

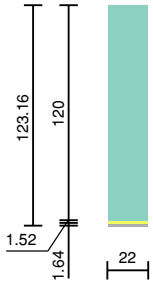

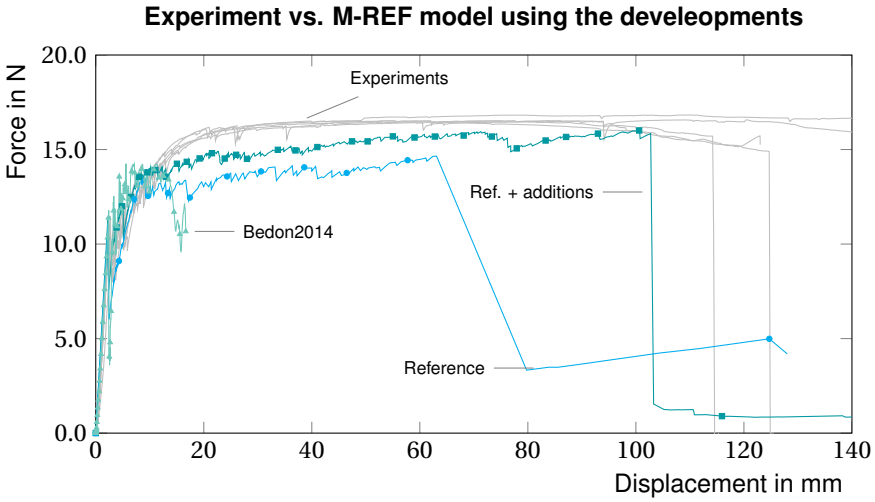

Figure 7.36: Force-displacement diagram of reference simulation containing all considerations

Analysis

Looking at the difference between the reference model based on the starting points a good progress is made. It is seen that the difference in the force resistance goes from an error of 11.9% based on the reference model to 3.5% using the additions[18]. This is mainly caused by the SG implementation. Also the deflections are increased from 62 to 102mm and the ultimate failure deflection of the model is almost in the range as the failure of the experiments, which lies between 123 and 174mm with a mean of 139mm. This increase in deflection is mainly to the use of plasticity in the reinforcement adherence. Although the amount of cracks are not in agreement with the experiments their pattern is developed with respect to the starting conditions and a higher crack density is reached. This is also observed in the experiments, but T-shaped crack are still present.

Using the SLA results to compare this with the NLA model, a significant differences is seen. The NLA curve has a higher resistance initial cracking and ultimate failure occurs after low deflection where the SLA curve follows the experiments quite accurately.

7.9.2. Validation of M-BEN1 case

As the post-tensioning during the experiments did not went as expected, it is still interesting to model these specimen as there are a few of differences with respect to stainless steel reinforcement. Aside from the difference in material, the adherence is also different. In the experiments of Louter et al. [2012a] the reinforcement is adhered to the glass using the SG interlayer as the section is partially integrated. In case of experiment BEN1, the reinforcement strips are adhered to the glass using an epoxy. This manner differs

[18]The error is calculated accoridng to the stated validation goal in Section 4.3.3, using the values at ultimate failure, $F_{u,exp,meam.} = 16.59$ and $F_{u,num.} = [14.62; 16.01]$

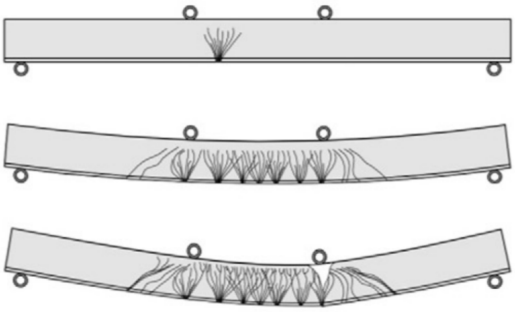

(a) Schematic crack sequence of SG-specimen from Louter et al. [2012a]

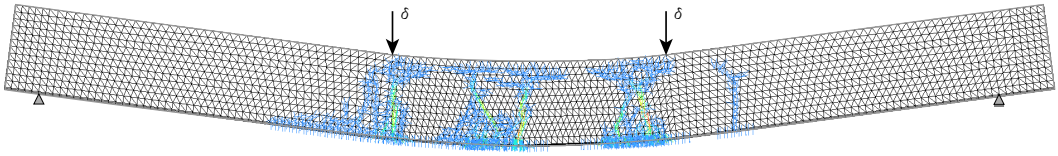

(b) Crack development of M-REF at before of ultimate failure

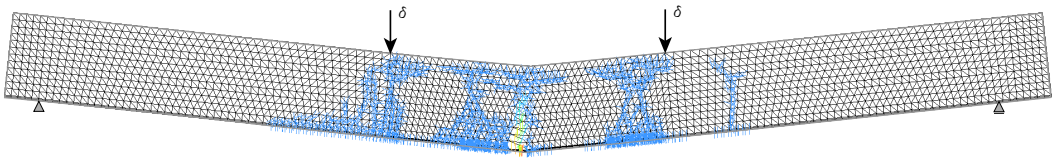

(c) Crack development of M-REF after ultimate failure

Figure 7.37: Crack sequence of the reference case

from the SG in stiffness, due to the thickness of approximate 0.1 instead of 1.52mm the overall stiffness of the interface is extremely higher, if Young's modulus change is disregarded. Therefore this aspect is looked into in Section 7.6.4 where a lot of differences are seen. Besides this, the lower Young's modulus of the reinforcement strip has an additional effect on the tearing of the glass as the reinforcement strip will elongate more than the glass. Especially since the tensile test showed that the Young's modulus is even lower as originally thought. For the validation the numerical simulation and the experimental data are shown in Figure 7.38. The simulation is based on the experimental values of the GFRP strips from the experimental Section 6.2.4. Furthermore, the model mainly consist out of the following enlisting of implementations treated in this thesis, further specification of this model is found in Appendix C.2.2.

Glass model Fracture energy of $3.0\mathrm{J/m^2}$ is used;

Reinforcement Brittle SLA model based on TEN-FIB values;

Final branch Final branches of negligible strength and high strain are used for both material models;

Interlayer No interlayer implementation in glass model;

Adherence Full rigid bound between glass and GFRP strips;

Mesh Uniform single diagonal mesh.

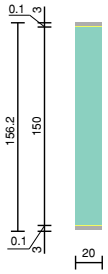

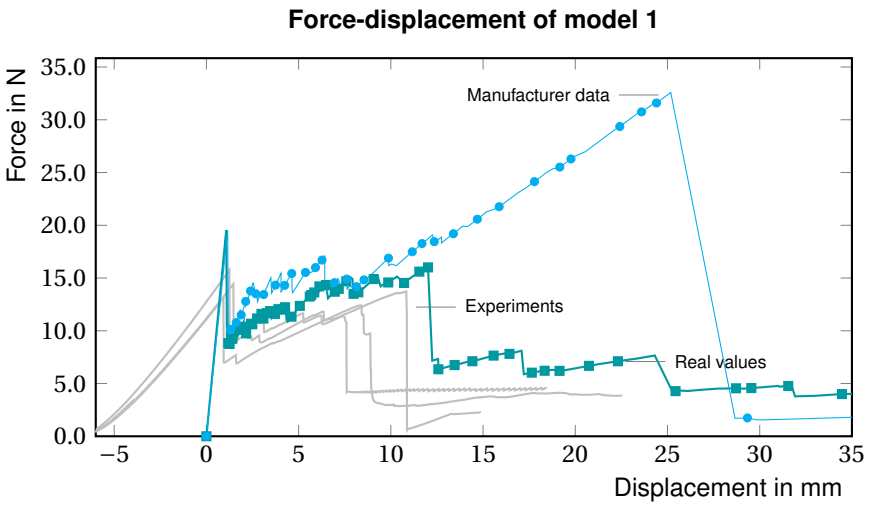

Figure 7.38: Force-displacement diagram of experiment BEN1 simulation

Analysis and discussion

The first observation is that the initial stiffness of the glass is a lot lower, this is explained via the steel frame which is used during the experiment. This deflection can be seen in the footage in Appendix B.2.1, and is corrected by synchronising the initial failure moments. The force stays roughly the same after fracture thus this effect is negligible hereafter. In Section 6.5 is explained how the lower material properties result in an earlier failure, this is shown here by using both the manufacturers data and the real values. The SLA simulation using the real values is in good agreement with the experiment. The resistance deviation at ultimate failure is 27% more than the average of the experiments at a displacement of 11.9mm where the experiments failed at the average of 8.7mm. The crack pattern shows a very similar failure, this is mainly due to the PVB interlayer, where diagonal cracks are developed and failure occurred also in this diagonal crack just as is observed in the BEN1-PT-2 specimen as presented in Figure 7.39.

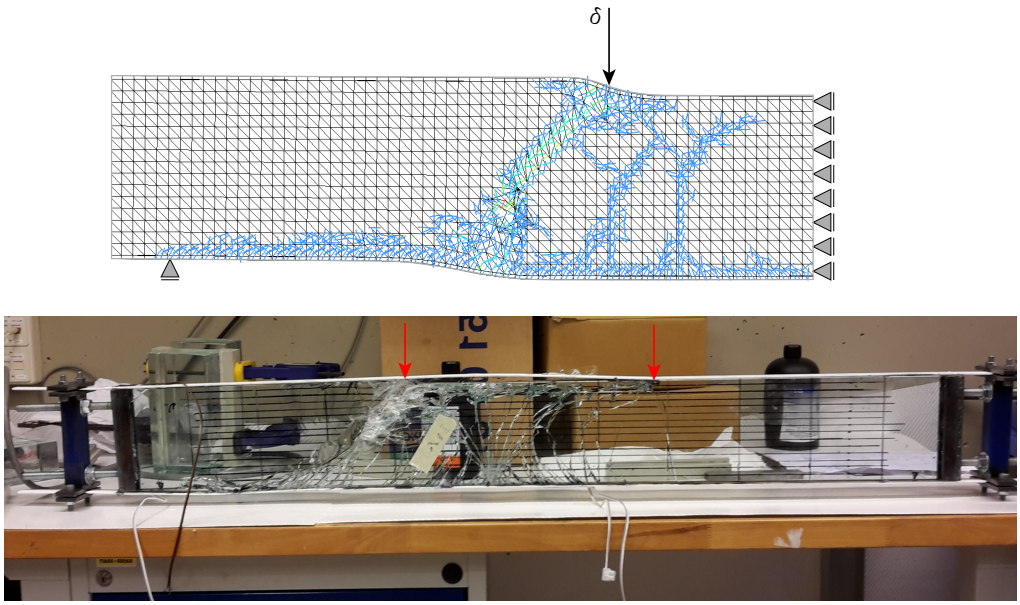

Figure 7.39: Crack pattern of numerical model M-BEN1 and specimen BEN1-PT-1

7.9.3. Experiment BEN2

In the experiments of BEN2 is seen how the FFR creates a quite complex failure behaviour involving internal slip and decreasing stiffness. Next to the challenge of physical understanding, the absence of truss elements brings additional challenges in the numerical simulation. With these uncertainties it is challenging

to distinguish the origin of differences in the computational results. As they could be both incorrect parameters and physical understanding. A numerical prediction does therefore not contribute to the understanding of reinforced glass failure and is therefore not treated.

8

Discussion

During the course of the thesis a lot of information is passed by, with differing relevance. In this chapter the conclusion/summaries made in the chapters are repeated and a discussion is made based on their relevance to the objective, which flaws are encountered and how they could be solved. These considerations are taken into account for the following conclusions and recommendations. Next to the three main subjects of the thesis the crack formation and relation to practise is discussed as these subjects are worth mentioning.

8.1. Post-tensioning

The objective of post-tensioning in RG beams to increase in initial failure resistance. With the research question whetherGFRP is a suitable material for post-tensioned reinforced beams. The aspects of post-tensioning beams and reinforcing with GFRP strips are discussed.
Some considerations about post-tensioning, during preparation of the specimen it was experienced that tensioning a beam is quite a challenge. As the force introduction can cause failure at every interface of force transition, it is a challenge to design this well. Eventually is chosen for an adhered connection with the actuator and to possibility of additional friction by tensioning the bolts. The tensioning process itself felt quite dangerous due to the uncertainty and the brittle behaviour of the structure, even thought everything was calculated and eventually only a tenth of the force was reached. While the applied force is very small in relation to practise it is in the opinion of the author to apply post-tensioning in more lateral stable systems as is done by Bos et al. [2004]. The idea of storing a lot of energy in such a brittle structure requires good engineering and more research in the prevention of explosive failure of the compression zone.
In hindsight, the initial design lacked lateral stability, had a low post-tension force and no eccentricity. This led to a theoretical insignificant increase in initial strength resistance.
In addition to the post-tensioning, the GFRP strips which were used in experiment BEN1 had an even lower Young's modulus than expected. This resulted in more crack opening and earlier reaching of ultimate failure. This is recognised as the lack of rotation capacity, a failure mode which is not often observed and therefore interesting. Most likely this would not have happen if a SG interlayer was used. But it does show that a glass beam has another failure mode aside from compression of glass or rupture of reinforcement.

8.2. Flexible reinforcement

The second goal is regarding the concept of laminating fibreglass texture inside the laminate and thus increasing flexibility in reinforced glass design. This concept is verified in the tensile and bending experiments in sections 6.2 and 6.4. Here it is observed that the estimated tensile strength and Young's modulus were not met and resulted in lower values. It is observed that the SG did not saturate the whole fabric this is probably due to the high density of the fabric. A possible solution is to limit the thickness/density of the fibreglass fabric to approximate 400 $\mathrm{gr/m2}$ and adhere between the foils instead of substitution of one. Another solution is to pre-manufacture the reinforcements in an autoclave and laminate the reinforcement with

high pressure, as the SG has the ability to melt and merge with the interlayer. Both solutions are should be feasible and lead to higher saturation of the fibres.
The performance in a beam were satisfying, although also here the fibres were not fully saturated thus only a part of the reinforcement contributed to the ultimate failure resistance, the resistance was is equal range of the initial failure. Meaning that with the above stated improvements its performance would increase and are able to function as a reinforcement. Due to slipping of the un-adhered fibres the beams' stiffness gradually decreased, resulting in only one extensive crack and a safe failure. Most likely will this slip be an issue on long term behaviour when constant load is applied. But this behaviour will probably change when the saturation is increased and no slipping occurs in the reinforcement.

8.3. SLA calculations

For the numerical calculations the goals were to extend the SLA with new developments and to implement post-tensioning. Therefore analyses are made of a few parameters and modelling choices which then are used to calculate experiment BEN1. As not all implementations require discussion a few are left out and only treated in the conclusion, the others are discussed below.

Plasticity model As mentioned it is a challenge to model the right plasticity model in a SLA. In the study two approaches are compared which are both used before and in the outcome of analyses are significant. This manner of defining the reinforcement has a large impact on the results. In the work of Rots et al. [2008] and Invernizzi et al. [2011] plasticity is described with a saw-tooth and state the acquired results to be in agreement with experiments. It can be explained in the way that the deflections from Rots are too small in order to observe difference in earlier failure deflection. Also the absence in bond-slip implementation could influence this behaviour as this phenomenon is observed in the experiments of Louter et al. [2012a]. According to the analysis the implementation of a saw-tooth reinforcement model highly influences the results and is not recommended as it introduces inaccuracies in the tensile strength, which is the driving parameter for the load resistance.

Glass model The fracture energy is a debatable parameter and is analysed by Bedon and Louter [2014] in a NLA in ABAQUS. In this study the only difference is observed in crack pattern, just as concluded by Valarinho et al. [2012b]. The three different snap-back models are compared in SLA together with the brittle model and no differences are found in the force-displacement curve nor in the crack pattern. Only a variety in crack strain is observed, this could be explained by the fixed cracking, which is applicable for this SLA version. Meaning after initial crack direction is set, the crack is only able to strain up to its next limit. Therefore the cracks will only be opened in its crack direction and the brittle model will do this faster as its branches allow higher strains. As the post-cracked behaviour of an element can not be influenced after cracking the differences between the analysed fracture energies are too small to be significant.The higher allowable strains in the brittle model could add up to influence the stress distribution and should therefore be applied with care. Influences of fracture energy on the crack pattern should be noticed when rotational cracking is used, but this is only one parameter which possible influences these differences.

SG implementation The absence of strength increase due SG in previous work (Louter et al. [2010b]; Louter [2011]) was given some thought. A transformation is done to add post-cracked resistances to the glass which are equivalent to the SG interlayer, using the post-cracked theory from the dummy branch. As the load resistance of the beam is increased to the experimental value directly after cracking, the model without reinforcement has an extra increase in post-cracked resistance. This is not seen using the SG implementation and is probably a result of de-bonding and visco-plastic behaviour of the material (Santarsiero et al. [2016]). As this is only a theory, this and de-bonding should be researched.

Adherence Experiment BEN1 has a quite rigid adherence layer and the work of Louter et al. [2010b] a truss element without interlayer is applied. The difference between elastic behaviour and full rigid connection of the adherence is analysed. This is done with respect to stress in the reinforcement and crack patterns. Differences in the crack pattern are significant as multiple cracks are developed using the rigid connection. This is also seen in the experiment observations. But this rigid connection results also in limited straining of the reinforcement. As the force-displacement curve does result in a more accurate approximation with adherence layer, the preliminary adherence layer is kept. Model M-BEN1 is simulated without this adherence layer due to the rigid connection of the thin epoxy adherence.

SLA adherence In addition to the previous analysis the SG is also analysed as a plastic material using reduction branches. The addition of a yield limit and plastic behaviour causes extra deflection and cracking to occur. The real physics behind this are debatable and should be researched.

Mesh The goal for mesh refinement was to reduce crack influence. This is done by creating a less uniform mesh by increasing divisions at the bottom and creating a better distribution of triangular elements, i.e. diagonals in both directions. As this mesh already resulted in more freedom in the crack development. The better option is to create a refined mesh by combining the Delaunay algorithm used by DeJong et al. [2009] and a linear density course as is done in th work of Bedon and Louter [2014].

Post-tensioning An attempt is done to apply post-tensioned reinforcement on model M-BEN1. At the time of this thesis the used version of SLA does not include initial conditions. This limitation is covered by analysing two work-around options in order to get the right results. One of these options was physical incorrect and therefore not recommended. As for the second option, the load model, gave the expected results. But due to the absence of experimental data this still needs validation. The analysed model does give the expected results, but it would be more accurate to use the initial conditions as the tension in the reinforcement does influence the cracking by its adherence to the glass.

8.3.1. Crack formation

The crack formation in the simulations performed in this thesis are getting closer to the expected crack patterns observed in the experiments. But T-shaped cracks are still found in the refined mesh simulation. Although this is on the edge of the scope of this thesis its formation should be discussed as a whole thesis can not be written without some thoughts about this subject. When looking at the development of the numerical crack and the crack in practise the difference is that in practise this crack is already a V-crack with 2 or more branches at the first instant of occurrence as seen in the background. This could be explained by thinking in the dynamic origin of the crack, as the energy is suddenly release in the formation of the crack (Bos [2009]), the crack formation becomes a dynamic process finding the way of the least resistance . Looking at the stress-release circle in fracture mechanics it might be possible for a brittle material to form multiple cracks origination from one weak spot, developing to the edges of this circle instead of the assumed one crack perpendicular to the principle stress.

8.4. Reinforced glass structures in practise

It is not the main topic in this thesis but it is found noteworthy to mention how all research is related to practise, mainly with respect to scaling and what issues should still be overcome. The research executed in this thesis and in previous work is all experimental, as mentioned by Martens et al. [2016c] half of the experiments had a span of 1.40 m and 75% of the concepts were tested with spans smaller or equal to 2.68 m having a minimum and maximum ranging from 0.40 m and 8.00 m. This data related to relative small experiments and it is arguable how this relates to practise, if the concept can be applied all the time and with all reinforcement types. As is seen that the ultimate failure is not reached for experiment BEN1 due to the low stiffness of the reinforcement.

Failure modes Looking at different applicable reinforcements which are be distinguished between brittle and plastic it should be questioned which failure modes exist within this concept, how to design the beam to prevent brittle failure and how to ensure prevention of this failure.

Multi lamination Also it is not uncommon to apply multiple laminated glass beams, but in research 3 layered laminates is the maximum which is observed. It is imaginable that a low height-to-span beam with multiple panes suddenly cracks, the large energy release might lead to either rupture of reinforcement as mentioned by Bos [2009] or maybe direct crack growth through the compression zone. These situations are not likely since near failure modes were not observed and multiple panes fail independently as mentioned. These full scale tests, proving the concept are only done to a limited amount by Bos [2009] and Louter et al. [2012a].

Humidity Besides scaling of the concept the mentioned humidity corrosion will affect the strength of glass over time. A solution is mentioned to apply HSG with internal pre-tension below 50 MPa, then again this combination is researched to limited extend.

9

Conclusions and Recommendations

The thesis is summarised in the conclusion and recommendation to create an overview for further research. Due to the results from the tests and limitations which are encountered, this thesis does not result in directly more answers but maybe even more questions which need attention. The conclusions are based on the research questions and summarise the conclusions of previous chapters.

9.1. Conclusions

Conclusions are made regarding the problem definition and research questions stated in Chapter 5. As this consist out of three subjects these are also brought back in the subsequent sections, answering the stated questions.

9.1.1. The suitability of GFRP post-tensioned reinforcement

Experiments are performed using GFRP strips as post-tensioned reinforcement.

- The post-tensioning process encountered a fault resulting in an insufficient post-tension force. Creating the inability to experimentally validate the post-tension effects;
- Lower elasticity resulted in earlier ultimate failure due to higher crack opening.

9.1.2. Performance of fibreglass fabric reinforcement in relation to integrated GFRP strips

Bending and pull-out experiments are executed using both types of reinforcement, designed to have equal ultimate failure resistance.

- It is observed that the SG did not fully saturate all fibres resulting in approximate 30% activation of the fibreglass reinforcement in the tensile experiment;
- From the tensile and bending experiments is concluded that the principle is feasible as reinforcement application and it is able to maintain integrity up to a significant ultimate failure resistance;
- The ultimate failure resistance did not meet a mean ratio of 83% and thus not fulfil the stated design/-validation requirements;
- The fibreglass fabric specimen achieved 49% regarding the ultimate failure resistance of the equivalent GFRP specimen;
- The observed slipping on the reinforcement could lead to undesired load term behaviour;
- The crack formation of the fibreglass specimen was less in relation to the GFRP specimen;
- The fibreglass fabric specimen failed at a lower deflection.

9.1.3. Influences of design and modelling alterations on the performance of a numerical RG beam

A reference model is used as starting point based previous work, developments and design considerations are analysed and graded based on the performance aspects. Furthermore, interlayer and post-tension implementations are treated.

- More insight is created by analysing different design considerations and modelling deviations, by grading the performance aspects individually using the reference case;
- The accuracy ultimate failure resistance of the method using the findings of the study improved with a decreased in deviation from 11.9% to 3.5% for the reference case;
- The implementation of the SG interlayer is able to fill a great part of the remaining resistance;
- Two methods are described to implement post-tensioning as initial conditions are not implemented in SLA. The load model is concluded to be the most favourable.

9.2. Recommendations

The executed research found a few answers but leaves maybe even more new questions, first recommendations within the scope of the thesis related to the treated subjects are listed and hereafter some recommendations from the boundaries of the scope containing recommendations regarding RG design in general.

9.2.1. Post-tensioning

- Design post-tension system with a higher effectiveness is recommended, e.g. higher stability structure and eccentricity;
- Prevention explosive ultimate failure should be researched, as this is an unfavourable failure mode;
- Improving the connection of the actuator and a GFRP reinforcement;

9.2.2. (Transparent) fibreglass reinforcement

- Solutions for higher saturation to decrease internal slip are recommended, e.g. lower density of the fibreglass, higher viscosity of the interlayer, pre-fabricated post-processing sheets, difference in configuration;
- Research in combining the transparent composite results (Seo et al. [2017]) with glass adherence interlayer;

9.2.3. Numerical calculations

- Improve plasticity implementation in SLA, e.g. a multi-linear saw-tooth curve for both the lower yield strength and the higher ultimate strength or implementing a bi-linear material model in SLA;
- Implement 3D elements with SLA for full modelling of interlayer to compare computational costs and accuracy;
- Modelling of visco-plastic behaviour during cracking of Sentryglas (Santarsiero et al. [2016]);
- Research differences between SLA and non-iterative energy based method (NIEM) (Neto et al. [2015]);

9.2.4. Reinforced glass in general and on boundary of the scope

- Experiment of external impact in combination with force controlled load[1]
- Physical behaviour of de-bonding of the SentryGlas during cracking.
- To research the crack development in a reinforced beam with respect to different interlayers and reinforcements.
- Create a better understanding of the failure modes and design approach
- Research in time dependent behaviour of reinforcement adhesives for their over time effectiveness;

[1] Although these experiments are have high risks they do represent the design philosophy of these systems and the dynamic impact could lead to rupture of reinforcement.

A

Appendix A - Calculations

A.1. Analytical resistance calculation

The analytical calculation in this thesis is held very basic, where the two failure moments are calculated. This analytical calculation is based on basic mechanics for the linear part and horizontal equilibrium[1] for the cracked part as is also seen in Louter [2011]. In the cracked section it is still assumed that strain occur linear as is measured in Valarinho et al. [2012b]. For the post-tension in this thesis is implemented of increase of glass fracture strength, since the force is assumed to be uniform. This is shown in equation A.2 Since GFRP reinforcement is assumed to behave linear and brittle only initial and ultimate failure are the interesting points and no yielding is taken into account. The deflection is calculated based on EI and set-up dimensions. The stiffness of the un-cracked section or initial failure moment is calculated in a linear manner according to equation A.3 and equation A.4 for the ultimate failure of the cracked section. In order for simplicity and understandability the resistances are expressed in load (F_i, F_u) so they can be put easily in perspective to the experiments. This is done according to calculation A.5.

$$u = \frac{\frac{1}{2}FL_1}{24EI}(3L^2 - 4{L_1}^2) \tag{A.1}$$

$$f_t = f_{t,g} + \frac{F_p}{A_{glass}} \tag{A.2}$$

$$M_i = f_t \frac{EI}{E_{mean} y_{bot}} \tag{A.3a}$$

$$EI = \sum_i (I_{yy,i} E_i + {a_i}^2 A_i E_i) \tag{A.3b}$$

Where:

f_t	=	Elastic tensile stress limit
L_1	=	Distance between support and load introduction point
M_i	=	Moment resistance at initial failure
E_{mean}	=	Mean Youngs' modulus
EI	=	Stiffness of the beam
$I_y y$		Moment of inertia along the y-axis
A	=	Area
y_{bot}	=	Distance from neutral line to bottom of glass section
a_i	=	Distance between neutral line of total section and part i

[1] The height of the compression zone is calculated according to horizontal equilibrium and linear strain distribution $F_{u,re} = F_c$ where $F_{u,re} = \varepsilon_{u,re} A_{re} E_{re}$ and $F_c = \frac{x_u b}{2}(\frac{x_u}{h - c_{re} - x_u} \varepsilon_{u,re} E_{glass})$. Resulting in equation A.4c

A

The ultimate fracture moment is calculated according to

$$M_u = F_{u,re} z \tag{A.4a}$$

$$z = h - c_{re} - x_u \tag{A.4b}$$

$$x_u = -\frac{F_{u,re} - \sqrt{2E_{glass}F_{u,re}b(h-c_{re})\varepsilon_{u,re} + 2{F_{u,re}}^2}}{E_{glass}b\varepsilon_{u,re}} \tag{A.4c}$$

Where:
- M_u = Moment resistance at ultimate failure
- $F_{u,re}$ = Force in reinforcement at ultimate failure
- z = Distance of internal arm between cumulated reinforcement and compression zone forces
- h= Height of the glass section
- x_u = Height of compression zone at ultimate failure
- E = Young's modulus
- $\varepsilon_{u,re}$ = Ultimate strain of reinforcement

$$F = \frac{2M}{L_1} \tag{A.5}$$

A.2. Buckling calculation

The buckling calculation is based on column buckling by from Blaauwendraad [2007].This is a analytical calculation with a second order stress check. As this calculation in incorporated in the analytical calculation in Matlab as a function its code is presented below[2]. The code is validated with the given example in the paper.

```
function [ P_Lower, P_critical, P_Upper ] = Buckling_strength( h_glass,...
h_glass_max,A_single_pane, L_beam, ...
t_interlayer, t_glass, E_glass, G_interlayer,n_panes)

%Buckling based on Blauwendraad - Buckling of laminated glass columns

%care for number of layers in section
%out of plane properties
if n_panes ==2
  %c.t.c from outer panes, 2 panes
  eccentricity=t_glass(1)/2+t_glass(2)/2+t_interlayer;
elseif n_panes==3
  %c.t.c from outer panes, 3 panes
  eccentricity=t_glass(1)/2+t_glass(3)/2+t_glass(2)+2*t_interlayer;
end

I_single_glass_weak=1/12*h_glass.*t_glass.^3;

%k-factors
k_panes=pi^2*E_glass*A_single_pane/L_beam^2;
k_interlayer=G_interlayer*h_glass_max/t_interlayer;

f_panes=1./k_panes;
f_interlayer=1/k_interlayer;
```

[2]The code is written for both 2 and 3 panes, as the work of Blaauwendraad was based on only 2 pane the implementation of 3 panes is based on applying the same concept

```
%Upper and Lower bounds
P_Lower=pi^2*E_glass*sum(I_single_glass_weak)/L_beam^2;
P_Upper=P_Lower+eccentricity^2/sum(f_panes) ;

%critical value
xi_factor=sum(f_panes)/(sum(f_panes)+(n_panes-1)*f_interlayer); %care #interlayers
P_critical=(1-xi_factor)*P_Lower+xi_factor*P_Upper;

end
```

The stress check is done via another function, which is presented below.

```
function [ Buckling_stress, unityCheck_Buckling, w] = Buckling_Safety( ...
  h_glass, A_single_pane, L_beam, P_pretension, P_critical, P_lower, ...
  f_t_design, t_interlayer, t_glass)

W_single_glass= 1/6*h_glass.*t_glass.^2;
e= t_glass(1)/2 + t_glass(2)/2 + t_interlayer ;
w_0=L_beam/300 ;
n=P_critical/P_pretension ;

w= n / (n-1) * w_0;

%Moments
M_total= w*P_pretension;
M_M = M_total * P_lower / P_critical ;
M_N=  M_total * (P_critical - P_lower ) / P_critical  ;

%Normal due eccentricity
N_e = M_N / e  ;

%Stresses
Buckling_stress(1) = -M_M/W_single_glass(1) + (N_e - 0.5*P_pretension)/ ...
  A_single_pane(1) - P_pretension/A_single_pane(1) ;
Buckling_stress(2) = M_M/W_single_glass(1) + (N_e - 0.5*P_pretension)/...
  A_single_pane(1) - P_pretension/A_single_pane(1) ;
Buckling_stress(3) = -M_M/W_single_glass(2) + (N_e - 0.5*P_pretension)/...
  A_single_pane(2) ;
Buckling_stress(4) = M_M/W_single_glass(2) + (N_e - 0.5*P_pretension)/...
  A_single_pane(2) ;

%Check
unityCheck_Buckling= Buckling_stress/f_t_design  ;

end
```

A.3. Specimen calculations

In the sections hereafter the in and- output files are presented for all bending tests

A.3.1. BEN1 - input

```
%global dimensions
L_beam=1100;
L1=375;
L2=L_beam-2*L1;
```

A

```
%glass
h_glass=[150 150];
h_glass_max=max(h_glass);
t_glass=[10 10 ];
n_panes=length(h_glass);
%number must be equal to the #elements in height and thickness

%interlayer
pre_laminated=1; %laminated before prestressing =1
t_interlayer=0.1;
G_interlayer=5;

material_re = mat_re{10};
%1=S-GFRP UD; 2=E-GFRP UD; 3=E-GFRP 0-90; 4- S2-GFRP UD
%5=SS EN1.4301; 6=GFRP Neto; 7=CFRP Louter;8=HT CFRP DPP; 9=HM CFRP DPP;
%10=Fibro; 11=plain UD E-Glass; 12=TEN-FIB data, 13=SG-GF composite;
h_re(1,m)=3; b_re(1,m)=20; cover_re(1,m)=-1; %distance from bottom

A_single_re(:,m)=h_re(:,m).*b_re(:,m); %area of single reinforcement
A_single_pane=h_glass.*t_glass;

F_p_input=20000;
f_t_design=17;

glass_type=1;
%1,2,3 for glas types AN, HS and FT respectively
material_glass=mat_glass{glass_type};
sigma_g_compr_u=450;
crack_stress_overwrite=0;

end
```

A.3.2. BEN2-FFR - input

```
%global dimensions
L_beam=800-2*25;
L1=275;
L2=L_beam-2*L1;

%glass
h_glass=[80 80];
h_glass_max=max(h_glass);
t_glass=[8 8];
n_panes=length(h_glass);
%number must be equal to the #elements in height and thickness

%interlayer
pre_laminated=0; %laminated before prestressing =1
t_interlayer=3*1.52;
G_interlayer=40;

material_re = mat_re{13};
%1=S-GFRP UD; 2=E-GFRP UD; 3=E-GFRP 0-90; 4- S2-GFRP UD
%5=SS EN1.4301; 6=GFRP Neto; 7=CFRP Louter;;8=HT CFRP DPP; 9=HM CFRP DPP;
%10=Fibro; 11=plain UD E-Glass; 12=TEN-FIB data, 13=SG-GF composite;
```

```
h_re(1,m)=16; b_re(1,m)=1.357; cover_re(1,m)=20; %distance from bottom


A_single_re(:,m)=h_re(:,m).*b_re(:,m); %area of single reinforcement
A_single_pane=h_glass.*t_glass;

UseDeterminedPrestress=1;
F_p_input=0;
f_t_design=17;

glass_type=1;
%1,2,3 for glas types AN, HS and FT respectively
material_glass=mat_glass{glass_type};
sigma_g_compr_u=450;
crack_stress_overwrite=0;
```

A.3.3. BEN2-REF - input

```
%global dimensions
L_beam=800-2*25;
L1=275;
L2=L_beam-2*L1;

%glass
h_glass=[80 80];
h_glass_max=max(h_glass);
t_glass=[8 8];
n_panes=length(h_glass);
%number must be equal to the #elements in height and thickness

%interlayer
pre_laminated=0; %laminated before prestressing =1
t_interlayer=3*1.52;
G_interlayer=40;

material_re = mat_re{1};
%1=S-GFRP UD; 2=E-GFRP UD; 3=E-GFRP 0-90; 4- S2-GFRP UD
%5=SS EN1.4301; 6=GFRP Neto; 7=CFRP Louter;;8=HT CFRP DPP; 9=HM CFRP DPP;
%10=Fibro; 11=plain UD E-Glass; 12=TEN-FIB data, 13=SG-GF composite;
h_re(1,m)=6; b_re(1,m)=0.8; cover_re(1,m)=13; %distance from bottom
h_re(2,m)=6; b_re(2,m)=0.8; cover_re(2,m)=26; %distance from bottom


A_single_re(:,m)=h_re(:,m).*b_re(:,m); %area of single reinforcement
A_single_pane=h_glass.*t_glass;

UseDeterminedPrestress=1;
F_p_input=0;

glass_type=1;
%1,2,3 for glas types AN, HS and FT respectively
material_glass=mat_glass{glass_type};
sigma_g_compr_u=450;
crack_stress_overwrite=0;
```

A

A.3.4. BEN1 - output

```
Reinforcement failure

Pretension_force_kN =

20


Initial_failure_kN =

19.0021


Initial_failure_P_kN =

21.8172


Ultimate_failure_kN =

37.0708


Initial_deflection =

1.9674


Ultimate_deflection =

34.9601


Buckling_stress =

-26.1431   -2.6188  -12.8098   10.7145


Buckling_deflection_hor =

5.7267

'Initial buckling force='    [55.5982]

'Ultimate compression'    [54]    [54]

'Additional glass stress due pre-te'    [6.6667]

'Less stress in reinforcement ='    [166.6667]
```

A.3.5. BEN2-FFR - output

```
Reinforcement failure

Pretension_force_kN =
```

```
0

Initial_failure_kN =

5.6897

Initial_failure_P_kN =

5.6897

Ultimate_failure_kN =

7.6590

Initial_deflection =

1.7179

Ultimate_deflection =

75.3550

Buckling_stress =

not applicable

Buckling_deflection_hor =

not applicable
'Initial buckling force='    [48.1277]
'Ultimate compression...'    [19.8882]    [19.8882]
'Additional glass stress due pre-te...'    [0]
'Less stress in reinforcement ='    [0]
```

A.3.6. BEN2-REF - output

```
Reinforcement failure

Pretension_force_kN =

0

Initial_failure_kN =
```

A

```
5.6383

Initial_failure_P_kN =

5.6383

Ultimate_failure_kN =

7.7856

Initial_deflection =

1.7027

Ultimate_deflection =

85.1226

Buckling_stress =

not applicable

Buckling_deflection_hor =

not applicable

'Initial buckling force='    [48.1277]

'Ultimate compression...'    [19.8720]    [19.8720]

'Additional glass stress due pre-te...'    [0]

'Less stress in reinforcement ='    [0]
```

A.4. Composite calculation

The composite calculation is a method to calculate the equivalent stiffness and tensile strength based on the fvf. The calculation is executed in a spreadsheet for x,y and z directions to cover all possibilities and store mostly used materials. In the following equations k is used to generalise the equation. In most cases only x-direction was applicable resulting in negligible contribution of the matrix to the tensile strength.

$$E_k = fvf E_{fibre} \rho_k + (1 - fvf) E_{matrix} \tag{A.6}$$

$$f_{tk} = fvf \rho_k f_{t\,fibre} + (1 - fvf) f_{t\,matrix} \tag{A.7}$$

In the work of Louter and Nielsen [2013] a study is regarding the stiffness of SG interlayer, in this thesis this

is calculated back to Young's modulus using the inverse of equation A.8.

$$G = \frac{E}{2(1-\nu)} \tag{A.8}$$

A.4.1. Shear resistance

Shear resistance is based on the shear stiffness of the SG, in this calculation it is assumed that de-bonding occurs when the interlayer is reaching plasticity and the stresses are redistributed. Yield deformation is assumed to occur over the diagonal of the thickness with an angle of $45°$, based on Poisson ratio 0.49. This is presented in equations A.9.

$$F_{bond} = A_{bond}\tau_{y,SG} \tag{A.9a}$$

$$\tau_{y,SG} = \gamma_y G_{SG} \tag{A.9b}$$

$$\gamma_y = \frac{u_y}{t_{SG}} \tag{A.9c}$$

$$u_y = \sqrt{t^2 + t^2} * \frac{\sqrt{2}}{2} * \varepsilon_{y,SG} \tag{A.9d}$$

Where: $\tau_{y,SG}$ = Yield shear stress of SentryGlas
γ_y = Yield shear strain
u_y = horizontal part of the $45°$ diagonal deformation over the thickness

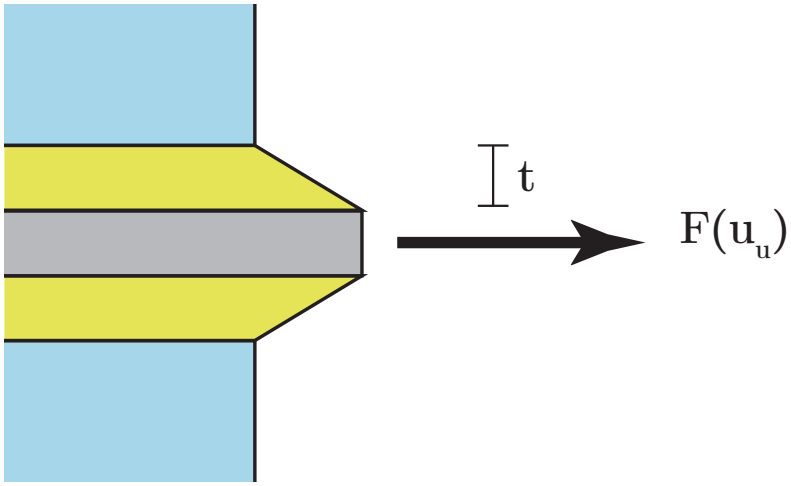

B

Appendix B - Experiments

B.1. Experiments BEN1

B.1.1. Pre-stress force

Based on the tensile test of experiment TEN-FIB the strains are calculated to limit the post-tension force. This calculation is based on basic constitutive law, $\sigma = E \cdot \varepsilon$ as elaborated in equations B.1. Using the input parameters $F_p = 20\text{kN}, A_{re} = 60\text{mm}^2, E_{re} = 15.33\text{GPa}$, a strain of $\varepsilon_p = 1.1 \cdot 10^{-}2$ is reached. This is equal to $\mu\varepsilon = 11000$ which value is read on the measuring software of strain gauges.

$$\varepsilon_p = \frac{\sigma_{re,p}}{E_{re}} \tag{B.1a}$$

$$\sigma_{re,p} = \frac{F_p}{A_{re}} \tag{B.1b}$$

B.1.2. Force introduction

After discovery of the fault of low post-tension force in the specimen of experiment BEN1. The option is taken to tighten the specimen even more in order to increase the normal force after curing. In hindsight this would have no affect as the adhesive was already cured and the horizontal stresses flow directly in the reinforcement due to the rigidity of the bound. To support this argument a small linear FEA is performed, its results are seen in Figure B.1. Here the beam for the dimension (lxbxh) 1100 x 20 x 150 is modelled with one symmetry axis at the right. At the top and bottom edges of the element supports in x-direction are added to simulate the cured epoxy. These supports are present up to 90% of the edge, to simulate the gap. On the left edge the two loads simulate the pretension force. In Figure B.1c is seen that the horizontal force is directly flown into the horizontal supports and therefore does not affect the compressive stress in the overall beam as it does in B.1b.

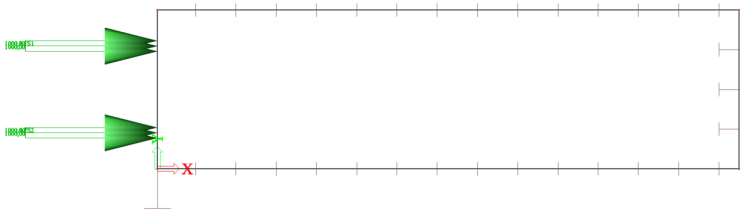

(a) OVerview of FE model

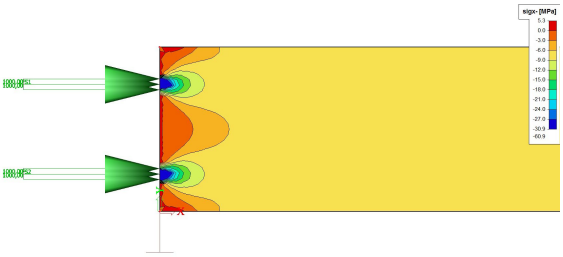

(b) σ_{xx} without edge constrains in x-directions

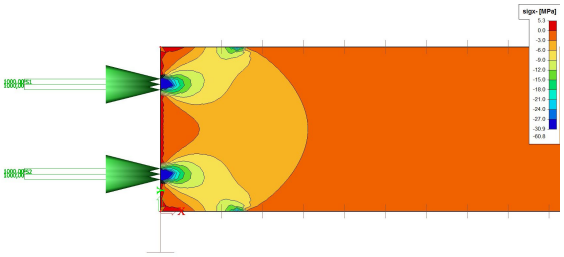

(c) σ_{xx} with edge constrains in x-directions

Figure B.1: Small FE calculation with and without constrains in x-direction

B.2. Photo sequence of experiments

B.2.1. Experiment BEN1

In the following figures a photo sequence is seen of one specimen of the performed experiments. No sequence is given of experiment PULL-FFR, since failure is not visible in the footage.

Experiment BEN1-3, 1200 mm PVB laminated glass with 20x3 GFRP strips adhered with both a post-tension of approximate 1000 N using DP490 epoxy.

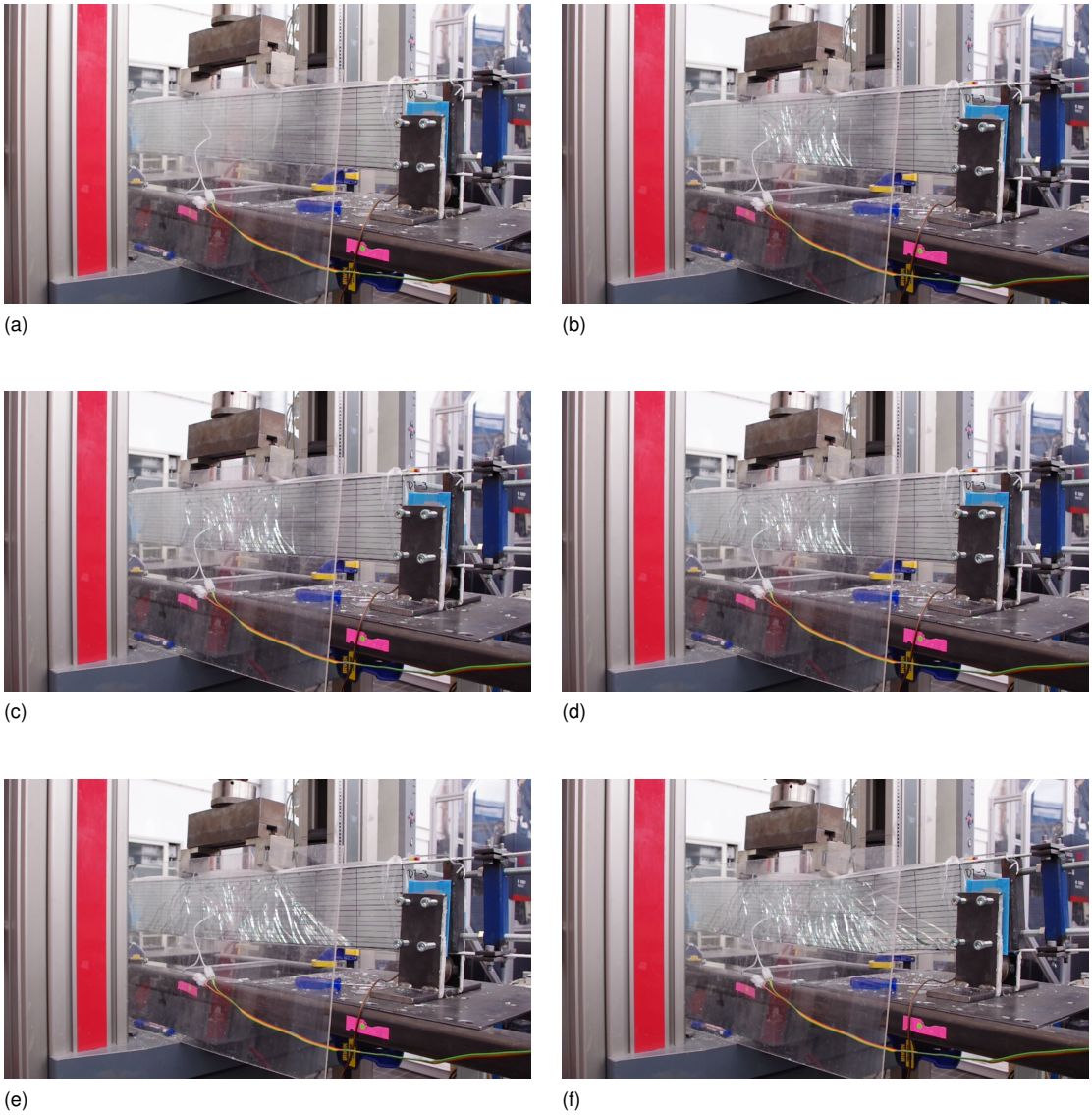

(a) (b) (c) (d) (e) (f)

Figure B.2: Photo sequence of experiment BEN1-3

Experiment BEN2-FFR-3, 800 mm SG laminated glass with integrated 16mm FFR. This specimen stands out due to the double cracks which occurred at the same time.

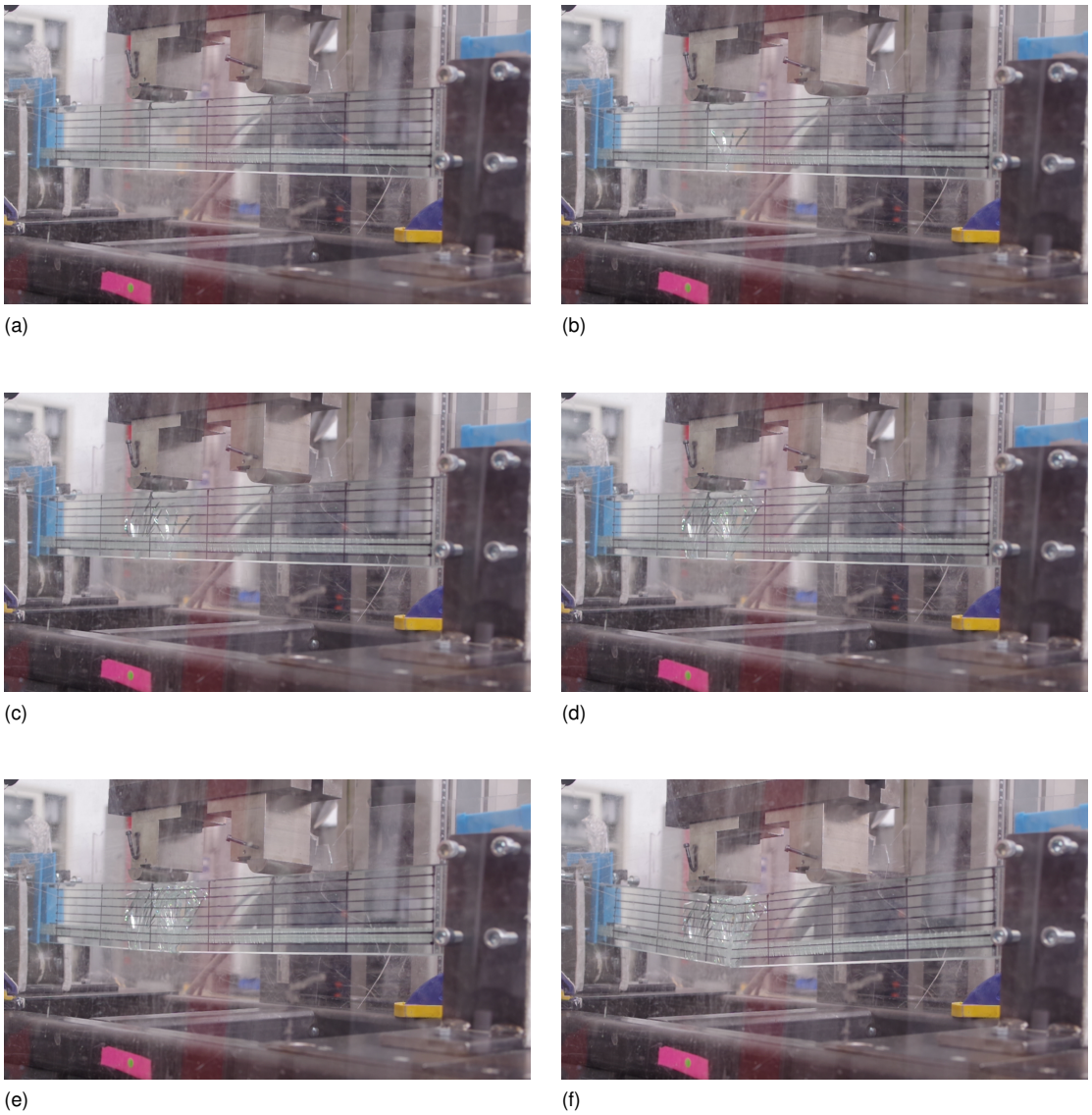

(a) (b)

(c) (d)

(e) (f)

Figure B.3: Photo sequence of experiment BEN2-FFR-3

Experiment BEN2-REF-3, 800 mm SG laminated glass with integrated 2x 0.8x6mm GFRP reinforcement. Crack development is much more concentrated and instant in relation to the PVB laminated beam.

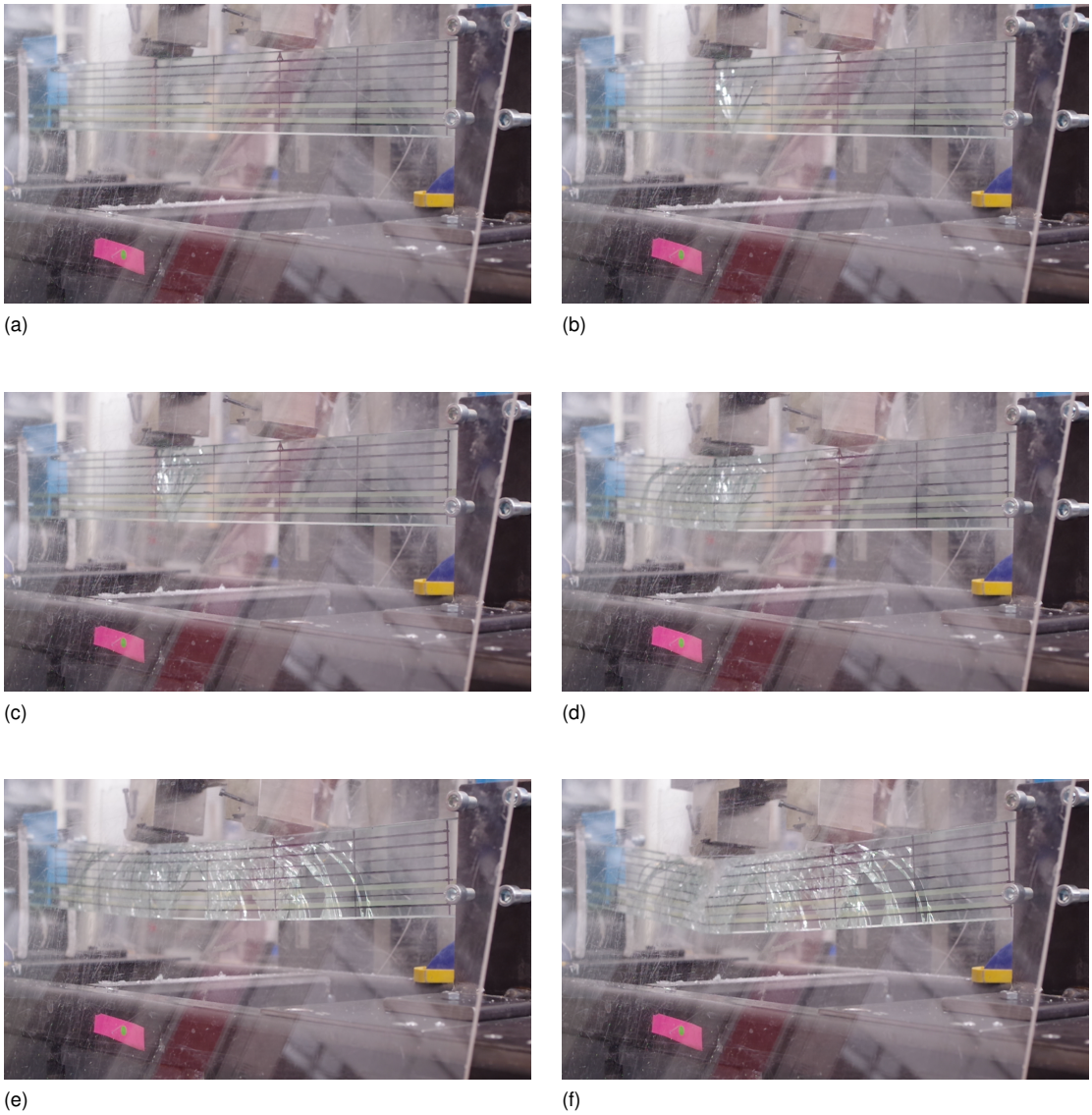

(a) (b)

(c) (d)

(e) (f)

Figure B.4: Photo sequence of experiment BEN2-REF-3

Experiment PULL-REF-4 en 5, pull-out experiment with SG laminated glass with integrated 0.8x6mm GFRP reinforcement.

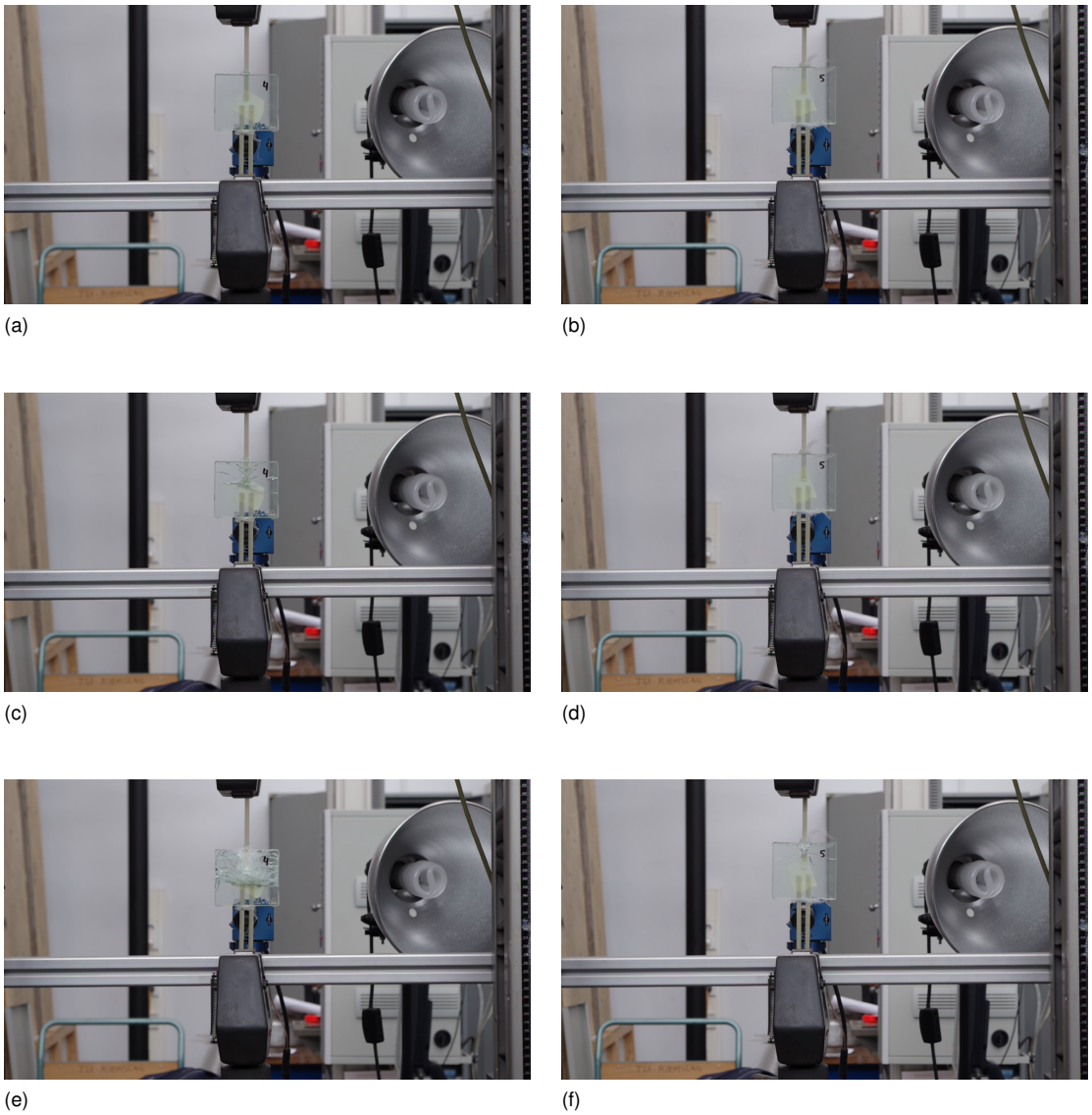

(a) (b)

(c) (d)

(e) (f)

Figure B.5: Photo sequence of experiment PULL-REF-4/5

Experiment TEN-FFR-1, pull-out experiment with SG laminated glass with integrated 0.8x6mm GFRP reinforcement.

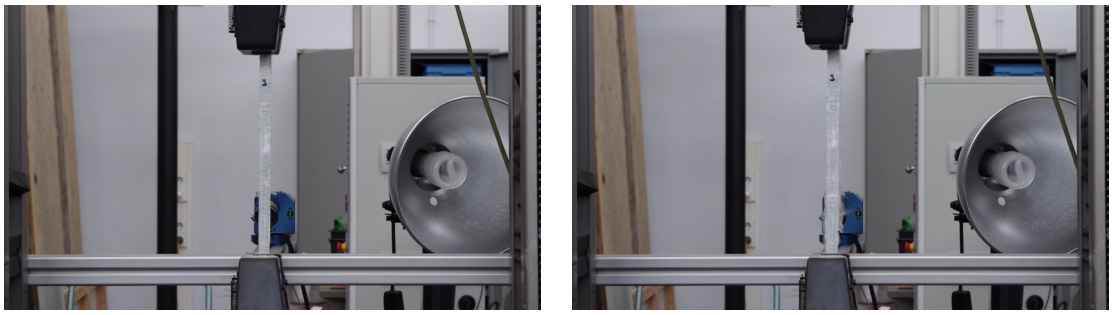

(a) (b)

Figure B.6: Photo sequence of experiment TEN-FFR-3

Experiment TEN-FIB-3, tensile experiment of 20x3 GFRP strips.

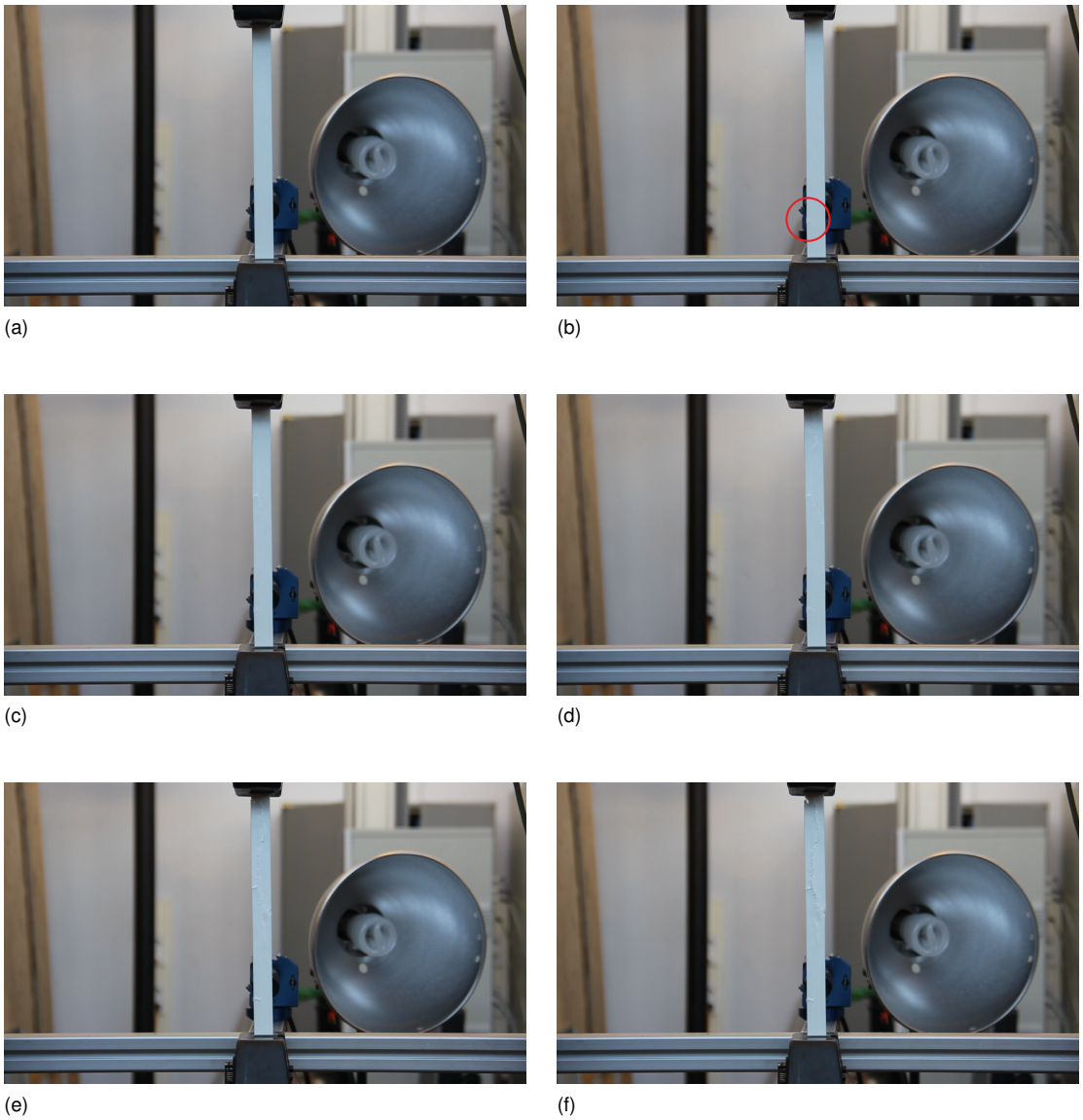

(a) (b)

(c) (d)

(e) (f)

Figure B.7: Photo sequence of experiment TEN-FIB-3

C

Appendix C - Numerical calculations

In this Appendix the input files for the numerical calculations are shown, starting with input data followed by the command files and at last the construction of the different saw-tooth models including their data points for both glass and reinforcement.

C.1. Input for data files

In this section the SLA input files of reference Model M-REF and Model M-BEN1 are shown.

C.1.1. Input data Model M-REF

```
FEMGEN MODEL       : BEDON2014_0130_gf3_0314
ANALYSIS TYPE      : Structural 2D
MODEL DESCRIPTION : Bedon2014, triangular mesh, h=10, fracture energy=3.0, sla reinforceme
'UNITS'
LENGTH    MM
TIME      SEC
TEMPER    KELVIN
FORCE     N
'COORDINATES' DI=2
    1       5.550000E+02      0.000000E+00
    2       5.647500E+02      0.000000E+00
    3       5.745000E+02      0.000000E+00
(...)
4171       2.000000E+01     -7.600000E-01
4172       3.000000E+01     -7.600000E-01
4173       4.000000E+01     -7.600000E-01
'ELEMENTS'
CONNECTIVITY
    1 CT12M  1 274 2 295 22 294
    2 CT12M  2 296 23 335 22 295
    3 CT12M  2 275 3 297 23 296
 (...)
 1779 CT12M  1904 3703 1952 3752 1951 3702
 1780 CT12M  1904 3607 232 3704 1952 3703
 1781 CT12M  232 965 253 3753 1952 3704
 1782 CQ16M  1037 3803 3754 3853 1329 1953 1059 3852
 1783 CQ16M  3754 3804 3755 3854 1330 1954 1329 3853
 1784 CQ16M  3755 3805 3756 3855 1331 1955 1330 3854
(...)
```

```
 1922 CQ16M   1034 1051 1035 4172 1057 1134 1056 4171
 1923 CQ16M   1035 1052 1036 4173 1058 1135 1057 4172
 1924 CQ16M   1036 1053 1037 3852 1059 1136 1058 4173
MATERIALS
/ 1-480 486-1781 /  1
/ 481-485 1831-1879 1900-1919 /  2
/ 1782-1830 1880-1899 1920-1924 /  3
GEOMETRY
/ 481-485 1831-1879 1900-1919 /  1
/ 1-480 486-1781 /  2
/ 1782-1830 1880-1899 1920-1924 /  3
DATA
/ 481-485 1831-1879 1900-1919 /  1
/ 1-480 486-1781 /  1
/ 1782-1830 1880-1899 1920-1924 /  1
'MATERIALS'
   1 YOUNG      7.000000E+04
     POISON     2.300000E-01
     TOTCRK FIXED
     TENSTR     4.500000E+01
     GF1        3.000000E-03
     TAUCRI     2
   2 YOUNG      2.000000E+05
     POISON     3.000000E-01
     TOTCRK FIXED
     TENSTR     5.500000E+02
     GF1        2.203000E+04
     TAUCRI     2
   3 YOUNG      1.192000E+02
     POISON     4.900000E-01
'FILOS'
/materi(1)/TSAWLW    TABLE
/materi(1)/TSAWDI    6.4286e-04    4.5000e+01
                     3.9105e-04    2.7000e+01
                     2.6514e-04    1.8001e+01
                     1.3924e-04    9.0008e+00
                     1.3333e-05    1.0000e-03
                     1.3333e-01    1.0000e-03
/materi(3)/TSAWLW    TABLE
/materi(3)/TSAWDI    0.002894737 550.00
                     0.012315783 770.00
                     0.021736857 790.00
                     0.031157878 798.00
                     0.040578857 800.00
                     0.05 806.00
                     0.1 817.75
                     0.15 829.50
                     0.2 841.25
                     0.25 853.00
                     0.275 800.00
                     4 0.00001
/loads(1)/LOTYPE REFLOD
'GEOMETRY'
   1 THICK      2.200000E+01
   2 THICK      2.200000E+01
   3 THICK      2.200000E+01
```

```
'GROUPS'
ELEMEN
   1 GLASS / 1-480 486-1781 /
NODES
   2 GLASS_N / 1-1025 1054-3753 /
ELEMEN
   3 INTER / 1782-1830 1880-1899 1920-1924 /
NODES
   4 INTER_N / 1-21 274-293 1032-1037 1049-1059 1132-1136 1329-1376
               1953-2001 3754-3901 4049-4108 4169-4173 /
ELEMEN
   5 RE / 481-485 1831-1879 1900-1919 /
NODES
   6 RE_N / 1026-1053 3754-3851 3902-4088 4109-4168 /
'SUPPORTS'
 / 21 42 63 84 105 126 147 168 189 210 231 252 273 334 395 456 517
   578 639 700 761 822 883 944 1005 4068 4108 4128 4168 /   TR     1
 / 253 1031 /   TR     2
'DATA'
 1  LINEAR
'LOADS'
CASE 1
DEFORM
 253 TR 2 -0.100000E+01
'DIRECTIONS'
1   1.000000E+00   0.000000E+00   0.000000E+00
2   0.000000E+00   1.000000E+00   0.000000E+00
3   0.000000E+00   0.000000E+00   1.000000E+00
'END'
```

C.1.2. Input data Model M-BEN1

```
FEMGEN MODEL      : BEN1_2305_no_adh_E15
ANALYSIS TYPE     : Structural 2D
MODEL DESCRIPTION : Experimental Young, no adherence
'UNITS'
LENGTH   MM
TIME     SEC
TEMPER   CELSIU
FORCE    N
'COORDINATES' DI=2
    1      0.000000E+00     0.000000E+00
    2      1.000000E+01     0.000000E+00
    3      2.000000E+01     0.000000E+00
(...)
 4551      5.756944E+02     1.531000E+02
 4552      5.854167E+02     1.531000E+02
 4553      5.951389E+02     1.531000E+02
'ELEMENTS'
CONNECTIVITY
    1 CT12M  1 97 2 103 7 102
    2 CT12M  2 104 8 113 7 103
    3 CT12M  2 98 3 105 8 104
(...)
 1828 CT12M  2966 3793 2984 3812 2983 3792
 1829 CT12M  2966 3759 2967 3794 2984 3793
 1830 CT12M  2967 3795 2985 3813 2984 3794
```

```
 1831 CQ16M   3814 3820 3815 3826 2 97 1 3825
 1832 CQ16M   3815 3821 3816 3827 3 98 2 3826
 1833 CQ16M   3816 3822 3817 3828 4 99 3 3827
(...)
 2072 CQ16M   4329 4366 4330 4533 4515 4551 4514 4532
 2073 CQ16M   4330 4367 4331 4534 4516 4552 4515 4533
 2074 CQ16M   4331 4368 4332 4535 4517 4553 4516 4534
MATERIALS
/ 1-1830 / 1
/ 1892-1952 2014-2074 / 2
/ 1831-1891 1953-2013 / 2
GEOMETRY
/ 1-1830 / 1
/ 1892-1952 2014-2074 / 1
/ 1831-1891 1953-2013 / 1
DATA
/ 1-1830 / 1
/ 1892-1952 2014-2074 / 1
/ 1831-1891 1953-2013 / 1
'MATERIALS'
   1 YOUNG      7.000000E+04
     POISON     2.300000E-01
     TOTCRK FIXED
     TENSTR     4.500000E+01
     GF1        3.000000E-03
     TAUCRI     2
   2 YOUNG      4.000000E+04
     POISON     3.000000E-01
     TOTCRK FIXED
     TENSTR     9.000000E+02
     GF1        1.012500E+02
     TAUCRI     2
   3 YOUNG      1.192000E+02    1.192000E+02
     POISON     4.900000E-01
     SHRMOD     4.000000E+01
'FILOS'
/materi(1)/TSAWLW     TABLE
:N5 h7 gf3
/materi(1)/TSAWDI     6.4286e-04    4.5000e+01
                      3.9105e-04    2.7000e+01
                      2.6514e-04    1.8001e+01
                      1.3924e-04    9.0008e+00
                      1.3333e-05    1.0000e-03
                      1.3333e-01    1.0000e-03
/materi(2)/TSAWLW     TABLE
:N5 Fibro Experiment data
/materi(2)/TSAWDI    3.7052e-02    5.6800e+02
                     3.7052e-02    4.2600e+02
                     3.7052e-02    2.8400e+02
                     3.7052e-02    1.4200e+02
                     3.7052e-02    1.0000e-07
                     3.7052e-00    1.0000e-07
/loads(1)/LOTYPE REFLOD
'GEOMETRY'
1 THICK      2.000000E+01
'GROUPS'
```

```
ELEMEN
   1 GLASS / 1-1830 /
NODES
   2 GLASS_N / 1-3813 /
ELEMEN
   3 RE_BOT / 1892-1952 /
NODES
   4 RE_BOT_N / 3814-3824 3831-3906 3945-3980 3999-4183 /
ELEMEN
   5 RE_TOP / 2014-2074 /
NODES
   6 RE_TOP_N / 4184-4189 4196-4238 4277-4332 4351-4553 /
ELEMEN
   7 INTER / 1831-1891 1953-2013 /
NODES
   8 INTER_N / 1-6 91-101 337-379 912-987 2660-2715 2968-3003 3796-3998
               4184-4368 /
'SUPPORTS'
 / 2715 2733 2751 2769 2787 2805 2823 2841 2859 2877 2895 2913 2931
  2949 2967 2985 3039 3093 3147 3201 3255 3309 3363 3417 3471 3525
  3579 3633 3687 3741 3795 3962 3998 4147 4183 4332 4350 4517 4535 /
TR     1
 / 4004 4423 /   TR     2
'DATA'
 1  LINEAR
'LOADS'
CASE 1
DEFORM
 4423 TR 2 -0.100000E+01
'DIRECTIONS'
1    1.000000E+00    0.000000E+00    0.000000E+00
2    0.000000E+00    1.000000E+00    0.000000E+00
3    0.000000E+00    0.000000E+00    1.000000E+00
'END'
```

C.2. Command files

C.2.1. Command file for Model M-REF

```
*FILOS
INITIA
*INPUT

*NONLIN
!SEGMENT DV03
:TYPE PHYSIC OFF

BEGIN EXECUT
  BEGIN LOAD
    STEPS  EXPLIC  SIZES 1.0(6525)
  END LOAD
END EXECUT

BEGIN OUTPUT FEMVIE
  BEGIN SELECT
    STEPS 1-10 25-6025(50)
  END SELECT
```

```
  DISPLA  TOTAL  TRANSL  GLOBAL
  FORCE  REACTI  TRANSL  GLOBAL
  STRAIN  TOTAL  GREEN  GLOBAL INTPNT
  STRESS  TOTAL  CAUCHY  GLOBAL INTPNT
  STRAIN CRACK INTPNT
  STATUS USER ITEM01
END OUTPUT

BEGIN OUTPUT TABULA
  DISPLA  TOTAL  TRANSL  GLOBAL
  FORCE  REACTI  TRANSL  GLOBAL
  BEGIN SELECT
    NODES 253
  END SELECT
  STRAIN  TOTAL  GREEN  GLOBAL INTPNT
  STRESS  TOTAL  CAUCHY  GLOBAL INTPNT
  BEGIN SELECT
    ELEMEN 1 1900
  END SELECT
  BEGIN LAYOUT
    LINPAG=10000
    COLLIN=150
    DIGITS results 10
  END LAYOUT
END OUTPUT

BEGIN OUTPUT TABULA
  STRAIN  TOTAL  GREEN  GLOBAL INTPNT
  STRESS  TOTAL  CAUCHY  GLOBAL INTPNT
  BEGIN SELECT
    ELEMEN 481-485 1831-1879 1900-1919
    NODES 1026-1053 3754-3851 3902-4088 4109-4168
  END SELECT
  BEGIN SELECT
    STEPS 2031
  END SELECT
  BEGIN LAYOUT
    LINPAG=10000
    COLLIN=150
    DIGITS results 10
  END LAYOUT
END OUTPUT

*END
```

C.2.2. Model M-BEN1

```
*FILOS
INITIA
*INPUT

*NONLIN
!SEGMENT DV03
:TYPE PHYSIC OFF

BEGIN EXECUT
  BEGIN LOAD
```

```
    STEPS  EXPLIC  SIZES 1.0(8000)
  END LOAD
END EXECUT

BEGIN OUTPUT FEMVIE
  BEGIN SELECT
    STEPS 1-10 25-8025(50)
  END SELECT
  DISPLA  TOTAL  TRANSL  GLOBAL
  FORCE  REACTI  TRANSL  GLOBAL
  STRAIN  TOTAL  GREEN  GLOBAL INTPNT
  STRESS  TOTAL  CAUCHY  GLOBAL INTPNT
  STRAIN CRACK INTPNT
  STATUS USER ITEM01
  END OUTPUT

BEGIN OUTPUT TABULA
  DISPLA  TOTAL  TRANSL  GLOBAL
  FORCE  REACTI  TRANSL  GLOBAL
  BEGIN SELECT
    NODES 4423
  END SELECT
  BEGIN LAYOUT
    LINPAG=10000
    COLLIN=150
    DIGITS results 10
  END LAYOUT
END OUTPUT

*END
```

C.3. Material models

C.3.1. Glass curves

Code used for the $G_f = 3.0\text{J/m}^2$ model;

```
/materi(1)/TSAWLW     TABLE
/materi(1)/TSAWDI     0.000642857  45
0.00034175  23.70143302
0.000181678 12.15780429
9.65822E-05 6.021081792
5.13442E-05 2.758731287
2.72951E-05 1.024429171
6.4286e-00    1.0000e-03
```

Code used for the $G_f = 5.5\text{J/m}^2$ model;

```
0.000642857 45
0.000380346 26.23605757
0.000225032 14.7461766
0.00013314  7.948188164
7.87724E-05 3.926158092
4.66057E-05 1.546523872
6.4286e-00    1.0000e-03
```

Code used for the $G_f = 8.0\text{J/m}^2$ model;

```
/materi(1)/TSAWLW     TABLE
/materi(1)/TSAWDI     0.000642857  45
```

```
                    0.000406464   27.9086037
                    0.000256999   16.55818039
                    0.000162495   9.381556856
                    0.000102742   4.843935318
                    6.49613E-05   1.974896818
                    6.4286e-00    1.0000e-03
```

C

Code used for the brittle model

```
/materi(1)/TSAWLW     TABLE
/materi(1)/TSAWDI     6.4286e-04    4.5000e+01
                      6.4286e-04    2.7000e+01
                      6.4286e-04    1.8001e+01
                      6.4286e-04    9.0008e+00
                      6.4286e-04    1.0000e-03
                      6.4286e-00    1.0000e-03
```

C.3.2. Stainless steel curves

Curve REF

```
/materi(2)/TSAWLW     TABLE
/materi(2)/TSAWDI     0.002894737 550.00
                      0.012315783 770.00
                      0.021736857 790.00
                      0.031157878 798.00
                      0.040578857 800.00
                      0.05 806.00
                      0.1 817.75
                      0.15 829.50
                      0.2 841.25
                      0.25 853.00
                      0.275 800.00
                      4 0.00001
```

Curve P5

```
/materi(2)/TSAWLW     TABLE
/materi(2)/TSAWDI     0.0043   859.9500
                      0.0048   859.9500
                      0.0053   859.9500
                      0.0058   859.9500
                      0.0064   859.9500
                      0.0071   859.9500
                      0.0078   859.9500
                      0.0087   859.9500
                      0.0096   859.9500
                      0.0106   859.9500
                      0.0117   859.9500
                      0.0129   859.9500
                      0.0143   859.9500
                      0.0158   859.9500
                      0.0175   859.9500
                      0.0193   859.9500
                      0.0213   859.9500
                      0.0236   859.9500
                      0.0261   859.9500
                      0.0288   859.9500
                      0.0318   859.9500
```

```
                    0.0352   859.9500
                    0.0389   859.9500
                    0.0430   859.9500
                    0.0475   859.9500
                    0.0525   859.9500
                    0.0580   859.9500
                    0.0641   859.9500
                    0.0709   859.9500
                    0.0783   859.9500
                    0.0866   859.9500
                    0.0957   859.9500
                    0.1058   859.9500
                    0.1169   859.9500
                    0.1292   859.9500
                    0.1428   859.9500
                    0.1578   859.9500
                    0.1745   859.9500
                    0.1928   859.9500
                    0.2131   859.9500
                    0.2355   859.9500
                    0.2603   859.9500
                    0.2750   821.8708
                    0.3750   0.0001
```

Curve P10

```
/materi(2)/TSAWLW    TABLE
/materi(2)/TSAWDI    0.0045   900.9000
                     0.0055   900.9000
                     0.0067   900.9000
                     0.0082   900.9000
                     0.0101   900.9000
                     0.0123   900.9000
                     0.0150   900.9000
                     0.0184   900.9000
                     0.0224   900.9000
                     0.0274   900.9000
                     0.0335   900.9000
                     0.0410   900.9000
                     0.0501   900.9000
                     0.0612   900.9000
                     0.0748   900.9000
                     0.0914   900.9000
                     0.1117   900.9000
                     0.1365   900.9000
                     0.1669   900.9000
                     0.2039   900.9000
                     0.2493   900.9000
                     0.2750   813.2218
                     0.375    0.00001
```

Stainless steel saw-tooth generation

The steel curves are generated using Matlab as their number is quite extensive. The main part of the Matlab code is seen below.

```
%Input values
p=0.1;
E(1)=200000;
```

```
f_t=819;
eps_u=0.275;

%Starting parameters
f_t_tooth(1)=f_t*(1+p);
eps(1)=f_t_tooth(1)/E(1);
i=2;

while eps<eps_u
    % Define lower tooth with reduced elasticity
    eps(i)=f_t_tooth(i-1)/E(i-1);
    f_t_tooth(i)=f_t*(1-p);
    E(i)=E(i-1)*(1-p)/(1+p);

    % Define new upper tooth with new elasticity
    i=i+1;
    f_t_tooth(i)=f_t*(1+p);
    E(i)=E(i-1);
    eps(i)=f_t_tooth(i)/E(i);
    i=i+1;
end
%Cut off last tooth at ultimate strain
if  eps(i-1)>eps_u
    eps(i-1)=eps_u;
    f_t_tooth(i-1)=eps_u*E(i-1);
end

%Filter only + values
k=1
for n=2:2:i
    Write_f_t(k)=f_t_tooth(n);
    Write_eps(k)=eps(n);
    k=k+1;
end
```

Bibliography

3M. Scotch-Weld. pages 1–4, 1996.

AGY. High Strength Glass Fibers. Technical report, 2006.

C. Bedon and C. Louter. Exploratory numerical analysis of SG-laminated reinforced glass beam experiments. *Engineering Structures*, 75:457–468, 2014. ISSN 01410296. doi: 10.1016/j.engstruct.2014.06.022. URL http://dx.doi.org/10.1016/j.engstruct.2014.06.022.

J. Belis. The Effect of Post-Tensioning On the Buckling Behaviour of a Glass T-Beam. 2004.

J. Belis, J. Depauw, D. Callewaert, D. Delincé, and R. Van Impe. Failure mechanisms and residual capacity of annealed glass/SGP laminated beams at room temperature. *Engineering Failure Analysis*, 16(6):1866–1875, 2009. ISSN 13506307. doi: 10.1016/j.engfailanal.2008.09.023. URL http://dx.doi.org/10.1016/j.engfailanal.2008.09.023.

F. Bernard. Analysis of the debonding risks and the failure of laminated glass thanks to a coupled analytical-numerical investigation. (2001), 2013.

J. Blaauwendraad. Buckling of laminated glass columns. 52(1), 2007.

F. P. Bos. Safety Concepts in Structural Glass Engineering. Toward an Integrated Approach. page 592, 2009.

F. P. Bos, F. A. Veer, G. J. Hobbelman, and P. C. Louter. STAINLESS STEEL REINFORCED AND POST-TENSIONED GLASS BEAMS. pages 1–9, 2004.

J. R. Correia, L. Valarinho, and F. A. Branco. Post-cracking strength and ductility of glass-GFRP composite beams. *Composite Structures*, 93(9):2299–2309, 2011. ISSN 02638223. doi: 10.1016/j.compstruct.2011.03.018.

M. DeJong, M. Hendriks, and J. Rots. Shear retention and mesh alignment during fracture using sequentially linear analysis. *Intl. Conf. on Fracture*, 12:1–10, 2009.

M. A. N. Díaz, J. M. C. Miguel, and B. L. Aguirregabiria. Prestressed glass beams. *Glass Performance Days*, pages 645–649, 2011.

O. Englhardt and K. Bergmeister. Hybrid structural elements an innovative high filigree glass-steel-system. *Glass Performance Days 2007*, 2007.

Fibrolux. Material Properties_ Fibrolux GmbH.pdf.

A. Graaf, M. Hendriks, and J. Rots. Sequentially linear analysis as an alternative to nonlinear analysis applied to a reinforced glass beam. *fib international PhD symposium in civil engineering*, 7:1–9, 2008.

M. Haldimann, A. Luible, and M. Overend. Structural use of glass. 10, 2008.

N. Hanenberg. MECHANICAL BEHAVIOUR OF LAMINATED HYBRID ADHESIVE POINT CONNECTIONS WHEN EXPOSED TO HUMIDITY CONDITIONS. *MSc Thesis*, 2016.

Huntsman. Araldite ® 2013. (April 2007):1–5, 2013.

S. Invernizzi, D. Trovato, M. A. N. Hendriks, and A. V. V. D. Graaf. Sequentially linear modelling of local snap-back in extremely brittle structures. *Engineering Structures*, 33(5):1617–1625, 2011. ISSN 0141-0296. doi: 10.1016/j.engstruct.2011.01.031. URL http://dx.doi.org/10.1016/j.engstruct.2011.01.031.

N. Khorasani. Design Principles For Glass Used Structurally. 2004.

A. Kott and T. Vogel. Remaining Structural Capacity of Broken Laminated Safety Glass. *Glass Processing Days 2003*, pages 403–407, 2003. ISSN 18736033. URL http://scholar.google.com/scholar?hl=en{&}btnG=Search{&}q=intitle:Remaining+Structural+Capacity+of+Broken+Laminated+Safety+Glass{#}0{%}5Cnwww.glassfiles.com.

J. Kraus. *Sequentially linear modelling of combined tension/compression failure in masonry structures*. 2014.

K. Kreher. Von Holz-Glas-Verbundträgern Unter Par. 2999, 2004.

Kuraray. SentryGlas ® Elastic Properties (SG5000). 89, 2014a.

Kuraray. PHYSICAL PROPERTIES OF SENTRYGLAS ®. 2014b.

Kuraray. interlayer Laminating Guide. Technical Report February, 2016.

C. Leung. Reinforcing glass with glass, Application of transparent reinforcement in structural glass beams. Technical report, Faculty of Civil Enineering & Geosciences, Delft, 2010.

C. Louter. High-strength fibre rods as embedded reinforcement in SentryGlas-laminated glass beams. *Glass Performance Days 2009*, pages 285–289, 2009. URL http://www.glassfiles.com/library/article.php?id=1414.

C. Louter and J. Cupaç. Exploratory experimental investigations on post-tensioned structural glass beams. 2:3–18, 2014. doi: 10.3233/FDE-130012.

C. Louter and J. H. Nielsen. Numerical analyses of the effect of SG-interlayer shear stiffness on the structural performance of reinforced glass beams. *COST Action TU0905, Mid-term Conference on Structural Glass*, 1:405–412, 2013. doi: 10.1201/b14563-55.

C. Louter, J. Belis, F. Bos, D. Callewaert, and F. Veer. Experimental investigation of the temperature effect on the structural response of SG-laminated reinforced glass beams. *Engineering Structures*, 32(6):1590–1599, 2010a. ISSN 01410296. doi: 10.1016/j.engstruct.2010.02.007. URL http://dx.doi.org/10.1016/j.engstruct.2010.02.007.

C. Louter, A. van de Graaf, and J. Rots. Modeling the Structural Response of Reinforced Glass Beams using an SLA Scheme. *Challenging Glass 2 - Conference on Architectural and Structural Applications of Glass*, (May), 2010b.

C. Louter, J. Belis, F. Veer, and J. P. Lebet. Structural response of SG-laminated reinforced glass beams; experimental investigations on the effects of glass type, reinforcement percentage and beam size. *Engineering Structures*, 36:292–301, 2012a. ISSN 01410296. doi: 10.1016/j.engstruct.2011.12.016. URL http://dx.doi.org/10.1016/j.engstruct.2011.12.016.

C. Louter, J. Belis, F. Veer, and J. P. Lebet. Durability of SG-laminated reinforced glass beams: Effects of temperature, thermal cycling, humidity and load-duration. *Construction and Building Materials*, 27(1):280–292, 2012b. ISSN 09500618. doi: 10.1016/j.conbuildmat.2011.07.046. URL http://dx.doi.org/10.1016/j.conbuildmat.2011.07.046.

C. Louter, M. Debonnaire, and J. Cupaç. Structural glass beams pre-stressed by externally bonded tendons. *GlassCon Global*, pages 460–469, 2014.

C. L. P. C. Louter. *Fragile yet Ductile*. PhD thesis, 2011.

P. Louter, F. Bos, and F. Veer. Performance of SGP and adhesively bonded metal-reinforced glass beams. *International symposium of the application of architectural glass ISAAG 2008 conference proceedings*, ISAAG 2008:203–210, 2008.

P. C. Louter. Adhesively bonded reinforced glass beams. *Heron*, 52(1-2):31–57, 2007. ISSN 00467316.

P. C. Louter, J. F. V. Heusden, F. A. Veer, and J. N. J. A. Vambersky. Post-tensioned Glass Beams. *ECF*, 2006.

K. Martens, R. Caspeele, and J. Belis. Development of composite glass beams – A review. *Engineering Structures*, 101:1–15, 2015. ISSN 01410296. doi: 10.1016/j.engstruct.2015.07.006. URL http://dx.doi.org/10.1016/j.engstruct.2015.07.006.

K. Martens, J. Belis, R. Caspeele, and J. Dispersyn. Numerical investigation of reinforced laminated glass beams. *IABSE Conference Nara 2015 'Elegance in Structures'*, 57:136, 2016a. ISSN 2363-5142. doi: 10.1007/s40940-016-0005-6.

K. Martens, R. Caspeele, and J. Belis. Experimental investigations of statically indeterminate reinforced glass beams. *Construction and Building Materials*, 119:296–307, 2016b. ISSN 09500618. doi: 10.1016/j.conbuildmat.2016.04.151. URL http://dx.doi.org/10.1016/j.conbuildmat.2016.04.151.

K. Martens, D. Ph, R. Caspeele, D. Ph, J. Belis, and D. Ph. Development of Reinforced and Posttensioned Glass Beams : Review of Experimental Research. 142(5):1–23, 2016c. doi: 10.1061/(ASCE)ST.1943-541X.0001453.

V. G. K. Menta, R. R. Vuppalapati, K. Chandrashekhara, and T. Schuman. Manufacturing of transparent composites using vacuum infusion process. *Polymers and Polymer Composites*, 22(9):843–850, 2014. ISSN 14782391. doi: 10.1016/j.biortech.2010.02.045.

NEN-EN. NEN-EN 10088-1. (november 2014), 2017a.

NEN-EN. NEN-EN 1993-1-4, 2017b.

NEN-EN 1990. NEN-EN 1990 + A1 + A1 / C2. 2002(december 2011), 2016.

NEN-EN 2608. Nen 2608. 2016.

P. Neto, J. Alfaiate, L. Valarinho, J. R. Correia, F. A. Branco, and J. Vinagre. Glass beams reinforced with GFRP laminates: Experimental tests and numerical modelling using a discrete strong discontinuity approach. *Engineering Structures*, 99:253–263, 2015. ISSN 1873-7323. doi: 10.1016/j.engstruct.2015.04.002. URL http://dx.doi.org/10.1016/j.engstruct.2015.04.002.

I. Niall, M. Barr, C. Gb, G. Cameron, C. Gb, S. Philip, C. Gb, X.-l. F. Cockcroft, I. Timothy, W. Matthews, H. Gb, K. A. Menear, H. Gb, F. Kerrigan, C. Gb, and A. Ashworth. (12) United States Patent (45) Date of Patent : dº ãº. 2(12), 2010.

J. H. Nielsen and J. F. Olesen. Post-crack capacity of mechanically reinforced glass beams (MRGB). *Fracture Mechanics of Concrete and Concrete Structures - Recent Advances in Fracture Mechanics of Concrete FraMCoS-7*, pages 1707–1712, 2010.

D. Palumbo, M. Palumbo, M. Mazzuchelli, A. Schiavon, and A. Rebeschini. A New Roof for the XIII th Century " Loggia de Vicari " (Arquà Petrarca -PD – Italy) Based on Structural Glass Trusses : a Case Study. *Proceedings of Glass Processing Days 2005*, pages 1–3, 2005.

S. Perkoff, S. Byers, and R. I. Limited. Destruction of glass surfaces : Inevitable or preventable ? (2), 2001.

M. Rademakers. Transparent Ductility. (June), 2009.

J. G. Rots and S. Invernizzi. Regularized sequentially linear saw-tooth softening model. *International Journal for Numerical and Analytical Methods in Geomechanics*, 28(7-8):821–856, 2004. ISSN 03639061. doi: 10.1002/nag.371.

J. G. Rots, S. Invernizzi, and B. Belletti. Fracture via a sequence of events : a saw-tooth softening model. *Fracture mechanics of concrete and concrete structures*, pages pp. 427–435, 2007.

J. G. Rots, B. Belletti, and S. Invernizzi. Robust modeling of RC structures with an " event-by-event " strategy. 75:590–614, 2008. doi: 10.1016/j.engfracmech.2007.03.027.

M. Santarsiero, C. Louter, and A. Nussbaumer. The mechanical behaviour of SentryGlas ionomer and TSSA silicon bulk materials at different temperatures and strain rates under uniaxial tensile stress state. *Glass Structures & Engineering*, 1(2):395–415, 2016. ISSN 2363-5150. doi: 10.1007/s40940-016-0018-1.

C

H. Schober. Ein Glashaus für die Therme in Badenweiler. 73:886–892, 2004.

Y. Seo, S. Cho, S. Kim, S. Choi, and H. Kim. Synthesis of refractive index tunable silazane networks for transparent glass fiber reinforced composite. *Ceramics International*, 43(10):7895–7900, 2017. ISSN 02728842. doi: 10.1016/j.ceramint.2017.03.112. URL http://linkinghub.elsevier.com/retrieve/pii/S0272884217304844.

Shin-Etsu Chemical Ltd. Silane Coupling Agents. *Silane coupling agents*, pages 1–24, 2015. URL http://www.shinetsusilicone-global.com/catalog/pdf/SilaneCouplingAgents{_}e.pdf.

E. Speranzini and S. Agnetti. Strengthening of glass beams with steel reinforced polymer (SRP). *Composites Part B: Engineering*, 67:280–289, 2014. ISSN 13598368. doi: 10.1016/j.compositesb.2014.06.035. URL http://dx.doi.org/10.1016/j.compositesb.2014.06.035.

E. Speranzini and P. Neri. Structural behaviour of GFRP reinforced glass beams. *Glass performance days-2011*, pages 604–609, 2011.

L. Valarinho, J. R. Correia, and F. Branco. Experimental Investigations on Continuous Glass-GFRP Beams . Preliminary Non- linear Numerical Modelling. June, 2012a.

L. Valarinho, J. R. Correia, F. Branco, and J. Sena-Cruz. Experimental investigations on continuous glass-GFRP Beams; preliminary nonlinear numerical modelling. *Challenging Glass 3: Conference on Architectural and Structural Applications of Glass, CGC 2012*, June:745–758, 2012b. doi: 10.3233/978-1-61499-061-1-745.

L. Valarinho, J. R. Correia, and F. A. Branco. Experimental study on the flexural behaviour of multi-span transparent glass-GFRP composite beams. *Construction and Building Materials*, 49:1041–1053, 2013. ISSN 09500618. doi: 10.1016/j.conbuildmat.2012.11.024. URL http://dx.doi.org/10.1016/j.conbuildmat.2012.11.024.

A. van de Graaf. SLA Users Manual 0.2.00, 2009.

F. Veer, J. Zuidema, and F. Bos. The strength and failure of glass in bending. *Glass processing days*, pages 1–3, 2005. URL http://www.zappi.bk.tudelft.nl/fileadmin/Faculteit/BK/Onderzoek/Projecten/Glass/Publications/2005/doc/VEER{_}2005ATPstrengthofglass.pdf.

F. A. Veer, P. C. Louter, and F. P. Bos. The strength of annealed, heat-strengthened and fully tempered float glass. *Fatigue and Fracture of Engineering Materials and Structures*, 32(1):18–25, 2009. ISSN 8756758X. doi: 10.1111/j.1460-2695.2008.01308.x.

B. Weller, A. Meier, and T. Weimar. Glass-Steel Beams as Structural Members of Façades. *Challenging Glass*, 2(May):517–524, 2010.

X. Zhang, Y. Shi, H. Hao, and J. Cui. The mechanical properties of Polyvinyl Butyral (PVB) at high strain rates. *Construction and Building Materials*, 93(September):404–415, 2015. ISSN 02641275. doi: 10.1016/j.matdes.2015.06.076. URL http://linkinghub.elsevier.com/retrieve/pii/S0264127515004268.